

## Secondary Reactions of Low-Molecular Weight Olefins During Fischer-Tropsch Synthesis

Deborah S. Jordan and Alexis T. Bell  
Materials and Molecular Research Division  
Lawrence Berkeley Laboratory  
and

Department of Chemical Engineering  
University of California, Berkeley, CA 94720

### INTRODUCTION

Low molecular weight olefins formed during Fischer-Tropsch synthesis can undergo secondary reactions and thereby influence the distribution of the final products. In the case of Ru catalysts, it has been postulated (1) that the low yields of  $C_2$  and  $C_3$  olefins over these catalysts may be due to the reincorporation of these products into growing chains. Ekerdt and Bell (2) observed that the addition of 2% ethylene to an  $H_2/CO$  mixture resulted in an enhanced yield of propylene. Subsequent studies by Kellner and Bell (1) demonstrated that at concentrations above 1% ethylene addition enhanced the rates of  $C_3$  and  $C_4$  formation but suppressed the synthesis of  $C_{6+}$  hydrocarbons. Kobori et al. (3) have examined the effects of ethylene, propylene, and 4-octene addition. When  $^{12}C$ -labeled olefins were added to a  $^{13}C/CO/H_2$  mixture, the isotopic distribution of products showed that the carbon from the additives was incorporated randomly into the products. Very recently Morris et al. (4) investigated the effects of ethylene and propylene addition on the hydrogenation of CO over Ru supported on silica, 13x-zeolite, titania, and magnesia. For  $Ru/SiO_2$  and  $Ru/13x$ -zeolite, ethylene addition markedly increased the rates of higher hydrocarbon formation without greatly influencing the methanation rate, whereas for  $Ru/TiO_2$  and  $Ru/MgO$ , ethylene addition enhanced the rate of higher hydrocarbon formation by a factor of less than two and reduced the methanation rate. With increasing proportion of ethylene in the feed, the yield of methane decreased and the yield of  $C_{3+}$  products increased. Propylene addition to CO hydrogenation over  $Ru/SiO_2$  increased the rates of  $C_2$  and  $C_{4+}$  hydrocarbon formation, without markedly affecting the methanation rate.

The objectives of this study were to investigate the influence of ethylene addition on the hydrogenation of CO over  $Ru/SiO_2$ , and to compare the product distribution obtained with those for CO hydrogenation in the absence of ethylene and ethylene homologation in the absence of CO. To enable identification of the source of carbon in the products,  $^{13}C$ -labeled CO and unlabeled  $C_2H_4$  were used. Products were analyzed by isotope-ratio gas chromatography-mass spectrometry. Among the issues investigated were the influence of ethylene addition on the reactions of CO and the participation of ethylene in processes of hydrocarbon chain initiation and growth. The influence of ethylene addition on methane formation was also examined.

### EXPERIMENTAL

A 4.3%  $Ru/SiO_2$  catalyst is used in this investigation. Details concerning its preparation and initial reduction are presented elsewhere (5). The dispersion of the catalyst is 0.27 as determined by  $H_2$  chemisorption at 373 K.

Hydrogen is purified by passage through a Deoxo unit (Engelhard Industries) and 5-Å molecular sieve. Helium (99.999%) and ethylene (99.95%) are used without further purification. Isotopically labeled carbon monoxide (Isotec, Inc.) consisting of 89.3%  $^{13}\text{C}$ O, 9.86%  $^{13}\text{C}^{18}\text{O}$ , and 0.36%  $^{12}\text{C}$ O is used as received.

Reactants are supplied from a gas flow manifold at a pressure of 1 atm to a stainless steel microreactor heated by a fluidized sand bath. The catalyst (0.51 g) is reduced in flowing  $\text{H}_2$  for 12 h at 573 K prior to each series of experiments. Reduction is continued at the reaction temperature of 493 K for 2 h before initiating an experiment. The reactant stream is then introduced, and the reaction allowed to continue for 15 min before product samples are taken for analysis. Reduction is resumed and maintained for at least 2 h between experiments. The activity of the catalyst was checked periodically by returning to base case conditions. The activity remained constant to within five percent of its standard activity.

The reactor effluent is analyzed by a combination of gas chromatography and mass spectrometry, to determine the product distribution and the  $^{13}\text{C}$  content of each of the products. The products are first separated by gas chromatography and then each eluted product is combusted to  $\text{CO}_2$ . The  $^{13}\text{C}$  content of the  $\text{CO}_2$  is determined by mass spectrometry. This analytical approach has been described by Sano et al. (6) and Matthews and Hayes (7), and is termed isotope-ratio gas chromatography-mass spectrometry.

## RESULTS AND DISCUSSION

The reaction of  $\text{C}_2\text{H}_4$  and  $\text{H}_2$  over Ru produces, in addition to  $\text{C}_2\text{H}_6$ ,  $\text{CH}_4$  and  $\text{C}_3+$  olefins and paraffins. A large fraction of the  $\text{C}_4+$  hydrocarbons are branched. As shown in fig. 1, the carbon number distribution of the  $\text{C}_3+$  products does not decrease monotonically, but rather, oscillates so that products with an even number of carbon atoms predominate. The formation of  $\text{CH}_4$  is ascribed to the hydrogenolysis of  $\text{C}_2\text{H}_4$  and the formation of  $\text{C}_3+$  hydrocarbons to homologation of  $\text{C}_2\text{H}_4$  via chain growth, involving  $\text{C}_1$  and  $\text{C}_2$  monomer units. An accurate description of the product distribution is achieved using the mechanism illustrated in Fig. 2 (8).

The addition of  $\text{C}_2\text{H}_4$  to synthesis gas has a strong influence on the hydrogenation of CO. Figures 3 and 4 show that above a  $\text{C}_2\text{H}_4/\text{CO}$  ratio of 1.0, the formation of hydrocarbons from CO is completely suppressed and only the hydroformylation of  $\text{C}_2\text{H}_4$  to form propanal (and some propanol) is observed. The presence of CO suppresses the hydrogenation of  $\text{C}_2\text{H}_4$  to  $\text{C}_2\text{H}_6$  but has relatively little effect on  $\text{C}_2\text{H}_4$  hydrogenolysis and homologation. The selectivities to  $\text{CH}_4$  and  $\text{C}_3+$  products are influenced by the partial pressures of  $\text{C}_2\text{H}_4$ , CO, and  $\text{H}_2$ . High selectivity to  $\text{C}_3+$  products and low selectivity to  $\text{CH}_4$  are observed for high  $\text{C}_2\text{H}_4$ , CO, and  $\text{H}_2$  partial pressures and low reaction temperatures. The observed distribution of products can be described theoretically using a modified version of the mechanism for  $\text{C}_2\text{H}_4$  homologation (8).

The results of the present study clearly indicate that ethylene formed via the hydrogenation of CO can undergo extensive secondary reaction. The presence of CO inhibits the hydrogenation of ethylene to ethane, and hence the formation of a stable  $\text{C}_2$  hydrocarbon product. A major portion of the readsorbed ethylene will participate in the initiation and propagation of chain growth. A significant fraction will react with adsorbed CO and hydrogen to form propanal (or propanol). Ethylene readsorption will also result in a suppression of  $\text{CH}_4$  formation. This would explain why the yield of  $\text{CH}_4$  produced over Ru catalyst is observed to decrease as the conversion of CO to products increases.

# ACKNOWLEDGMENT

This work was supported by the Division of Chemical Sciences Office of Basic Energy Sciences, United States Department of Energy, under contract DE-AC03-76SF00098.

# REFERENCES

1. Kellner, C. S., and Bell, A. T., J. Catal. 70, 418 (1981).
2. Ekerdt, J. G., and Bell, A. T., J. Catal. 62, 19 (1980).
3. Kobori, Y., Yamasaki, H., Naito, S., Onishi, T., and Tamaru, K., Chem. Soc. Faraday Trans. 1 78, 1473 (1982).
4. Morris, S. R., Hayes, R. B., Wells, P. B., and Whyman, R., J. Catal. 96, 23 (1985).
5. Winslow, P., and Bell, A. T., J. Catal. 86, 158 (1984).
6. Sano, M., Yotsui, Y., Abe, H., and Sasaki, S., J. Biomed. Mass Spec. 3, 1 (1976).
7. Matthews, D. E., and Hayes, J. M., Anal. Chem. 50, 1465 (1978).
8. Jordan, D.S., and Bell, A. T., J. Phys. Chem., submitted.

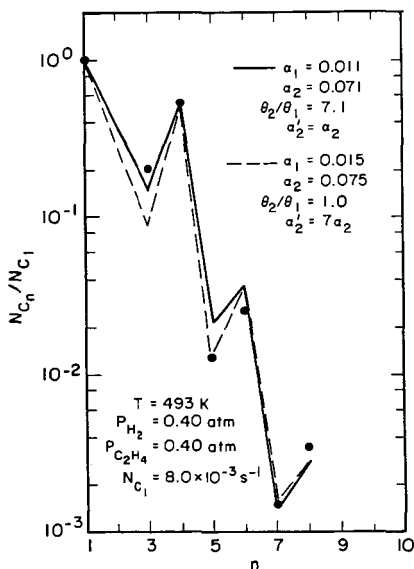


Fig. 1 Distribution of  $C_1$  through  $C_8$  hydrocarbons produced by reaction of  $H_2$  and  $C_2H_4$  at 493 K.  $P_{H_2} = P_{C_2H_4} = 0.40 \text{ atm}$ . Solid and dashed lines represent a theoretical description of the data for two sets of parameters.

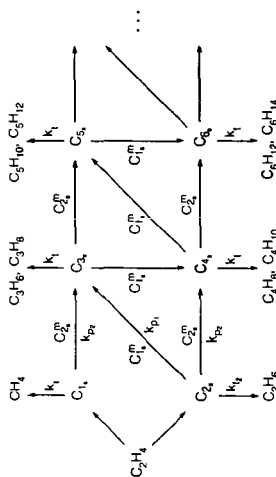


Fig. 2 Proposed scheme of chain growth for the reaction of  $H_2$  and  $C_2H_4$

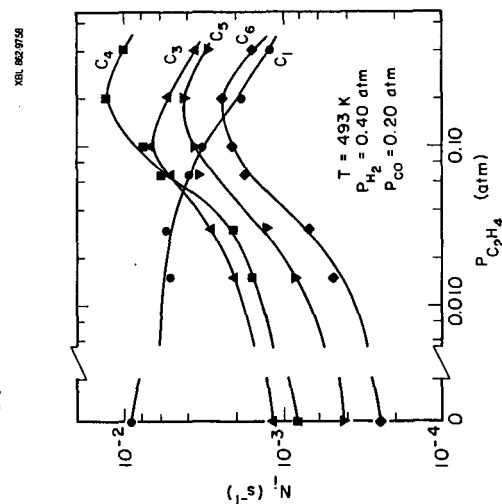


Fig. 3 Influence of  $\text{PCl}_4$  on the rates of production of  $\text{C}_1$  through  $\text{C}_6$  hydrocarbons.  $T = 493 \text{ K}$ ,  $\text{P}_{\text{H}_2} = 0.40 \text{ atm}$ ,  $\text{P}_{\text{CO}} = 0.20 \text{ atm}$ .

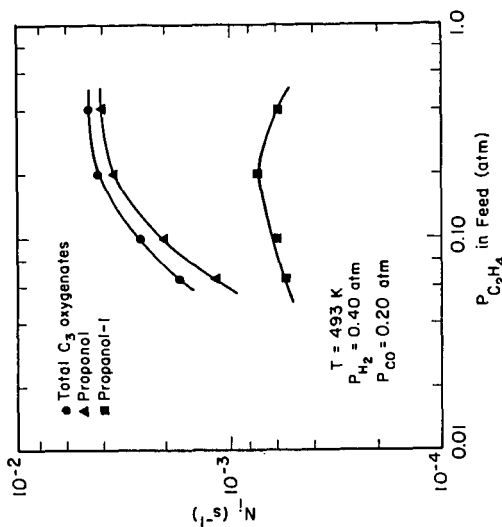


Fig. 4 Influence of  $P_{C_2H_4}$  on the rates of production of  $C_3$  oxygenates.  $T = 493$  K,  $P_{H_2} = 0.40$  atm,  $P_{CO} = 0.20$  atm.

## CHEMICAL TRAPPING OF CO/H<sub>2</sub> SURFACE SPECIES

John A. Williams, Donna G. Blackmond, and Irving Wender

Department of Chemical & Petroleum Engineering  
University of Pittsburgh  
Pittsburgh, PA 15261

### Introduction

CO hydrogenation reactions over supported metal catalysts can produce a wide spectrum of hydrocarbon and oxygenated compounds depending to a large extent on the type of metal used. Elucidating the nature of the intermediate species formed on metal surfaces may provide the key to understanding the pathways through which these reactions proceed on different metals. The number of different techniques which have been employed in search of this understanding attests not only to the importance of but also to the difficulties inherent in the identification of reactive surface species.

One common method of obtaining evidence of the participation of a postulated reaction intermediate is the use of labelled molecules during reaction (1,2). Other kinds of experiments have involved generating certain labelled or unlabelled species on the catalyst surface and then reacting them to prove their participation in CO hydrogenation reactions (3). Another elegant kind of tracer experiment is carried out by instantaneously switching a CO/H<sub>2</sub> reaction mixture to a stream in which an isotopic analog of one of the reactive components is present (4) and then monitoring the reaction kinetics during the transient period that follows. Other creative experiments have used reactive molecules not part of the reaction scheme to scavenge surface intermediates (5).

Each of these experiments has added greatly to our knowledge of the chemistry of the catalyst surface under reaction conditions. The unanswered questions that remain, however, have emphasized the need for unequivocal surface species identification. This in turn has led us to investigate a novel technique which has recently been developed (6) for chemically trapping adsorbed species. This trapping technique involves introducing an alkylating reagent onto the catalyst surface after it has been contacted with the CO/H<sub>2</sub> reactants. It is postulated that the reagent reacts with the surface intermediate species by alkylating it at each point of former attachment to the catalyst surface. Identification of the products of this alkylation reaction may then lead to back-deduction of the identity of the surface species itself. The schematic in Figure 1 portrays the reaction of alkylating reagents such as CH<sub>3</sub>I and (C<sub>2</sub>H<sub>5</sub>)<sub>2</sub>SO<sub>4</sub> with some postulated intermediate species. The ideas behind the develop-

ment of this technique draw upon methods used in the determination of mechanisms of organic reactions (7).

Chemical trapping experiments to date have been of limited use in elucidating catalytic reaction mechanisms because they have not been carried out under reaction conditions. Moreover, questions have been raised about whether the trapping reagents actually react quantitatively with surface species in the manner postulated. The purpose of our investigation is to delineate how the trapping reagent reacts with the catalyst surface and to employ the technique to probe the nature of reactive surface intermediates on supported metal catalysts during CO hydrogenation reactions.

### Discussion of Experiments

Preliminary chemical trapping experiments were carried out in-situ under CO hydrogenation conditions on a 3% RuKY zeolite catalyst. The addition of  $\text{CH}_3\text{I}$  to a  $\text{CO}/\text{H}_2$  reaction stream resulted in a profound alteration of the typical ASF product distribution for this catalyst. A dramatic decrease in  $\text{C}_1$ - $\text{C}_3$  hydrocarbons was observed concomitant with a similarly sharp increase in  $\text{C}_4$ - $\text{C}_6$  hydrocarbons. The distribution of  $\text{C}_4$  products was also significantly altered as shown in Figure 2. These results indicate that addition of the trapping reagent causes perturbations in the observed  $\text{CO}/\text{H}_2$  products which may be caused by alkylation of surface species by the reagent. However, the complexity of the results make it difficult to clearly identify surface species or to understand the action of the trapping reagent on these surface species.

The complex action of the trapping reagent on metal-adsorbate bonds might be made more clear with the substitution of model organometallic complexes for the catalyst-adsorbate systems under study. These model complexes simulate organic species adsorbed on metal surfaces. The interaction of the organic ligands with chemical trapping reagents may provide important clues about how these reagents interact with species adsorbed on the surface of a metal catalyst. Figure 3 shows the structure of two organometallic complexes now under study using the chemical trapping technique.

The investigations involving model complexes are being coupled with further in-situ trapping experiments on supported Ni and Pd catalysts during  $\text{CO}/\text{H}_2$  reactions. These two metals yield very different product distributions, but both are generally less complex than those obtained from Ru. Coupled with investigations on model organometallic systems, these trapping studies promise to provide a framework for understanding differences in CO hydrogenation reaction pathways over different metals.

### References

- (1) Kummer, J. T., DeWitt, T.W., and Emmett, P. H., *J. Am. Chem. Soc.*, 70, 3632 (1948).
- (2) Araki, M. and Ponec, V., *J. Catal.*, 49, 439 (1976).
- (3) Brady, R. C. and Petit, R., *J. Am. Chem. Soc.*, 102, 6181 (1980).
- (4) Biloen, P., Helle, J. N., and Sachtler, W.M.H., *J. Catal.*, 58, 95 (1979).
- (5) Eckert, J. G. and Bell, A. T., *J. Catal.*, 62, 19 (1980).
- (6) Deluzarche, A., Hindermann, J. P., Kiennemann, A., and Kieffer, R., *J. Mic. Cat.*, 31, 225 (1985).
- (7) Gould, E. S., in *Mechanism and Structure in Organic Chemistry*, Holt, Rinehart and Winston, New York (1959).

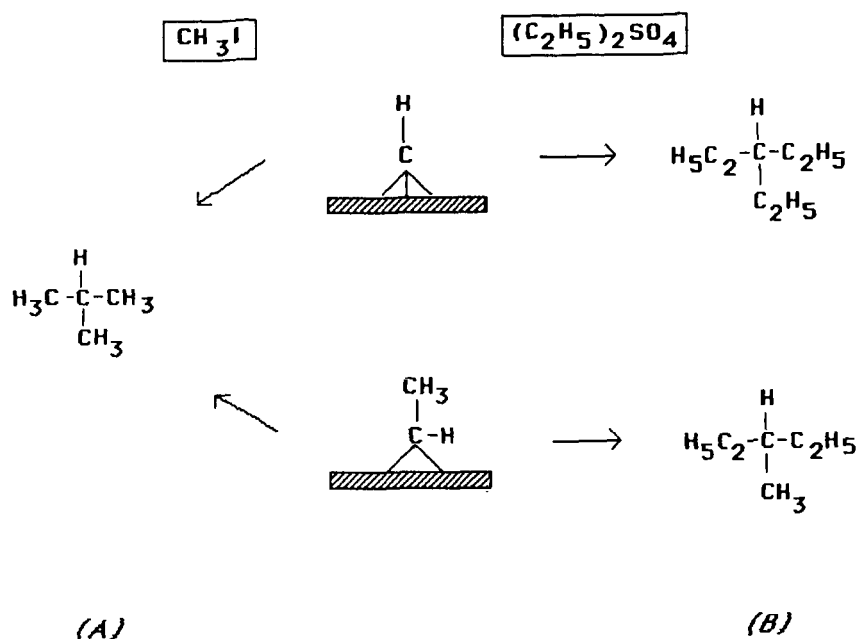


FIGURE 1. Schematic of the reaction of alkylating reagents with some postulated surface intermediate species

(A) products derived from a  $\text{C}_1$  alkylating reagent

(B) products derived from a  $\text{C}_2$  alkylating reagent



Figure 2A. Total Product Distribution

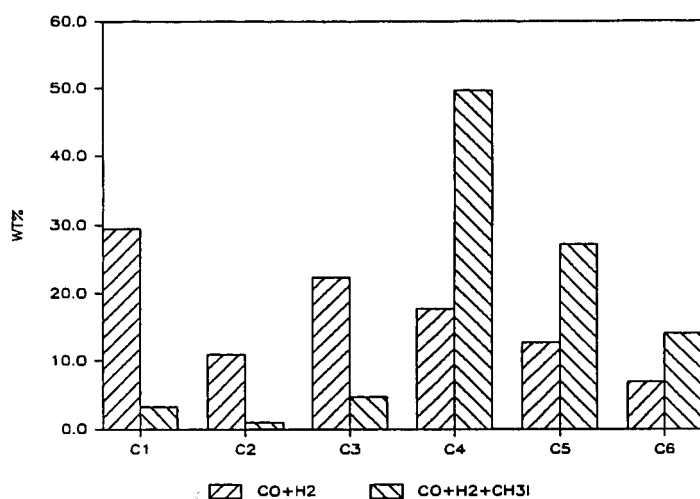
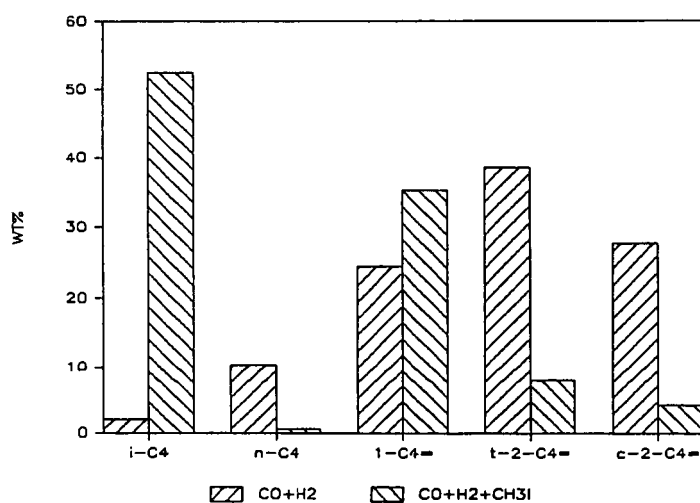
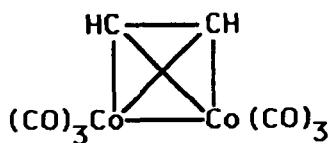


Figure 2B. Composition of C4 Products



(A)



(B)

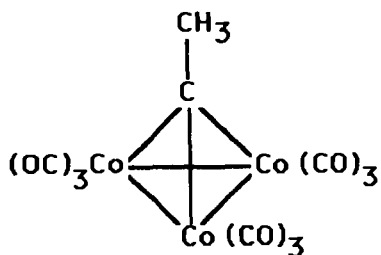


FIGURE 3. Organometallic complexes under study as model metal-adsorbate systems for chemical trapping

(A) *acetylene dicobalt hexacarbonyl*

(B) *ethyl tricobalt enneacarbonyl*

## Isosynthesis Mechanisms Over Zirconium Dioxide

Ronald G. Silver, Shiaw C. Tseng, and John G. Ekerdt

Department of Chemical Engineering  
University of Texas  
Austin, Texas 78712

### Introduction

The isosynthesis process refers to the selective conversion of synthesis gas into branched aliphatic hydrocarbons over metal oxide catalysts. Thoria and zirconia are the most active oxides that catalyze the formation of hydrocarbons containing four to eight carbon atoms, with isobutane as the major product [1]. The reaction requires high pressures, 30-600 atm, and high temperatures, 375 to 475 C.

The reactions occurring during isosynthesis have not been as thoroughly studied as have the reactions occurring during CO hydrogenation to methanol or during Fischer-Tropsch synthesis. The earliest research was conducted in the 1940's [1]. The effects of oxide composition and synthesis conditions are reported and mechanisms, based on these early studies, have been proposed [1,2,3]. These proposed mechanisms relied on the acid/base nature of the catalytically active oxides and involved acid-catalyzed reactions between methanol or dimethyl ether and olefins. More recently, two additional isosynthesis mechanisms have been proposed [4,5]. Both of the recent mechanisms propose CO insertion into an oxygenated hydrocarbon fragment to explain chain growth and involve aldol condensation as one of the termination reactions. The CO insertion and the aldol condensation reactions differ in that different oxygenated fragments and C<sub>1</sub> fragments are proposed to be involved.

The activation of CO on zirconia has been reported in a series of papers [6,7,8,9]. The activation is proposed to involve the initial formation of a surface formate and its subsequent reduction to a methoxide via an oxymethylene. The oxymethylene carbon is bonded to the Zr cations through two oxygen atoms [7]. This proposed structure was based on limited infrared data and other structures, such as those involving carbon bonded directly to a Zr cation, may be present.

### Experimental

The high pressure studies were conducted in a 70 mm section of 6.35 mm OD stainless steel tubing. All of the experiments were conducted at 35 atm and a total flow rate of 100 cc/min. The reactor effluent was analyzed on a gas chromatograph.

A fresh charge (2.0 grams) of zirconia was used for each experiment. The zirconia was pretreated at 425 C in flowing oxygen for 60 min followed by heating at 425 C in flowing hydrogen for 60 min. The treated zirconia was exposed to CO/H<sub>2</sub> at a constant ratio of 1/1 for the data presented in the tables.

Zirconia was prepared by adding concentrated ammonium hydroxide to a 20.3 wt%  $\text{Zr}(\text{NO}_3)_4$  solution (Nyacol). The resulting hydrous  $\text{ZrO}_2$  was washed with distilled water and dried in air at 120 C for 24 hr. The  $\text{ZrO}_2$  was subsequently calcined in air for 4 hr at 600 C. The  $\text{ZrO}_2$  had a BET area ranging from 30-45  $\text{m}^2/\text{g}$  and was monoclinic. The activity of the  $\text{ZrO}_2$  was a strong function of the degree of drying and the calcination conditions. A thorough drying was necessary to achieve high activity to methanol, dimethyl ether and hydrocarbons. (The causes for this are currently under investigation.)

### Results

A series of experiments was conducted over the zirconia at temperatures ranging from 250 to 425 C and at varying flow rates. Below 350 C methanol and dimethyl ether were the only products formed in significant quantities. Hydrocarbon production was observed above 350 C. The product distribution trends were similar to those reported over thorium [1].

Experiments were performed to test the mechanisms that have been proposed. These involved adding reactants into the  $\text{CO}/\text{H}_2$  feed gas that should, on the basis of the different mechanisms, adsorb, transform into a reactive intermediate, and become incorporated into the isosynthesis products. The effect of adding propylene, methanol, formaldehyde, acetone, n-propanol, propionaldehyde and 2-methyl-propionaldehyde has been measured. These were added at low concentrations (50-500 ppm) to minimize their effect on existing surface species and reactions.

Propylene was added at the level it was produced at and it passed through the reactor unreacted and had a negligible effect on the  $\text{C}_4$  products. This, and other olefin addition experiments, suggests that olefins are not incorporated into the isosynthesis products and it is unlikely that isosynthesis intermediates can be derived from hydrocarbon products. These results also provide evidence that the early acid-based mechanisms [1,2,3] are not correct.

In many cases, the oxygenated additives did not appear to incorporate, in appreciable amounts, into the next higher synthesis products, but rather underwent self-condensation or underwent reduction. The propionaldehyde and acetone additions have provided the most information. Table 1 presents the effect of adding 200 ppm of propionaldehyde to the feed. (Isosynthesis produced at most 4 ppm of propionaldehyde at the conditions reported here.) Table 2 presents the effect of adding 250 ppm of acetone to the feed. The acetone experiments were conducted over a batch of zirconia that had a lower activity; presumably this was caused by a variation in the preparation of the zirconia.

Methane, methanol and dimethyl ether decreased, while ethylene, propylene, propane, isobutene, and the  $\text{C}_4$  alcohols increased in concentration in the presence of added propionaldehyde. Propionaldehyde appeared to react with the methane/methanol precursor to form isobutene. Our atmospheric studies [6,7,8] have demonstrated that the

methane/methanol precursor is a methoxide. The amount of propionaldehyde fed can be accounted for in the increase in ethylene, C<sub>3</sub> hydrocarbons and oxygenates, isobutane and the C<sub>4</sub> alcohols.

The majority of the acetone was reduced to propane and propylene. There was a significant increase in the amount of isobutanol formed and an unexpected decrease in isobutene. The linear butenes were moderately affected. Methanol and dimethyl ether decreased substantially in the presence of acetone. Acetone was expected to form an aldehydic-like species by analogy to previous work with formaldehyde [6,7,8].

Isobutanol was seen to increase and isobutene was seen to decrease in the presence of acetone. Both were expected to increase. The significant drop in isobutene, in parallel with the methanol decrease, may be related to acetone interfering with methanol production. Aldol condensation appears to require the methanol precursor (see next section). The majority of the isobutene loss could be associated with the isobutene formed via aldol condensation.

### Discussion

The acetone addition experiments support the CO insertion scheme proposed by Mazanec [4]. This scheme is represented in Figure 1 for a bound aldehyde originating from acetone. This scheme involves CO insertion into a bound aldehyde, I, to form a cyclic acyl, II. The substituents of the cyclic acyl influence subsequent transformations, 1,2-shift of hydrogen (favored over alkyl [4]) through the second valence bond structure, III, or step-wise hydrogenation to the alcohol via the intermediate IV.

The other CO insertion scheme has been proposed by Vedage et al. [5] on the basis of extensive studies of alcohol synthesis over a variety of metal oxide systems. An alkoxide is proposed to undergo CO insertion to form an alkionate which is subsequently reduced to the alcohol. There is an important distinction between the two mechanisms. Secondary alcohols are not observed during isosynthesis; therefore, secondary alkoxides are not formed and the alkoxide-based CO insertion mechanism [5] can only lead to linear products.

Acetone addition led to an increase in isobutanol and a parallel loss of isobutene, which may be related to a suppression of aldol condensation (see below). Isopropanol was not detected, suggesting that acetone did not form the branched alkoxide required, in Vedage et al.'s scheme, to form the increased isobutanol. Additional studies in which n-propanol was added to the feed did not lead to a measurable change in any C<sub>4</sub> product providing additional evidence that alkoxides are unlikely intermediates in CO insertion reactions over zirconia.

Aldol condensation has been proposed as the termination reaction that can account for branching in the synthesis of alcohols [5] and that can account for the non-Flory distribution observed during isosynthesis [4]. The propionaldehyde addition experiments showed a

loss in methanol, methane and dimethyl ether, and an increase in isobutene. These observations suggest that the branching reaction involves the methanol/methane precursor, the methoxide [8,9]. Figure 2 presents the aldol condensation scheme that was suggested by Mazanec [4]. Propionaldehyde is proposed to adsorb as structure V and transform into the enolate anion, VI. The enolate reacts with methoxide to form the next higher aldehyde, that is subsequently reduced to the branched hydrocarbon or alcohol. The alternative scheme involves a reaction between the enolate anion, VI, and a formyl [5]. All the previous work over zirconia [6,7,8,9] is consistent with the conversion of CO via a formate rather than a formyl intermediate. This observation along with the effect propionaldehyde had on the methanol/methane yield supports the aldol condensation scheme represented in Figure 2.

#### Acknowledgements

This work was supported by the Division of Chemical Sciences, Office of Basic Energy Sciences, U.S. Department of Energy under Contract DE-AS05-80ER10720.

#### References

1. Pichler, H., and Ziesecke, K-H., Bureau of Mines Bull. 448 (1950).
2. Storch, H. H., Golumbic, N., and Anderson, R. B., "The Fischer-Tropsch and Related Synthesis", Wiley, New York, 1951.
3. Cohn, E. M., in "Catalysis" (P. H. Emmett, Ed.) Vol. 4, Reinhold, New York, 1956.
4. Mazanec, T. J., J. Catal. 98, 115 (1986).
5. Vedage, G. A., Himelfarb, P. B., Simmons, G. W., and Klier, K. in "Solid State Chemistry in Catalysis", (R. K. Grasselli and J. F. Bradzil) ACS Symposium Series 279, 1985.
6. He, M-Y., and Ekerdt, J. G., J. Catal. 87, 238 (1984).
7. He, M-Y., and Ekerdt, J. G., J. Catal. 87, 381 (1984).
8. He, M-Y., and Ekerdt, J. G., J. Catal. 90, 17 (1984).
9. Jackson, N. B., and Ekerdt, J. G., "Methanol Synthesis Mechanism Over Zirconium Dioxide", J. Catal. (in press).

Table 1 Isosynthesis Products at 425 C and 35 atm  
over  $\text{ZrO}_2$  Made from  $\text{Zr}(\text{NO}_3)_4$

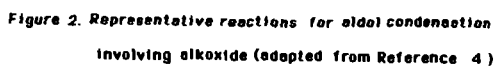
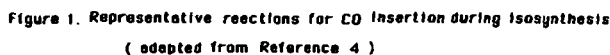
Feed Gas	$\text{H}_2/\text{CO}/\text{He}$	$\text{H}_2/\text{CO}/\text{He}$ with 200 ppm of $\text{C}_2\text{H}_5\text{CHO}$
$\text{CH}_4$	1312 <sup>(a)</sup>	863
$\text{C}_2\text{H}_4$	104	123
$\text{C}_2\text{H}_6$	103	103
$\text{C}_3\text{H}_6$	67.0	204
$\text{C}_3\text{H}_8$	19.0	27.0
i- $\text{C}_4\text{H}_{10}$	6.1	5.5
i- $\text{C}_4\text{H}_8$	252	301
n- $\text{C}_4\text{H}_{10}$	4.0	4.7
1- $\text{C}_4\text{H}_8$	28.5	30.7
t-2- $\text{C}_4\text{H}_8$	27.7	27.6
c-2- $\text{C}_4\text{H}_8$	26.4	26.1
$(\text{CH}_3)_2\text{O}$	486	455
$\text{CH}_3\text{OH}$	171	155
$\text{C}_2\text{H}_5\text{CHO}$	0	0
n- $\text{C}_3\text{H}_7\text{OH}$	3.1	6.8
n- $\text{C}_4\text{H}_9\text{OH}$	12.3	16.9
i- $\text{C}_4\text{H}_9\text{OH}$	7.9	12.6
i- $\text{C}_4\text{H}_8/\text{CH}_3\text{OH}$	1.47	1.94

(a) ppm

Table 2 Isosynthesis Products at 425 C and 35 atm  
over  $\text{ZrO}_2$  Made from  $\text{Zr}(\text{NO}_3)_4$

Feed Gas	$\text{H}_2/\text{CO}/\text{He}$	$\text{H}_2/\text{CO}/\text{He}$ with 250 ppm of acetone
$\text{CH}_4$	1307 <sup>(a)</sup>	834
$\text{C}_2\text{H}_4$	155	128
$\text{C}_2\text{H}_6$	64.3	34.5
$\text{C}_3\text{'s}$	93.1	338
i- $\text{C}_4\text{H}_{10}$	1.2	1.8
i- $\text{C}_4\text{H}_8$	72.3	37.5
n- $\text{C}_4\text{H}_{10}$	2.9	11.5
1- $\text{C}_4\text{H}_8$	20.5	23.2
$\text{CH}_3\text{OH}$	665	356
$(\text{CH}_3)_2\text{O}$	913	25.2
$(\text{CH}_3)_2\text{CO}$	0	0
$(\text{CH}_3)_2\text{CHCHO}$	3.9	6.4
i- $\text{C}_4\text{H}_9\text{OH}$	31.9	69.8
n- $\text{C}_4\text{H}_9\text{OH}$	13.3	5.4

(a) ppm





# EFFECTS OF H<sub>2</sub>O AND CO<sub>2</sub> ON THE ACTIVITY AND COMPOSITION OF IRON FISCHER-TROPSCH CATALYSTS

Mark A. McDonald

U.S. Department of Energy  
Pittsburgh Energy Technology Center  
P.O. Box 10940  
Pittsburgh, Pennsylvania 15236

## INTRODUCTION

The composition of an iron Fischer-Tropsch (F-T) catalyst is strongly affected by the % conversion of H<sub>2</sub>-CO syngas (1,2). At low % conversion, the strongly reducing syngas mixture tends to convert metallic or oxidic iron species to a bulk iron carbide phase or phases. As % syngas conversion increases, H<sub>2</sub> and CO are converted to organic products, and to H<sub>2</sub>O and CO<sub>2</sub>. The gas mixture can therefore oxidize an iron catalyst (3). However, the catalyst's synthesis behavior (activity, selectivity, activity and selectivity maintenance) also depends strongly on % syngas conversion (4). Thus, an iron catalyst's composition and synthesis behavior are not easily correlated under typical F-T reaction conditions.

This study was designed to determine how the build-up of H<sub>2</sub>O and CO<sub>2</sub> during reaction affect F-T catalyst composition and synthesis behavior. Reaction rate measurements were conducted at differential % syngas conversion using catalyst wafers mounted in an *in-situ* cell. This cell allowed Mössbauer effect spectroscopy of the used catalyst for determination of the catalyst composition. Additional H<sub>2</sub>O and CO<sub>2</sub> were added to syngas to determine the effects on catalyst composition, activity, and selectivity. Furthermore, these experiments were carried out at pressures well above atmospheric, the pressure range required for good iron F-T catalyst behavior (5). Thus, results presented here are more closely related to the state of working F-T catalysts than are previous *in-situ* Mössbauer studies of iron catalysts, which were done almost exclusively at atmospheric pressure. This paper focuses on initial experiments involving the addition of only H<sub>2</sub>O, not CO<sub>2</sub>, to a syngas stream.

## EXPERIMENTAL METHODS

Flows of 1/1 H<sub>2</sub>/CO, H<sub>2</sub>, CO<sub>2</sub>, CO and He were obtained from cylinders, with purification traps located downstream from each cylinder. Two Brooks 5850 mass flow controllers regulated flows from one or two cylinders at a time. Water was added to the gas streams with an ISCO 314 syringe pump. The water flowing from the pump was vaporized and combined with the gas stream. Gas lines were heated downstream to prevent water condensation. The syringe pump was filled from a distilled water reservoir. The water in this reservoir was sparged 4-10 h with He to remove dissolved gases.

The spectroscopy cell used for reaction experiments was constructed at West Virginia University under the supervision of Dr. Pedro Montano. The cell pressure was regulated with a Tescom back-pressure regulator located downstream. Reaction products were analyzed using a Hewlett-Packard 5730 gas chromatograph. A flame ionization detector analyzed organic products eluted from a capillary column, while a thermal conductivity detector analyzed other gases (CO<sub>2</sub>, CO) eluting from a Porapak R column. The Mössbauer spectrometer is an MS-900 manufactured by Ranger Scientific. The source was 100 millicuries of <sup>57</sup>Co in Rh, obtained from New England Nuclear.

The iron catalyst was prepared by incipient wetness impregnation of Davison 952 silica with aqueous Fe(NO<sub>3</sub>)<sub>3</sub> solution, yielding a catalyst precursor of

approximately 12 wt% Fe following drying and calcination. Approximately 0.15 g of this precursor was pressed into a wafer and mounted in the reaction cell for each experiment. The cell was then pressure tested by heating in a He flow to 383 K for 2 h, then given a standard reduction in flowing  $H_2$  at 523 K for 14 h, 623 K for 8 h, and finally 698 K for 14 h. Before exposure to syngas, the catalyst was cooled in  $H_2$  flow to 523 K. All gas treatments reported here were carried out at 2.06 MPa (20.3 atm).

## RESULTS

Rates of synthesis of  $CH_4$  and  $CO_2$  obtained after 2 h exposure to 1/1  $H_2/CO$  are shown in Table 1, reported as (moles product)/(mole total Fe  $\cdot$  s). Product selectivities to light hydrocarbons are also listed, shown as mole/mole  $CH_4$ . The catalyst reached maximum conversion after two hours on stream, and maintained essentially constant activity and selectivity during the entire 24 h of synthesis.

In a separate experiment, a catalyst sample given the same reduction pre-treatment and 24 h exposure to syngas was then exposed to syngas containing 12%  $H_2O$ . Catalyst activity declined fifty-fold during the first four hours on stream, to a level of activity approaching the accuracy of chromatographic analysis. (Thus, no data are given.) Production of  $CO_2$  declined rapidly over the same period of time.

Mössbauer effect spectra of catalyst samples are shown in the Figure 1. Figure 1a shows the spectrum of the initially reduced catalyst. This spectrum displays the characteristic six-peak spectrum of  $\alpha$ -Fe, demonstrating thorough reduction occurred before exposure to syngas. The spectrum may also contain an  $Fe^{+2}$  component overlapping with the fourth peak, although no computer fitting of the spectrum has been yet made. Figure 1b shows that during 24 h of syngas exposure, the catalyst was completely converted to iron carbide. The six-peak spectrum is that of  $\epsilon'$ -carbide (6,7), although a small amount of  $\chi$ -carbide may also be present. The sample exposed to an additional 24 h of syngas containing 12%  $H_2O$  gave essentially the same spectrum (Figure 1c), even though catalyst activity declined dramatically during this treatment. Thus, the decline in activity upon exposure to syngas + 12%  $H_2O$  was not accompanied by any measurable bulk oxidation of iron carbide.

## DISCUSSION

At least two processes need to be considered in discussing the effects of adding the oxidant  $H_2O$  to syngas: (a) bulk oxidation of the iron catalyst by  $H_2O$ , and (b) oxidation of CO by  $H_2O$  to form  $H_2 + CO_2$ , the water-gas shift reaction. The latter reaction is clearly favored thermodynamically under these conditions (8), and is typically equilibrated for K-promoted F-T catalysts operating at non-differential conversions and slightly higher temperatures than used here (9). However, for the experimental conditions reported here, there is little reason to expect the reaction to approach equilibrium. Thus, it is sufficient to consider only the first process and to neglect the water-gas shift reaction. (This statement is equivalent to saying that one need only consider the oxidation of iron by  $H_2O$  and need not consider the reverse process, the reduction of iron oxide by CO.)

For the run in which  $H_2O$  was added to syngas, the  $(H_2O)/(H_2)$  ratio was clearly above that required to oxidize  $\alpha$ -Fe to  $Fe_3O_4$  (8). However,  $\epsilon'$ -carbide, not  $\alpha$ -Fe, was present before exposure to  $H_2O$ -containing syngas, and the thermodynamics of the iron carbides are not well-defined (3). The absence of any detectable bulk carbide oxidation during  $H_2O$  exposure thus may be due to either the unfavorable thermodynamics or kinetics of bulk oxidation.

Nevertheless, the addition of  $H_2O$  to syngas certainly made the gas much more oxidizing. The loss of catalyst activity upon exposure to  $H_2O$ -containing syngas suggests that surface oxidation of the catalyst took place. This would be consistent with the idea that reduced iron species are required for hydrocarbon synthesis from syngas (10,11).

The severe loss of catalyst activity upon exposure to  $H_2O/H_2/CO$  was larger than the magnitude of effects reported by other workers (9,11,12). In fixed-bed experiments, Karn *et al.* reported that 10-30%  $H_2O$  added to 1/1  $H_2/CO$  had relatively little effect on % CO conversion (12). The main effect was to decrease the %  $CH_4$  in the outlet stream while increasing %  $CO_2$ . Thus, the extent of water-gas shift reaction was increased while hydrocarbon synthesis was inhibited. The increase in water-gas shift and inhibition in methane synthesis was most noticeable at low % conversions (high space velocities). At higher % conversions, less inhibition of methane production was observed, attributed to the enhanced  $H_2/CO$  ratio resulting from water-gas shift.

In slurry-phase F-T synthesis experiments, Satterfield *et al.* (9) reported trends similar to those of Karn *et al.* but of smaller magnitude. Addition of 12%  $H_2O$  slightly increased the rate of CO consumption, due to an increase in  $CO_2$  production from water-gas shift. The rate of CO conversion to organic products appears to have declined very slightly. The magnitude of these trends was not much larger even for addition of up to 42%  $H_2O$ ; the increase in  $CO_2$  production and decrease in CO conversion to organic products still were each only about a factor of two. It should be noted that these runs had  $H_2 + CO$  conversions over 50%. Since these authors used a mixed reactor, it is probably most reasonable to compare results presented here with their experiments containing 42%  $H_2O$  in the feed, since in each case the reactor concentrations of  $H_2O$  were in the same range.

Reymond *et al.* (13) reported trends somewhat closer to those reported here. In studies at atmospheric pressure and differential % conversion, addition of only 0.6%  $H_2O$  to 9/1  $H_2/CO$  produced about a three-fold drop in rates of both  $CH_4$  and  $CO_2$  synthesis.

The difference among these studies are attributable to differences in reactor type and catalyst used. Studies of  $H_2O$  addition carried out at high % conversion showed relatively small changes in reaction rates (9,12). Additional  $CO_2$  was produced, synthesis of F-T products was inhibited, but these trends became less pronounced as % conversion increased. In contrast, reactions carried out under differential % conversion (13) showed much larger effects of  $H_2O$  addition on catalyst activity but no clear effect on selectivity.

These trends can be rationalized from the following observations. The studies carried out at high % conversion (9,12) had substantial concentrations of  $H_2O$ ,  $CO_2$ , and organic products in the outlet stream, while concentrations of  $H_2$  and CO were well below concentrations in the inlet stream. In addition, K-promoted catalysts were used in both studies. High % conversions and K-promotion both favor equilibration of the water-gas shift reaction (9,14), so this reaction is likely to approach equilibrium under these conditions. Addition of  $H_2O$  to the feed perturbs the water-gas shift reaction away from equilibrium and makes the gas mixture more oxidizing. Therefore, the % CO conversion to  $CO_2$  (water-gas shift) increases while F-T activity drops. As % conversion is increased (space velocity is lowered), the water-gas shift reaction approaches equilibrium and the oxidizing effect of  $H_2O$  addition is minimized. F-T synthesis is not as strongly inhibited under these conditions.

In contrast, at differential % conversions, the  $H_2O$  concentration in the feed is essentially the same as in the outlet. The water-gas shift reaction is not equilibrated, so the increase in  $H_2O$  concentration is accompanied by a much larger drop in activity.

#### DISCLAIMER

Reference in this paper to any specific commercial product, process, or service is to facilitate understanding, and does not necessarily imply its endorsement or favoring by the United States Department of Energy.

#### REFERENCES

1. Shen, W.M., Dumesic, J.A., and Hill, C.G., Rev. Sci. Instrum. 52, 858 (1981).
2. Madon, R.J., and Taylor, W.F., J. Catal. 69, 32 (1981).
3. Højlund-Nielsen, P.E., and Bøgild-Hansen, J., J. Molec. Catal. 17, 183 (1982).
4. Dry, M.E., in "Catalysis: Science and Technology," Vol. 1 (Anderson, J.R., and Boudart, M., Eds.), Springer-Verlag, Heidelberg, 1981, p. 159.
5. Storch, H.H., Golumbic, N., and Anderson, R.B., "The Fischer-Tropsch and Related Synthesis," Wiley, New York, 1951.
6. Amelse, J.A., Butt, J.B., and Schwartz, L.H., J. Phys. Chem. 82, 588 (1978).
7. Niemantsverdriet, J.W., van der Kraan, A.M., van Dijk, W.L., and van der Baan, H.S., J. Phys. Chem. 84, 3363 (1980).
8. Anderson, R.B., "The Fischer-Tropsch Synthesis," Academic Press, Orlando, Fla., 1984.
9. Satterfield, C.N., Hanlon, R.T., Tung, S.E., Zou, Z.-M., and Papaefthymiou, to be submitted to Ind. Eng. Chem. Proc. Des. Dev.
10. Vogler, G.L., Jiang, X.-Z., Dumesic, J.A., and Madon, R.J., J. Catal. 89, 116 (1984).
11. McDonald, M.A., and Boudart, M., to be submitted to J. Catal.
12. Karn, F.S., Shultz, J.F., and Anderson, R.B., "Actes Congr. Intern. Catalyse, 2<sup>e</sup>", Vol. 2, Paris, 1961, p. 2439.
13. Reymond, J.P., Meriaudeau, P., Pommier, B., and Bennett, C.O., J. Catal. 64, 163 (1980).
14. Arakawa, H., and Bell, A.T., Ind. Eng. Chem. Proc. Des. Dev. 22, 97 (1983).

TABLE 1. Rates and Selectivities of F-T Synthesis  
(523 K, 2.06 MPa, 1/1 H<sub>2</sub>/CO, 2 h on stream)

Product		Rate/10 <sup>-4</sup> mol (mol Fe · s) <sup>-1</sup>	
CH <sub>4</sub>		3.2	
CO <sub>2</sub>		0.75	
Product		Selectivity/mol (mol CH <sub>4</sub> ) <sup>-1</sup>	
CH <sub>4</sub>		1.00	
ΣC <sub>2</sub>		0.31	
ΣC <sub>3</sub>	C <sub>2</sub> H <sub>4</sub>	0.18	.077
	C <sub>2</sub> H <sub>6</sub>		.235
ΣC <sub>4</sub>	C <sub>3</sub> H <sub>6</sub>	0.095	.118
	C <sub>3</sub> H <sub>8</sub>		.064
ΣC <sub>5</sub>		0.050	

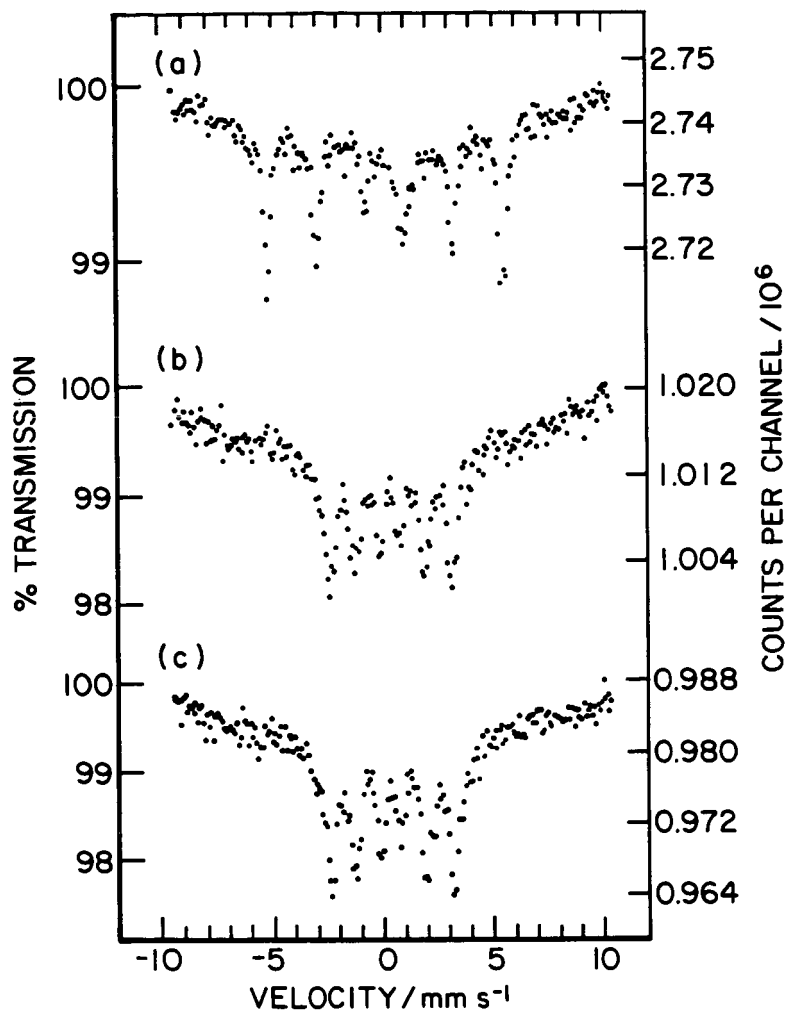


FIGURE 1. Mössbauer Effect Spectra of  $\text{Fe/SiO}_2$

- (a) Reduced catalyst
- (b) Reduced catalyst, reacted 24 h in 1/1  $\text{H}_2/\text{CO}$
- (c) Reduced catalyst, reacted 24 h in 1/1  $\text{H}_2/\text{CO}$ ,  
24 h in 1/1  $\text{H}_2/\text{CO} + 12\% \text{H}_2\text{O}$

THE INFLUENCE OF PARTICLE SIZE AND STRUCTURE ON THE MÖSSBAUER  
SPECTRA OF IRON CARBIDES FORMED DURING FISCHER-TROPSCH SYNTHESIS

R. R. Gatte and J. Phillips

The Pennsylvania State University  
133 Fenske Laboratory  
University Park, PA 16802

Introduction

Characterization of the active and stable phase of iron-based Fischer-Tropsch catalysts has been a topic of investigation for several years (1-10). Yet, a great deal of controversy still surrounds the identity of the phase(s) present during synthesis. This stems from the fact that neither x-ray nor Mössbauer studies have proven capable of unambiguously characterizing the metastable carbides formed.

Investigations of the metastable, octahedral carbides (as they have been termed (5)) have been going on for many years (11-18), dating back to at least 1949 (12). The iron structure has been assigned as HCP (or 'nearly' HCP) with the carbon atoms occupying the octahedral holes. The most notable of these are the  $\epsilon$  and  $\epsilon'$  carbides. X-ray results have, however, been rather unsatisfactory for many reasons. For instance, the commercial catalysts studied contained many metallic additives and in most cases the small crystallite sizes gave rise to broad, poorly resolved lines.

In recent years, emphasis has shifted toward the use of Mössbauer spectroscopy for in-situ studies of the carburization behavior (1-10, 13-15, 18). Again, a number of conflicting reports have appeared. Many workers suggest that  $\chi$  and  $\epsilon'$  are the active phases, with  $\epsilon'$  being present in smaller particles (4,10). Others have argued that the dominant phases are  $\epsilon$  and  $\epsilon'$  (2,8,9). Still others have suggested that the identities of  $\epsilon$  and  $\epsilon'$  are actually the reverse of what has been generally reported (5). It should be clear from a careful review of these studies that the ambiguity arises from the difficult interpretation of the spectra obtained. This may be due to the fact that these phases are present as very small particles (ca. 10 nm diameter), which introduces relaxation effects into the spectra. Further, the characteristic peaks attributed to  $\epsilon$  and  $\epsilon'$  carbide are, in most cases, present as background lines superimposed on a strong spectral component of  $\alpha$ -Fe or Fe-oxide.

It will be shown that if spectra are collected for a single sample over a range of temperatures, and if relaxation effects are properly accounted for, the Mössbauer results can give not only accurate identification of the phase(s) present but also quantitative particle size information and qualitative information regarding particle structure and the nature of particle/support interaction.

Discussion

In this study a Mössbauer modelling routine, described in earlier work (19-21), designed to account for collective magnetic excitations (22,23), superparamagnetic relaxation (24) and quadrupole shift distribution (25,26), was used to generate theoretical iron-carbide spectra which could then be analyzed using a conventional least-squares fitting routine (27). Several parameters (including, temperature, anisotropy energy constant, quadrupole shift distribution, and particle size distribution) were systematically varied to check the effect on the observed spectra. The starting parameters were those of  $\chi$ -carbide (25).

From the results (shown in Figures 1-4, and Tables I-III) the following conclusions can be drawn:

- 1.) At least one phase of octahedral carbide forms during Fischer-Tropsch synthesis.
- 2.) The partially relaxed spectrum of this phase can be reasonably well fit with a single sextuplet with  $H_{hf} \approx 170$  kOe and  $\delta_{IS} \approx .25$  mm/s (28). However, due to the clear asymmetry of the spectrum, more than one sextuplet is probably present.
- 3.) A wide particle size distribution cannot account for the broadness observed in the peaks attributed to  $\epsilon'$ -carbide, and the unrelaxed hyperfine field of this phase is probably larger than 170 kOe.
- 4.) The particle sizes reported on the basis of x-ray data cannot be correct (i.e., 35Å particle radius), since it is impossible to obtain a defined sextuplet for a particle size this small. Relaxation effects become overwhelming.

All of these conclusions will be discussed in greater detail.

#### References

1. Amelse, J. A., Butt, J. B., and Schwartz, L. H., J. Phys. Chem. 82, 558 (1978).
2. Raupp, G. B. and Delgass, W. N., J. Catal. 58, 337, 348 (1979).
3. Unmuth, E. E., Schwartz, L. H., and Butt, J. B., J. Catal. 63, 404 (1980).
4. Niemantsverdriet, J. W., Van der Kraan, A. M., Van Dijk, W. L., and Van der Baan, H. S., J. Phys. Chem. 84, 3363 (1980).
5. LeCaër, G., Dubois, J. M., Pijolat, M., Perrichon, V., and Bussiere, P., J. Phys. Chem. 86, 4799 (1982).
6. Van der Kraan, A. M. and Niemantsverdriet, J. W., to appear in "Industrial Applications of the Mössbauer Effect," G. J. Long and J. G. Stevens, eds., Plenum, NY (1986).
7. Loktev, S. M., Makarenkova, L. I., Slivinskii, E. V., and Entin, S. D., Kinet. Katal. 13(4), 1042 (1972).
8. Maksimov, Yu. V., Suzdalev, I. P., Arents, R. A., and Loktev, S. M., Kinet. Katal. 15(5), 1293 (1974).
9. Maksimov, Yu. V., Suzdalev, I. P., Arents, R. A., Goncharov, I. V., Kravtsov, A. V., Loktev, S. M., Kinet. Katal. 13(6), 1600 (1972).
10. Vaishnava, P. P., Ktorides, P. I., Montano, P. A., Mbadcam, K. J., and Melson, G. A., J. Catal. 96, 301 (1985).
11. Barton, G. H. and Gale, B., Acta Cryst. 17, 1460 (1964).
12. Hofer, L.J.E., Cohn, E. M., and Peebles, W. C., J. Am. Chem. Soc. 71, 189 (1949).
13. Arents, R. A., Maksimov, Yu. V., Suzdalev, I. P., Imshennik, V. K., and Krupianskiy, Yu. F., Fiz. Met. Metalloved. 36(2), 277 (1973).
14. Le Caër, G., Simon, A., Lorenzo, A., and Genin, J. M., Phys. Stat. Sol. A6, K97 (1971).
15. Mathalone, Z., Ron, M., Pipman, J., and Niedzwiedz, S., J. Appl. Phys. 42(2), 687 (1971).



16. Hofer, L.J.E. and Cohn, E. M., J. Am. Chem. Soc. 81, 1576 (1959).
17. Bernas, H., Campbell, J. A., and Fruchart, R., J. Phys. Chem. Solids 28, 17 (1967).
18. Le Caer, G., Dubois, J. M., and Senateur, J. P., J. Solid State Chem. 19, 19 (1976).
19. Phillips, J., Clausen, B., and Dumesic, J. A., J. Phys. Chem. 81, 1814 (1980).
20. Phillips, J., and Dumesic, J. A., Appl. Surf. Sci. 7, 215 (1981).
21. Phillips, J., Chen, Y., and Dumesic, J. A., in New Surface Science in Catalysis (edited by M. L. Deviney and J. Gland) ACS Symposium Series, (1985).
22. Mørup, S. and Topsøe, H., Appl. Phys. 11, 63 (1976).
23. Mørup, S., Topsøe, H., and Lipka, J., J. Phys. (Paris) Colloq. 37, C6-287 (1978).
24. Wickmann, H. H., "Mössbauer Effect Methodology," Vol. 2, edited by I. J. Gruverman (Plenum, NY, 1966) p. 39.
25. Lin, S. C. and Phillips, J., J. Appl. Phys. 58(5), 1943 (1985).
26. Bradford, E. and Marshall, W., Proc. Phys. Soc. London 87, 731 (1966).
27. Sørensen, K., International Report No. 1, Laboratory of Applied Physics II (Technical University of Denver, 1972).
28. Ron, M., "Applications of Mössbauer Spectroscopy," edited by R. L. Cohen (Academic, NY, 1980), Vol. 2, p. 329.

TABLE I: Comparison of input and fitted Mössbauer parameters for a bulk  $\chi$ -carbide phase.

<u>Parameter</u>	<u>Fe Site</u>	<u>Input Values</u>	<u>Fitted Values</u>
$H_{hf}(kOe)$	I	196.0	196.5
	II	217.0	217.5
	III	118.0	117.5
$\delta_{IS}(mm/sec)$	I	+0.15	+0.149
	II	+0.17	+0.169
	III	+0.15	+0.143
$\Delta E_Q(mm/sec)$	I	0.00	-0.003
	II	+0.027	+0.025
	III	-0.012	-0.021
Relative Intensity	I	3:2:1	3.9:3.2:1.2
	II	3:2:1	4.0:2.1:1.7
	III	1.5:1:0.5	2.0:1.4:0.4
Linewidths (mm/sec)	I	.25:.23:.23	.5:.43:.35
	II	.25:.23:.23	.48:.48:.46
	III	.25:.23:.23	.61:.68:.79

\*Other input parameters were (i) anisotropy energy constant = 1,000,000 erg/cm<sup>3</sup>, (ii) average particle size = 200Å, (iii) temperature = 300 K, (iv)  $\sigma = 1.20$

TABLE II: Mössbauer parameters obtained from a 20-peak fit of the spectra in Figure 1.

<u>Spectrum</u>	<u>Spectral Component</u>	<u>H<sub>hf</sub>(kOe)</u>	<u>δ<sub>IS</sub>(mm/s)</u>	<u>ΔE<sub>Q</sub>(mm/s)</u>	<u>Linewidths (mm/s)</u>	<u>% Area</u>
1a.	X-I	192.3	.146	.020	.57: .62: .67	24.7
	X-II	215.4	.233	.016	.78: .77: .62	24.0
	X-III	106.7	.241	-.027	.61: .62: .61	10.3
	Doublet	---	.157	.590	.76	41.0
1b.	X-I	192.6	.140	.009	.61: .50: .1.4	35.3
	X-II	212.3	.178	.023	.55: .55: .44	28.6
	X-III	110.3	.183	-.019	.72: .88: .51	20.1
	Doublet	---	.152	.533	.60	16.0
1c.	X-I	192.0	.146	-.002	.49: .69: .62	36.6
	X-II	212.4	.165	.027	.57: .53: .1.0	38.8
	X-III	113.9	.162	-.020	.52: .64: .63	19.8
	Doublet	---	.181	.879	.75	4.8

TABLE III: Mössbauer parameters obtained from an 8-peak fit of the spectra in Figure 1 and 2.

<u>Spectrum</u>	<u>Spectral Component</u>	<u>H<sub>hf</sub>(kOe)</u>	<u>δ<sub>IS</sub>(mm/s)</u>	<u>ΔE<sub>Q</sub>(mm/s)</u>	<u>Linewidths (mm/s)</u>	<u>% Area</u>
1a.	Sextuplet	197.7	0.155	0.014	.77: .70:1.6	58.4
	Doublet	---	0.158	0.643	.73	41.6
1b.	Sextuplet	200.4	0.155	0.013	.75: .61:1.7	73.8
	Doublet	---	0.159	0.748	.79	26.2
1c.	Sextuplet	202.0	0.154	0.013	.74: .59:1.0	92.8
	Doublet	---	0.210	1.209	1.40	7.2
2a.	Sextuplet	199.4	0.155	0.013	.75: .69:1.19	55.0
	Doublet	---	0.160	0.681	.73	45.0
2b.	Sextuplet	197.6	0.155	0.014	.78: .61:1.02	79.2
	Doublet	---	0.165	1.594	2.12	20.8
2c.	Sextuplet	198.2	0.157	0.013	.73: .55: .54	91.4
	Doublet	---	0.182	2.300	.692	8.6

#### FIGURE CAPTIONS

- Figure 1. Effect of anisotropy energy constant on spectrum. (a)  $K = 750,000$  erg/cm<sup>3</sup>; (b)  $K = 1,500,000$  erg/cm<sup>3</sup>; (c)  $K = 3,000,000$  erg/cm<sup>3</sup>. Other input parameters were (i) average particle size = 55Å; (ii)  $\sigma = 1.20$ ; (iii)  $T = 300K$ .
- Figure 2. Effect of narrowness of particle size distribution on spectrum. (a)  $\sigma = 1.25$ ; (b)  $\sigma = 1.10$ ; (c)  $\sigma = 1.05$ ; (d) log-normal distribution function for several  $\sigma$  values. Other input parameters were (i) average particle size = 55Å; (ii)  $T = 300K$ ; (iii) anisotropy energy constant = 1,000,000 erg/cm<sup>3</sup>.
- Figure 3. Effect of a variation of  $\epsilon_0$  (equation (3), Ref. 25). (a)  $\epsilon_0 = 0$ ; (b)  $-0.5\epsilon_{\text{Curie}} < \epsilon_0 < 0.5\epsilon_{\text{Curie}}$ ; (c)  $-0.75\epsilon_{\text{Curie}} < \epsilon_0 < 0.75\epsilon_{\text{Curie}}$ . Other input parameters were (i) average particle size = 80Å; (ii)  $\sigma = 1.20$ ; (iii)  $T = 300K$ ; (iv) anisotropy energy constant = 1,000,000.
- Figure 4. Effect of temperature on spectrum. (a)  $T = 350K$ ; (b)  $T = 300K$ ; (c)  $T = 80K$ . Other parameters were (i) average particle size = 55Å; (ii)  $\sigma = 1.20$ ; (iii) anisotropy energy constant = 1,000,000 erg/cm<sup>3</sup>. Values of  $H_{\text{hf}}$  and  $\delta_{\text{IS}}$  were taken from Ref. 25 at each temperature.

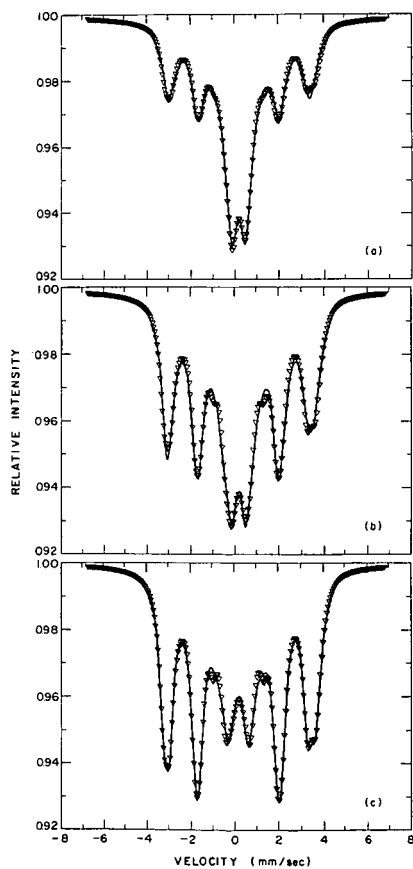


FIGURE 1

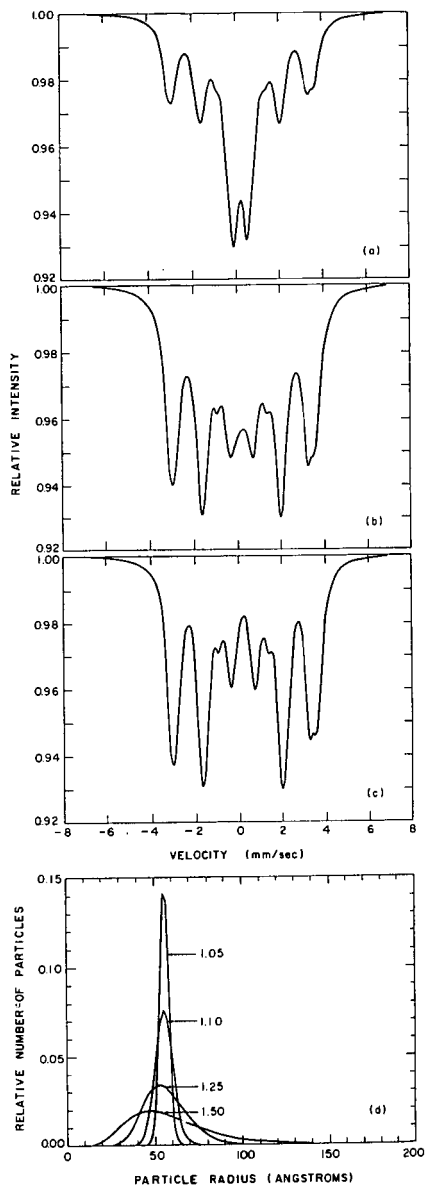


FIGURE 2

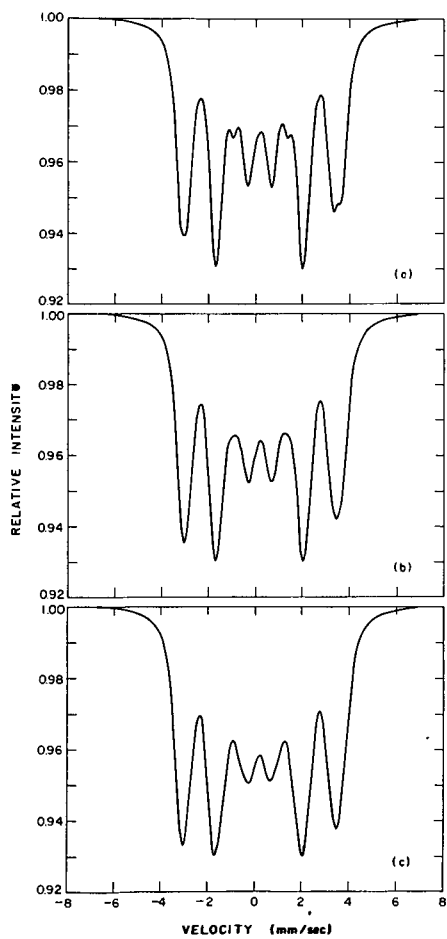


FIGURE 3

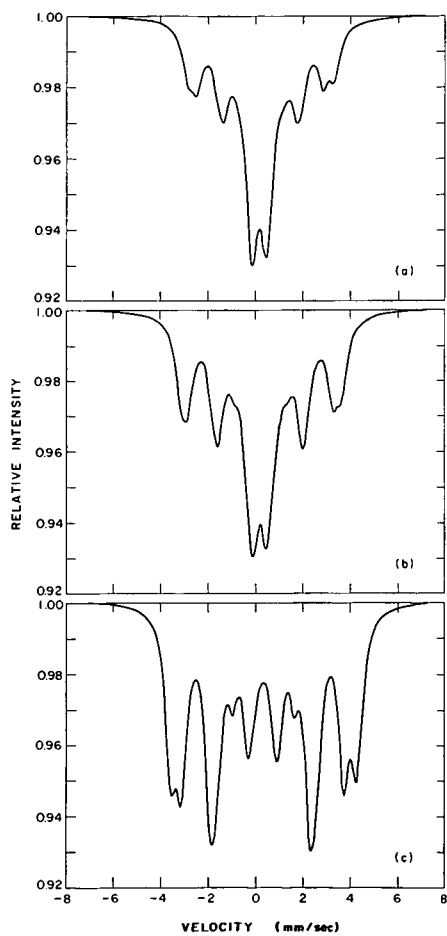


FIGURE 4

## NICKEL CRYSTALLITE THERMOMETRY DURING METHANATION

Douglas K. Ludlow and Timothy S. Cale

Chemical & Bio Engineering Department  
Arizona State University  
Tempe, AZ 85287

### ABSTRACT

A magnetic method to measure the average temperature of superparamagnetic nickel crystallites has been applied during CO methanation. The method takes advantage of the temperature dependence of the low field magnetization of such catalysts; however, the adsorption of carbon monoxide and the formation of surface carbon species complicate the interpretation of results. Calibrations to account for temperature change and the adsorption of reactants are described. The calibration for the effects of CO is based on the assumption that the interaction of CO with nickel is the same for methanation and disproportionation. Interphase heat transfer calculations based on the thermometric data compare favorably with previous results from ethane hydrogenolysis, and give no indication of microscopic temperature differences between the nickel crystallites and support.

### INTRODUCTION

The temperature of the active sites is of fundamental importance for the proper interpretation of catalytic kinetics. This information is not currently obtainable; however, a magnetic method to determine the bed average nickel crystallite temperature during ethane hydrogenolysis has been developed in this laboratory (1,2). This paper presents some early results of an effort to extend this magnetic crystallite thermometry to carbon monoxide methanation over nickel catalysts. This system is being studied because of its history, practical importance, more complicated magnetochemistry and higher heat of reaction.

The basis of nickel crystallite thermometry is the temperature dependence of the intrinsic magnetization, or magnetic moment per volume, of nickel crystallites in superparamagnetic samples (1,2,3). This can be determined from low field magnetization data. In order to perform the magnetic thermometry during ethane hydrogenolysis, ethane is introduced into a stream of hydrogen and helium which is flowing through a short catalyst bed. This initiates the exothermic ethane hydrogenolysis reaction. The sample moment decreases rapidly as the bed average nickel crystallite temperature increases. The relationship between sample moment and average crystallite temperature, determined by calibration, is then applied. In addition, any change in moment due to changes in surface coverage must be accounted for (1,2). One of the principle reasons that ethane hydrogenolysis over nickel was the system chosen to demonstrate the magnetic thermometry is that ethane does not affect the magnetic moment of nickel crystallites when hydrogen is present (4,5). However, the introduction of ethane reduces the hydrogen partial pressure slightly, which does affect moment. The moment change due to hydrogen partial pressure change is accounted for as explained elsewhere (2).

A principle conclusion of the research on ethane hydrogenolysis performed to date is the absence of microscopic nickel crystallite to support gradients. In contrast, Matyi, et. al. (6) present evidence for microscopic catalytic crystallite to support temperature differences for CO hydrogenation over iron. The higher heat of reaction for CO hydrogenation certainly makes these gradients more likely than during ethane hydrogenolysis. The presence of any microscopic gradients would interfere with the interpretation of kinetic information; therefore, it is of interest to pursue catalytic crystallite thermometry during methanation. If they are found to exist, then much of the experimental information on CO hydrogenation will have to be reviewed.



In contrast to the simple magnetochemistry found for the ethane hydrogenolysis system, thermometry during methanation is complicated by the fact that carbon monoxide affects the sample moment (7,8) of supported nickel catalysts in a complicated manner. In fact, an understanding of the interaction between CO and nickel is the primary hurdle to overcome in order to perform magnetic thermometry during methanation.

Adsorption and formation of surface species, as well as changes in crystallite size, have an effect on the net magnetization of a nickel catalyst in a fixed field. Therefore, these must be considered in order to perform accurate crystallite thermometry. There have been numerous studies concerned with the nature and role of surface carbon species (carbon and carbides) that form during methanation (4,7-18). The formation of nickel carbonyls, which leads to catalyst deactivation through metal loss and crystallite size changes, has also been studied (19,20).

Using gravimetric analyses, Gardner and Bartholomew (15) found that there was an initial rapid weight gain for the first few minutes after initiating methanation, followed by a more gradual uptake. They concluded that three forms of surface species are present during methanation: (1) easily desorbed species such as CO, CH<sub>4</sub>, H<sub>2</sub>, etc., (2) species reactive with H<sub>2</sub>, such as atomic carbon and (3) unreactive species. Their results also suggest that the species adsorbed after the initial rapid weight gain corresponds to a nonreactive surface species, such as a polymeric carbon. In addition, the weight gain during the initial stages of rapid adsorption decreased with increasing temperature. McCarty and Wise (21), using temperature-programmed surface reaction (TPSR) studies, also reported the formation of two carbon species,  $\alpha$  and  $\beta$ . These correspond to cases 2 and 3 above, respectively.

The interaction of CO with Ni/SiO<sub>2</sub> catalysts has been studied using saturation magnetization methods by Martin et. al. (13), and Mirodotas, et.al. (17), and by low field magnetization techniques by Kuijpers, et.al. (18). Martin et. al. (13), working with samples containing only small amounts of carbon, concluded that the carbon was interstitially dissolved in the nickel lattice. Mirodotas, et. al. (17) and Kuijpers, et. al. (18), using much higher coverages, concluded that there is bulk carbon dissolution and nickel carbide formation during CO disproportionation, whereas mainly surface carbide formation dominates during methanation. Kuijpers, et. al. (18) also performed static volumetric adsorption analyses between each magnetic measurement. They noted an initial rapid adsorption, followed by a more gradual and linear drop of pressure in their adsorption manifold. The similarity of this result to the observations of Gardner and Bartholomew (15) during methanation is noteworthy. They also noted that the sample magnetization drops to very low levels (up to 90% loss of magnetization) due to bulk carbide formation during disproportionation, whereas the adsorption of hydrogen onto the same samples reduces the relative magnetization by 26% at most.

Since crystallite growth and metal loss would interfere with the magnetic thermometry, it is important to operate in a region where these are minimized. Shen, Dumesic and Hill (19) established a criteria for "safe" operating conditions for methanation over nickel catalysts, where the catalyst no longer deactivated rapidly due to metal loss or particle growth. The criteria is to maintain the equilibrium nickel tetracarbonyl pressure at less than ca.  $7.5 \times 10^{-8}$  Torr. For this work, all experiments were performed in the "safe" operating region. However, because the AC permeameter design currently used can only operate up to a temperature ca. 510 K, conditions were near the "unsafe" operating region. Thus some changes in nickel crystallite size is to be expected. In addition, van Meerten et. al. (20) found nickel crystallite growth during methanation, even though the catalyst was not deactivating dramatically. This indicates a crystallite size dependence on methanation activity. If microscopic crystallite to support temperature gradients exist, then the more active crystallites will be hotter than the less active crystallites. This would further complicate the interpretation of the thermometric results. Conversely, if these gradients do not exist, then a crystallite size effect on activity has little impact on the magnetic thermometry. In that case, the measured temperature is the local temperature of the support and crystallites of all sizes.

## EXPERIMENTAL

A one half gram sample of a 25% nickel on silica catalyst, with an average equivalent spherical diameter of 0.018 cm, was packed into a quartz reactor (22,23) to a bed length of 0.6 cm. The catalyst was from the same batch as the catalysts used in previous crystallite thermometry experiments (1,2). The catalyst sample was reduced in flowing hydrogen at 673 K for 5 hrs and "cleaned" (23) in flowing helium at 723 K for 1/2 hr. Before beginning thermometric experiments, the catalyst was "aged" under reaction conditions until the magnetization no longer changed much. To perform the thermometry, the catalyst sample is initially brought to equilibrium with a flowing stream of hydrogen and helium. The average crystallite temperature is then that of the bulk stream. Reaction is initiated by introducing carbon monoxide at essentially constant total pressure.

An AC permeameter (3,22) is used to follow the changes in magnetic moment of the nickel catalyst sample upon initiation of reaction. The output voltage of the permeameter is related to average catalyst bed temperature via a calibration. Corrections for the change in sample moment due to adsorption and surface species formation are taken into account as described elsewhere in this paper. Reaction products are analyzed using a Carle Analytical gas chromatograph to determine the extent of reaction. Details of the equipment are presented elsewhere (1,2,22). Modifications of the gas handling system which was used for ethane hydrogenolysis were required in order to perform CO methanation. Ultra high purity hydrogen (99.999%, Alphagaz) passes through a palladium Deoxo purifier (Engelhard), a Linde gas purifier column (Model 120: indicating silica gel and molecular sieve), and a 7 micron filter (Nupro) before passing through a Linde mass flowmeter (Model FM 4570). The hydrogen is then mixed with ultra high purity helium (99.999%, Alphagaz) which has similarly passed through a Linde gas purifier column, 7 micron filter, and mass flowmeter. In order to remove remaining components that react with nickel, the hydrogen/helium mixture passes through a  $\text{Ni/SiO}_2$  "guard" reactor at 600 K, as well as another silica gel trap. The gas mixture then flows to a manifold where carbon monoxide can be added to the mixture before entering the reactor. The carbon monoxide (99.3%, Air Products) passes through a 7 micron filter and mass flowmeter before passing through a carbonyl trap, which consists of a column of copper turnings (19,20) heated to 500 K. The carbon monoxide is further purified by passing through an Oxy-Trap (Alltech Associates, Inc., Model 4002) heated at 400 K and an Alltech gas purifier column (Model 8125: indicating silica gel and molecular sieve). The carbon monoxide then passes through a needle valve. A ball valve is used to introduce the carbon monoxide into the hydrogen/helium stream just before the sample reactor.

## RESULTS AND DISCUSSION

An example of the rapid decrease in AC permeameter voltage which occurs upon introducing carbon monoxide into the flowing stream of hydrogen and helium is shown in Figure 1. This corresponds to the decrease in sample moment due to the average crystallite temperature rise as well as to the adsorption of carbon monoxide. After this rapid decrease, the sample signal remains relatively constant. When the reaction is terminated by stopping the carbon monoxide flow, there is a rapid increase in sample moment followed by a more gradual increase in moment which levels off within 5 to 10 minutes. This is also shown in Figure 1.

As with ethane hydrogenolysis, the temperature and adsorption calibrations were performed after an initial aging period, in order to minimize any post calibration changes. In order to monitor catalyst aging, a series of methanation experiments was performed with the  $\text{H}_2/\text{CO}$  ratio kept at 7. Figure 2 shows the decrease in conversion relative to that of the fresh catalyst. The catalyst was left in flowing hydrogen for a period of 16 hours between samples 10 and 11, and for a period of 17 hours between samples 26 and 27. This is taken to account for the higher conversion in run 11; however, there is no corresponding increase between samples 26 and 27. Nevertheless, the activity of the catalyst seems to level off and remain comparatively constant.

The temperature calibration is performed by perturbing the average bed temperature by temporarily removing the catalyst bed from the AC permeameter/oven while flowing hydrogen and helium over the catalyst. After allowing the sample to cool 5 to 10 K, as measured by a thermocouple at the bed exit, the catalyst sample is returned to the optimal sensing location within one of the secondary coils. The AC permeameter signal and exit fluid temperatures are then monitored as the catalyst bed heats. This is repeated several times. The sensitivity (mV/K), determined using least squares regression is assumed constant over the small temperature range considered. As mentioned, this calibration will be affected by changes in crystallite size and by the formation of "permanent" nonmagnetic nickel compounds. Thus, it is important that these do not change significantly between a calibration and the corresponding thermometry experiments.

The calibration procedure used in this study to account for changes in magnetization due to changes in CO uptake takes advantage of the similarity between the uptake results reported during methanation (15) and disproportionation (17,18), discussed previously. The formation of bulk carbide during the CO disproportionation calibration would result in large magnetization decreases and invalidate the procedure; therefore, the possibility of its formation was investigated. Previous studies (17,18) found the formation of bulk carbide during CO disproportionation. However, Mirodatos et. al. (17) using both static and flow experiments, only found bulk carbidization at times greater than 30 minutes for their flow conditions. For experiments in this laboratory, when carbon monoxide is introduced into a helium stream flowing through the catalyst bed, there is a rapid decrease in sample moment, followed by a more gradual decrease in moment, as shown in Figure 3. When disproportionation is allowed to run for longer periods of time, the moment decrease approaches a limiting value after 10 to 15 minutes with a final moment loss of only 6 to 8% of the total sample moment. This relatively small moment loss indicates that no significant amount of bulk carbidization has occurred. When the reaction is terminated, leaving only helium flowing through the catalyst bed, there is a gradual increase in moment which reaches a limiting value after 15 to 20 minutes with a recovery of greater than 90% of the lost moment.

If hydrogen flow is initiated through a catalyst that has previously been exposed to CO disproportionation, there is a rapid increase in sample moment, indicating the removal of a hydrogen reactive surface species. This is in agreement with the results of other laboratories (15,17). There is no discernible change in the sample moment when the hydrogen flow is terminated, leaving only helium flowing. With repeated cycles of 10 minutes of a H<sub>2</sub>/He mixture followed by 20 minutes of pure He flow through the catalyst bed, there is a rapid increase in sample moment after each hydrogen introduction. However, the magnitude of the moment increase declines somewhat with each successive initiation of hydrogen flow. Analysis of the effluent shows that methane is evolved after each hydrogen introduction. Similar results are also obtained for the catalyst after methanation with an H<sub>2</sub>/CO ratio of at least seven. There is no marked difference in the response of the sample moment to the initiation of hydrogen flow after either the methanation or disproportionation experiments. These results indicate the formation of carbon species, during both methanation and disproportionation, all forms of which are not available for reaction with hydrogen, but with which they become available for reaction. This corresponds to the interstitially dissolved carbon reported by other researchers (13,17,18), where the surface carbon is removed by the hydrogen, and is replaced by the migration of the interstitially dissolved carbon.

The use of CO disproportionation for a calibration to account for carbon monoxide adsorption effects is substantiated by these results because: (1) they indicate no significant formation of bulk carbide, at least not in the short time required for the calibrations, and (2) they indicate that there is no significant difference in the carbon formed during both methanation and disproportionation. The results do not preclude the possibility of the formation of the filamentous carbon species reported by other researchers (24-26) during the CO disproportionation calibration. Such filamentous carbon species can deactivate the catalyst, but have no effect on the sample moment (18).

Baseline drift is usual when using an AC permeameter. Therefore for thermometry, we rely on the rapid change in sample moment which occurs within the first 1/2 to 1 minute after introducing carbon monoxide into the hydrogen and helium stream. As mentioned, there is also a rapid decrease in sample moment when carbon monoxide is introduced into a helium stream (see Figure 3). The magnitude of the rapid decrease depends upon the carbon monoxide partial pressure, and is reproducible. This is in apparent agreement with the results of Gardner and Bartholomew (15) and Kuijpers et.al. (18). For calibration purposes, this magnitude is assumed to correspond to the adsorption of carbon monoxide which occurs upon the initiation of methanation. The calibration is performed by introducing carbon monoxide at various partial pressures into helium. The carbon monoxide is allowed to flow only long enough to record the initial rapid decrease in sample moment (2 to 3 minutes). The results were fit to the following equation using least squares regression:

$$\Delta \text{Signal (mV)} = 0.00462 * (P_{\text{CO}} (\text{Torr}))^{0.662} \quad 1)$$

As indicated, with the termination of methanation there is a rapid increase in moment within the first minute after the carbon monoxide flow is stopped, which is followed by a more gradual increase. However, when the carbon monoxide flow is stopped during CO disproportionation there is only a gradual increase in sample moment, as shown in Figure 3. In the absence of a rapid moment change, a time of 60 seconds was arbitrarily chosen to represent the signal increase corresponding to desorption upon reaction termination. Again, the change is reproducible, and dependent upon the carbon monoxide partial pressure present before reaction termination. The results with this choice of time scale is represented by the equation

$$\Delta \text{Signal (mV)} = 0.00071 * (P_{\text{CO}} (\text{Torr}))^{1.05} \quad 2)$$

obtained using least squares regression.

The introduction of carbon monoxide in order to initiate methanation slightly decreases the hydrogen partial pressure, which effects the sample moment. A calibration for the moment change due to hydrogen partial pressure changes is performed by slightly changing the hydrogen partial pressure during reaction. Hydrogen partial pressure affects the reaction rate, however for the small changes that are required for the calibration, the extent of conversion changes at most only 2 to 5%. A small decrease in signal results from a decrease in hydrogen partial pressure. Just the opposite was observed if the hydrogen partial pressure was changed during ethane hydrogenolysis (2). Thus, it seems that the decrease in hydrogen partial pressure leads to an increase in the crystallite surface coverage by carbon, instead of a decrease in surface coverage by hydrogen. The moment change is reproducible and dependent upon the change in hydrogen partial pressure. There is no significant difference in the magnitude of the moment decrease with decreasing partial pressure and the moment increase with an equivalent increase in hydrogen partial pressure. The results are correlated using least squares regression and fit to the equation

$$\Delta \text{Signal (mV)} = 0.00003 (\Delta P_{\text{H}} (\text{Torr}))^{1.27} \quad 3)$$

It is important to note that this effect is one to two orders of magnitude less than that for changes in carbon monoxide partial pressure, and seldom has significance in the thermometry experiments since the hydrogen partial pressure changes only slightly.

The average crystallite temperature rise due to the initiation of methanation is determined by first measuring the magnitude of the signal change upon the initiation of reaction. Signal changes due the increase in CO partial pressure and decrease in hydrogen partial pressure are then subtracted. The result is then divided by the temperature sensitivity (mV/K) to determine the temperature rise.

The validity of the calibration technique was tested by comparing the results of this study with the those for ethane hydrogenolysis. Assuming that no microscopic crystallite to support gradients exist, it is possible to determine the interphase Nusselt number using the described thermometry (1,2,27,28). The average crystallite temperature rise determined from crystallite thermometry is used to calculate the average solid temperature. This information, along with the average bulk fluid temperature rise, and the conversion (heat release) allows the direct

calculation of interphase Nusselt number within the differential reactor assumption. The flow conditions ( $0.3 < Re < 0.6$ ) were not varied enough in this study to determine the functional dependence of the interphase Nusselt number (Nu) on Reynolds number (Re). The interphase Nu was determined for runs for which the catalyst bed was operated under differential conditions, taken as less than 5% conversion. The resulting Nu are scattered uniformly around the results from the previous study using ethane hydrogenolysis (2,27,28). The average Nu determined from the methanation data matches the previously determined relationship. If the results obtained during ethane hydrogenolysis are accepted, then the calibration method used in this work seems valid. Due to the limited Re range covered, these preliminary results are inconclusive, but also indicate the absence of microscopic temperature differences between the crystallite and support. A significantly smaller interphase Nu would be expected if these microscopic temperature differences existed. If this conclusion is correct, then any crystallite size dependence of activity does not interfere with the thermometry.

The possibility of crystallite growth during the initial aging period was investigated. This is not critical to this work, but it is of interest. Samples with larger nickel crystallites exhibit a larger magnetization than those with smaller crystallites, at a fixed field (3). As discussed, the calibrations were performed on the "aged" catalyst. Therefore, the sample moment would be larger than that for the fresh sample, at a given field, if crystallite growth occurred. This assumes that there is no significant loss of nickel. Thus, the fresh catalyst would show smaller magnetization changes than the aged sample for a given temperature change. Therefore, if the temperature calibration performed on the aged sample is applied, a smaller "measured" solid temperature rise is indicated from crystallite thermometry. The average solid temperature rise expected for given flow and conversion data can be estimated using the interphase heat transfer data from the ethane hydrogenolysis study (2,27,28). As discussed above, the interphase heat transfer results using data gathered on the aged catalyst have already been shown to agree with these previous results. Figure 4 shows a plot of the difference between the "measured" solid temperature and the "predicted" temperature during the initial aging period. The results show that initially, the "measured" solid temperatures were much smaller than that predicted. The difference between the measured and predicted temperatures decreased as the catalyst aged. Subsequent data reflects scatter. The crystallite growth inferred from these results is in agreement with the results of van Meerten et. al. (20). Those researchers performed crystallite size estimates as the catalyst aged and found crystallite growth. However, contrary to the results of that laboratory, a significant loss of activity was found in this work. A strong size dependence of activity is not apparent.

### CONCLUSIONS

Nickel crystallite thermometry has been performed during CO methanation. The analysis and calibrations are more complicated than for ethane hydrogenolysis, because of the more complicated magnetochemistry involved. The calibration scheme used to account for CO adsorption and the formation of surface species seems to work satisfactorily. The scheme used is based on results that show no significant formation of bulk carbide during the disproportionation calibration and no significant difference in the carbon species formed during methanation and disproportionation. In addition, interphase Nusselt number estimates are in good agreement with those obtained during ethane hydrogenolysis. However, it would be more satisfying to have a calibration based on methanation, rather than disproportionation.

An alternate calibration scheme in which the methanation rate is decreased while maintaining the same CO adsorption conditions is under development. The approach is to decrease the reaction rate while holding the adsorption/surface carbon species formation effects constant. The effect due to the temperature rise will decrease. Thus, it should be possible to extrapolate to zero rate in order to isolate the moment change due only to adsorption. Preliminary results following

this line of reasoning are inconclusive, and further work is necessary to determine whether such a calibration scheme can be developed.

#### ACKNOWLEDGEMENTS

Financial assistance from the Petroleum Research Fund and the National Science Foundation is gratefully acknowledged.

#### REFERENCES

1. Cale, T. S., and Ludlow, D. K., J. Catal. **86**, 450 (1984).
2. Cale, T. S., J. Catal. **90**, 40 (1984).
3. Selwood, P. W., "Chemisorption and Magnetization" Academic Press, New York, 1975.
4. Martin, G. A., and Imelik, B., Surf. Sci. **42**, 157 (1974).
5. Martin, G. A., Dutarte, R., and Dalmon, J. A., in "Growth of Properties of Metal Clusters", Bourdon, J. (ed.) p. 467, Elsevier, Amsterdam, 1980.
6. Matyi, R. J., Butt, J. B., and Schwartz, L. H., J. Catal. **91**, 185 (1985).
7. Geus, J. W., Nobel, A. P. P., and Zwietering, P., J. Catal. **1**, 8 (1962).
8. Primet, M., Dalmon, J. A., and Martin, G. A., J. Catal. **46**, 25 (1977).
9. Mulay, L. N., Everson, R. C., Mahajan, O. P., and Walker, P. L., Jr., AIP Conf. Proc., **29** (Magn. Magn. Mater., Annu. Conf., 21st), 536 (1975).
10. Farrauto, R. J., J. Catal. **41**, 482 (1976).
11. Wentrock, P. R., Wood, B. J., and Wise, H., J. Catal. **43**, 363 (1976).
12. Martin, G. A., Dalmon, J. A., and Primet, M., C. R. Hebd. Seances. Acad. Sci. Ser. C **284**(4), 163 (1977).
13. Martin, G. A., Primet, M., and Dalmon, J. A., J. Catal. **53**, 321 (1978).
14. Falconer, J. L., and Zagli, A. E., J. Catal. **62**, 280 (1980).
15. Gardner, D. C., and Bartholomew, C. H., Ind. Eng. Chem. Fundam. **20**, 229 (1981).
16. Kuijpers, E. G. M., Breedijk, A. K., van der Wal, W. J. J., and Geus, J. W., J. Catal. **81**, 429 (1983).
17. Mirodatos, C., Dalmon, J. A., and Martin, G. A., Stud. Surf. Sci. Catal. **19**, 505 (1984).
18. Kuijpers, E. G. M., Kock, A. J. H. M., Nieuwesteeg, M. W. C. M. A., and Geus, J. W., J. Catal. **95**, 13 (1985).
19. Shen, W. M., Dumesic, J. A., and Hill, C. G., Jr., J. Catal. **68**, 152 (1981).
20. van Meerten, R. Z. C., Beaumont, A. H. G. M., van Nisselrooij, P. F. M. T., and Coenen, J. W. E., Surf. Sci. **135**, 565 (1983).
21. McCarty, J. C., and Wise, H., J. Catal. **57**, 406 (1979).
22. Cale, T. S., and Ludlow, D. K., Anal. Instrum. **13**(2), 183 (1984).
23. Cale, T. S., and Richardson, J. T., J. Catal. **79**, 378 (1983).
24. Rostrup-Nielsen, J. R., J. Catal. **27**, 343 (1972).
25. Tøttrup, P. B., J. Catal. **29**, (1976).
26. Gardner, D. C., and Bartholomew, C. H., Ind. Eng. Chem. Prod. Res. Dev. **20**, 80 (1981).
27. Lawson, J. M., Ludlow, D. K., and Cale, T. S., Proceedings IASTED International Conference, AIMS '84, 26 (1984).
28. Cale, T. S., and Lawson, J. M., Chem. Eng. Commun. **39**, 241 (1985).

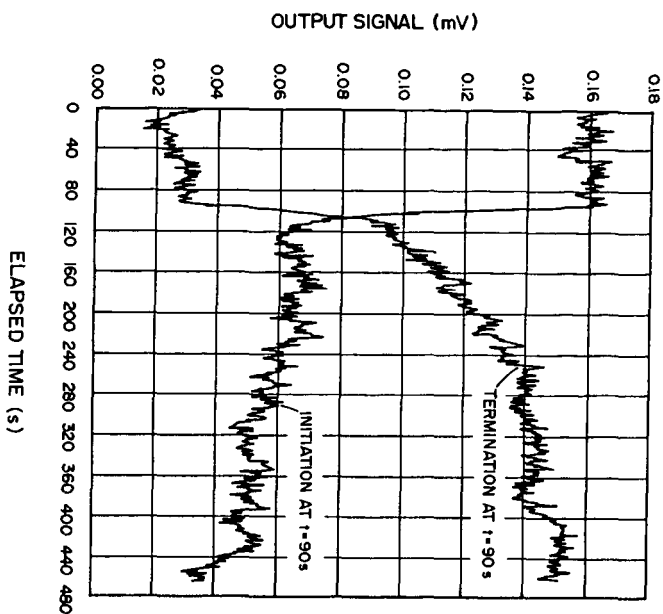


Figure 1. Examples of the changes in AC permeameter output voltage that occur upon the initiation and termination of CO methanation.

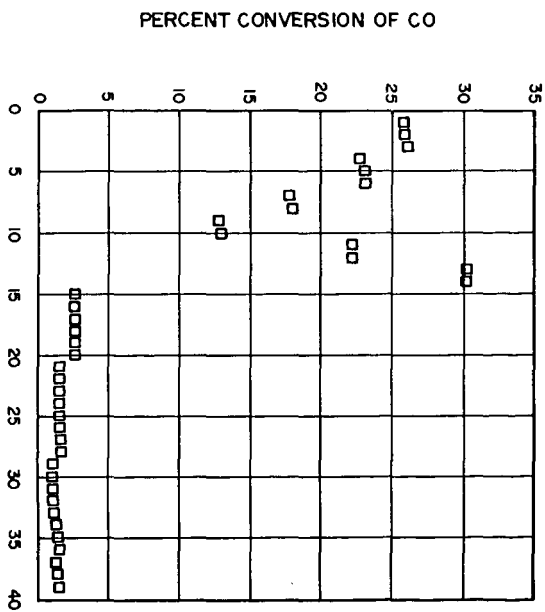


Figure 2. Conversion data during initial aging period. The  $H_2/CO$  ratio is seven. The catalyst was left in flowing hydrogen for 16 and 17 hours between samples 10-11 and 26-27, respectively.

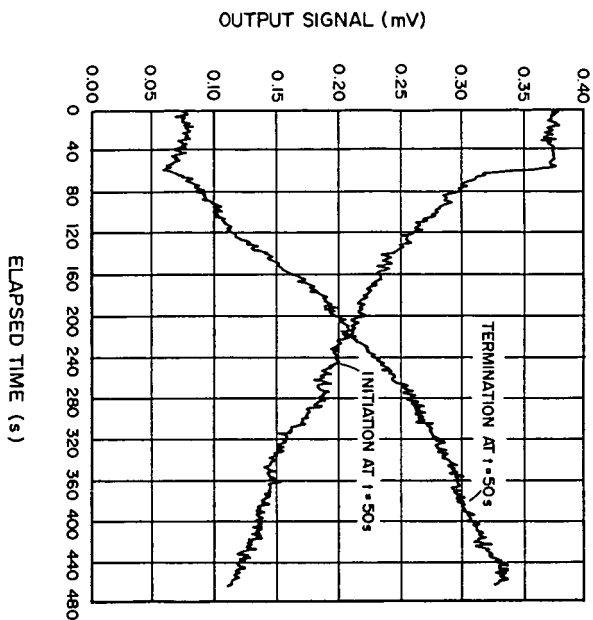


Figure 3. Examples of the changes in AC permeameter output voltage that occur upon the initiation and termination of CO disproportionation. (See text for explanation.)

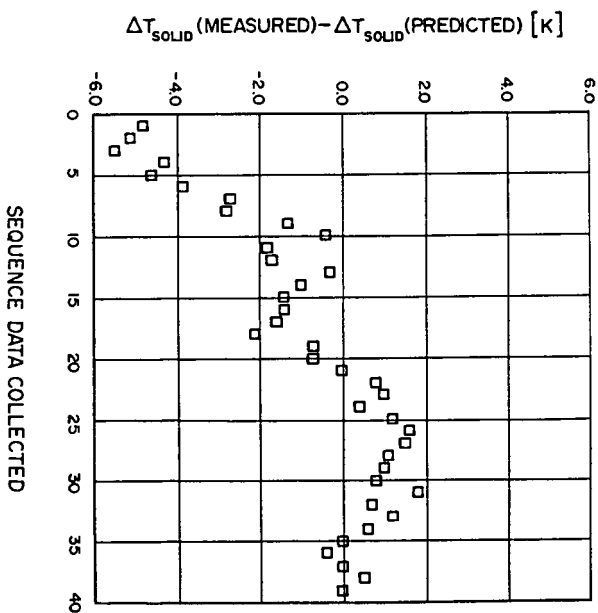


Figure 4. Difference in the "predicted" and "measured" solid temperature rise during initial aging period. (See text for explanation.)



## SUPPORTED MOLECULAR CATALYSTS FOR CO HYDROGENATION

H. Henry Lamb and B. C. Gates

Center for Catalytic Science and Technology  
Department of Chemical Engineering  
University of Delaware  
Newark, DE 19711

### INTRODUCTION

The metal-oxide support is known to exert a strong influence on the activity and selectivity of heterogeneous CO hydrogenation catalysts (1). Ichikawa demonstrated that catalysts derived from  $[\text{Rh}_4(\text{CO})_{12}]$  deposited on basic MgO produced methanol from  $\text{CO} + \text{H}_2$  with >95% selectivity, whereas  $[\text{Rh}_4(\text{CO})_{12}]$ -derived catalysts supported on more acidic metal oxides such as  $\gamma\text{-Al}_2\text{O}_3$  and  $\text{SiO}_2$  produced chiefly methane with only traces of oxygenated products being formed (2). Only limited data is currently available relating these differences in catalytic performance to differences in catalyst structure (3). However, it was recently demonstrated that under high-temperature CO hydrogenation conditions (275°C, 10 atm) anionic osmium carbonyl clusters (e.g.,  $[\text{Os}_{10}\text{C}(\text{CO})_{24}]^{2-}$ ) are formed on MgO from adsorbed  $[\text{H}_2\text{Os}(\text{CO})_4]$  (4). This finding is in contrast to the cluster fragmentation and  $\text{Os(II)}$  subcarbonyl formation observed under similar conditions for osmium clusters adsorbed on  $\gamma\text{-Al}_2\text{O}_3$  and  $\text{SiO}_2$  (5); the nature of the support dictates the surface organometallic chemistry.

Here we present the results of an investigation confirming the presence of  $[\text{Os}_{10}\text{C}(\text{CO})_{24}]^{2-}$  on the surfaces of conventional MgO-supported CO hydrogenation catalysts prepared by aqueous impregnation with  $[\text{H}_2\text{OsCl}_6]$  (6). The carbido carbonyl cluster is synthesized in high yield from  $\text{Os(IV)}$  on MgO exposed to CO hydrogenation conditions.

### EXPERIMENTAL

The MgO support (MX-65-1 powder, MCB reagents) was contacted with an aqueous solution of  $[\text{H}_2\text{OsCl}_6]$  having sufficient volume (~2 ml/g) to yield a heavy paste. The material was dried at 70°C in vacuum, and the resultant light-blue powder was analyzed by X-ray fluorescence (XRF) spectroscopy and found to contain 1.3 wt % Os.

Samples (0.30 g) of MgO impregnated with  $[\text{H}_2\text{OsCl}_6]$  were treated with  $\text{H}_2$  or a  $\text{H}_2 + \text{CO}$  mixture in a tubular flow reactor. The samples were thoroughly dried by pretreatment in flowing He for 1 h at 150°C. Conventional Os/MgO catalysts (7) resulted from reduction with  $\text{H}_2$  at 275°C and 1 atm for 10 h. These catalysts were subsequently exposed *in-situ* to  $\text{H}_2 + \text{CO}$  (equimolar) at 275°C and 1 or 10 atm for 8 h. A sample of  $[\text{H}_2\text{OsCl}_6]$  and MgO was treated directly with  $\text{H}_2 + \text{CO}$  (equimolar) at 275°C and 1 atm for 5 h. In each case the sealed reactor tube was unloaded in a dry box. The  $\text{H}_2$ -reduced materials were metallic gray after exposure to CO hydrogenation conditions; the sample exposed directly to  $\text{H}_2 + \text{CO}$  was reddish-pink. The gases employed were Matheson UHP grade and were further purified by passage over activated 5A molecular sieve and supported  $\text{Cu}_2\text{O}$  ( $\text{H}_2$  and He only).

$[\text{Et}_4\text{N}]_2[\text{Os}_{10}\text{C}(\text{CO})_{24}]$  was synthesized following the procedure of Hayward and Shapley (8). The metal cluster was adsorbed on MgO (pretreated in vacuum at 400°C) from dry tetrahydrofuran (THF) solution. The resultant reddish-pink solid was recovered by filtration, washed with fresh THF, and dried in flowing nitrogen.

Acetone solutions of  $[\text{PPN}][\text{Cl}]$  ( $\text{PPN}^+ = \text{N}(\text{PPh}_3)_2^+$ ) were used to extract  $[\text{Os}_{10}\text{C}(\text{CO})_{24}]^{2-}$  from the catalyst surfaces by ion exchange.  $[\text{PPN}]_2[\text{Os}_{10}\text{C}(\text{CO})_{24}]$  in the extract solutions was detected by infrared spectroscopy.

Infrared spectra were obtained with a Nicolet 7199 Fourier transform spectrometer. Powders were pressed, forming self-supporting wafers which were loaded (without exposure to air) into a leak-tight glass cell fitted with NaCl windows. The thermostated cell could be connected to a manifold for evacuation or gas treatments.

Ultraviolet-visible spectra of powders under  $N_2$  were recorded with a Cary 219 spectrophotometer equipped with a diffuse reflectance attachment.

Extended X-ray absorption fine structure (EXAFS) measurements were conducted at the Cornell High Energy Synchrotron Source (CHESS).  $[Os_{10}C(CO)_{24}]^{2-}/MgO$  formed by the  $H_2 + CO$  reduction of Os(IV) on MgO and a sample of  $[Et_4N]_2[Os_{10}C(CO)_{24}]$  and MgO were examined.

#### RESULTS AND DISCUSSION

In the presence of CO or an equimolar mixture of  $H_2 + CO$  at 275°C and 1 atm, Os(IV) on MgO is reduced and carbonylated to yield  $[Os_{10}C(CO)_{24}]^{2-}$  ionically bound to the MgO surface. The formation of  $[Os_{10}C(CO)_{24}]^{2-}$  under these conditions has been confirmed by IR, UV-Vis, and EXAFS spectroscopies, in addition to the isolation of  $[PPN]_2[Os_{10}C(CO)_{24}]$  from the surface by cation metathesis with  $[PPN][Cl]$  in acetone.

Treatment of MgO impregnated with  $[H_2OsCl_6]$  in  $H_2 + CO$  (equimolar) at 275°C and 1 atm for 5 h in a flow reactor, resulted in a change in color of the solid from light blue to reddish pink, indicative of the formation of  $[Os_{10}C(CO)_{24}]^{2-}$ . The UV-Vis diffuse reflectance spectrum (200-800 nm) of the product is in excellent agreement with that of  $[Et_4N]_2[Os_{10}C(CO)_{24}]$  deposited on MgO from THF. Extraction of a portion of the material with  $[PPN][Cl]$  in acetone resulted in a white solid and a brownish-red solution. The infrared spectrum of the solution contains only strong bands assigned to  $[PPN]_2[Os_{10}C(CO)_{24}]$  (Table 1).

The synthesis of  $[Os_{10}C(CO)_{24}]^{2-}$  on the MgO surface was also monitored by in-situ infrared spectroscopy. Slowly heating a wafer of  $[H_2OsCl_6]$  and MgO to 275°C in flowing  $H_2 + CO$  at atmospheric pressure, first produced Os(II) subcarbonyls ( $\nu_{CO} = 2105(m), 2030(s), 1936(s) \text{ cm}^{-1}$ ) on MgO (9). However, near 275°C there was a dramatic increase in absorption in the carbonyl stretching region, and after 1.5 h under these conditions strong bands assigned to  $[Os_{10}C(CO)_{24}]^{2-}/MgO$  (Table 1) were present. A similar experiment conducted using pure CO instead of  $H_2 + CO$  also resulted in the formation of the carbido carbonyl cluster in high yield.

TABLE 1

Molecular Cluster	$\nu_{CO} \text{ (cm}^{-1}\text{)}$	Ref.
$[PPN]_2[Os_{10}C(CO)_{24}]$	2034(s), 1992(s) (acetone)	(8)
$[Et_4N]_2[Os_{10}C(CO)_{24}]$ and MgO	2079(vw), 2062(w), 2030(s), 1998(sh), 1986(sh), 1975(vs), 1966(sh)	This work
$[Os_{10}C(CO)_{24}]^{2-}$ from Os(IV) on MgO	2104(vw), 2080(w), 2040(s), 1998(sh) 1989(s), 1979(sh), 1963(sh)	This work

Confirmation of the identity of the surface species was obtained from EXAFS spectroscopy. The reduction and carbonylation were again effected in-situ and comparison made to the spectrum of  $[Et_4N]_2[Os_{10}C(CO)_{24}]$  deposited on MgO. Close agreement was found for the EXAFS oscillations above the Os  $L_{III}$  edge over the range of the wavevector from  $k = 3$  to  $12 \text{ \AA}^{-1}$ . A final structure determination awaits detailed analysis of the data.

Even reduction of MgO impregnated with  $[H_2OsCl_6]$  with  $H_2$  to yield supported Os aggregates (7) did not completely inhibit the formation of  $[Os_{10}C(CO)_{24}]^{2-}$ . The highly stable molecular cluster was isolated in low yields by ion exchange of  $H_2$ -reduced samples exposed to  $H_2 + CO$  at 275°C and 1 or 10 atm for 8 h. The presence of the cluster in the lightly colored extract solutions was confirmed by infrared spectroscopy. In addition, Deeba *et al.* have reported that MgO-supported catalysts derived from the decomposition of adsorbed  $Os_3(CO)_{12}$  gave evidence for the presence of molecular clusters following use in CO hydrogenation to produce  $C_1$ - $C_4$  hydrocarbons at 300°C and 7 atm (10). Comparing the infrared data reported for their used catalysts ( $\nu_{CO}$  = 2080(m), 2048(sh), 2039(s), 2010(sh), 1986(vs), 1950(sh)  $cm^{-1}$ ), with those of  $[Os_{10}C(CO)_{24}]^{2-}/MgO$ , we infer that this molecular cluster was formed on these catalysts as well.

In summary,  $[Os_{10}C(CO)_{24}]^{2-}$  represents an extremely stable molecular structure on the surfaces of Os/MgO CO hydrogenation catalysts. The basicity of the MgO support appears to be essential; analogous structures do not form on the more acidic  $\gamma$ - $Al_2O_3$  and  $SiO_2$  surfaces (4), and the surface-mediated synthesis of  $[Os_{10}C(CO)_{24}]^{2-}$  parallels the syntheses of high-nuclearity Group VIII - metal clusters in basic solution (11). What direct role this metal cluster has in the catalysis remains to be elucidated.

#### ACKNOWLEDGEMENT

The authors wish to acknowledge Dr. D. C. Koningsherger for his valuable assistance in the EXAFS measurements. This work was supported by the National Science Foundation (grant CPE8218311) and the Exxon Education Foundation.

#### REFERENCES

- (1) Katzer, J. R., Sleight, A. W., Gajardo, P., Michel, J. P., Gleason, E. F., and McMillan, S., *Fara. Disc.*, **72**, 121 (1981).
- (2) Ichikawa, M., *Bull. Chem. Soc. Jpn.*, **51**, 2268 (1978).
- (3) (a) Solymosi, F., Tombácz, I., and Kocsis, M., *J. Catal.*, **75**, 78 (1982);  
(b) Erdöhelyi, A. and Solymosi, F., *J. Catal.*, **84**, 446 (1983).
- (4) Lamb, H. B. and Gates, B. C. *J. Am. Chem. Soc.*, **108**, 81 (1986).
- (5) Eds., Gates, B. C., Guzzi, L., and Knözinger, H., "Metal Clusters in Catalysis," Elsevier, Amsterdam, in press.
- (6) Lamb, H. B., Krause, T. R., and Gates, B. C., *J. Chem. Soc., Chem. Commun.*, in press.
- (7) Odebunmi, E. O., Matrana, B. A., Datye, A. K., Allard, L. F., Jr., Schwank, J., Manogue, W. B., Hayman, A., Onuferko, J. B., Knözinger, H., and Gates, B. C., *J. Catal.*, **95**, 370 (1985).
- (8) Hayward, T. C. and Shapley, J. R., *Inorg. Chem.*, **21**, 3816 (1982).
- (9) Psaro, R., Dossi, C., and Ugo, R., *J. Mol. Catal.*, **21**, 331 (1983).
- (10) Deeba, M., Scott, J. P., Barth, R., and Gates, B. C., *J. Catal.*, **71**, 373 (1981).
- (11) Chini, P., Longoni, G., and Albano, V. G., *Adv. Organomet. Chem.*, **14**, 285 (1976).

## Methanation and HDS Catalysts Based on Sulfided, Bimetallic Clusters

M. David Curtis, Johannes Schwank, Levi Thompson,  
P. Douglas Williams, and Oswaldo Baralt

Departments of Chemistry and Chemical Engineering,  
The University of Michigan, Ann Arbor, MI 48109

### INTRODUCTION

Environmental concerns have led to an increased interest in hydrotreating catalysts, i.e. catalysts for hydrodesulfurization (HDS) or hydrodenitrogenation (HDN) (1-3). Although HDS may be catalyzed by bulk or supported  $\text{MoS}_2$  and related sulfides, the most effective catalysts are those derived from "sulfided cobalt molybdate" supported on  $\text{Al}_2\text{O}_3$ . These catalysts are prepared conventionally by impregnating the alumina support with solutions of molybdate ions and cobaltous ions. The impregnated support is then calcined to convert the adsorbed species to their respective oxides. The supported metal oxides are then converted to sulfides ("sulfided") with a mixture of  $\text{H}_2$  and  $\text{H}_2\text{S}$  (or the feed stream itself) at temperatures in the range 300-400°C. Alternate promoters, e.g. Ni and Fe, may be used in the place of Co, but the resulting catalysts usually show a lower activity.

Despite intensive study, the exact nature of the active "CoMoS" phase is still uncertain, and hence the role of the Co promoter and the exact mechanism of HDS remain obscure. XPS and Mössbauer Emission Spectroscopy has been used to show that a "CoMoS" phase, distinct from  $\text{Co}_9\text{S}_8$  or  $\text{MoS}_2$ , is present and that the activity of the catalyst parallels the amount of this CoMoS phase present (4).

More recently, EXAFS has been used to study these cobalt molybdate catalysts in both the oxidized and sulfided states (5-11). The most popular model has Co-atoms coordinated to sulfur at the edges of basal planes of small (10-30Å) crystallites of  $\text{MoS}_2$  (see Figure 1). The EXAFS results also are best fit by assuming the  $\text{MoS}_2$  rafts are essentially two dimensional.

The promoter metal, Co or Ni, is intimately involved in the active site. The activities of the promoted  $\text{MoS}_2$  can be  $10^2$  that of unpromoted  $\text{MoS}_2$ , usually with the Co/Mo ratio  $\approx 1.0$  (12). It is therefore surprising that Co-Mo vectors have never been identified in the EXAFS studies of these catalysts. Therefore, the location of the Co relative to the Mo in these CoMoS catalysts is still uncertain. New approaches are necessary to probe the nature of the active site of these sulfided catalysts.

### MOLECULAR MODELS OF PROMOTED $\text{MoS}_2$ PHASES

We have prepared discrete, molecular clusters which may serve as models for the active sites in promoted molybdenum sulfide catalysts (13-15). These clusters are composed of one metal each from the sets, {Mo,W} and {Fe,Co,Ni}; they contain sulfur in the cluster framework and organic ligands, e.g. carbonyls, cyclopentadienyls (Cp), etc. on the periphery of the cluster. The structures of representative clusters are shown in Figure 2.

These clusters have been deposited on oxide supports by dissolving the molecular cluster in an appropriate solvent, e.g.  $\text{CH}_2\text{Cl}_2$ , and then adding the calcined support. With the low loadings (1% total

metal) employed in this study, the clusters are quantitatively adsorbed onto the support from solution. The solvent is then removed and the solid dried under vacuum. The supported clusters are then subjected to temperature-programmed decomposition (TPDE) in a stream of  $H_2$  or He. The exit gas stream is analyzed for  $CO$ ,  $CO_2$ , hydrocarbons, etc. by GC and GC/MS. Figure 3 shows a typical TPDE curve for the  $MoFeS$  cluster, 1, (Figure 2).

In the TPDE of cluster 1 on  $\gamma-Al_2O_3$ , ca. 5  $CO$  per cluster are lost at  $100^\circ C$ , and heating to  $400^\circ C$  causes gradual loss of one additional  $CO$ /cluster. In addition, small quantities of  $Me_2S$ ,  $CH_4$ , and  $CO_2$  are lost between  $150^\circ C$  and  $400^\circ C$ . The average composition of the remaining surface species is found to be  $C_5Mo_2Fe_2S_{1.8}O_xH_y$  (the oxygen and hydrogen are uncertain since surface  $OH$  groups may contribute to the formation of  $CO_2$ ,  $CH_4$ , etc.). Similar results are obtained for all the clusters investigated. The high carbon retention observed even with TPDE in flowing  $H_2$  is attributed to carbide formation.

The facile loss of  $CO$  by the supported cluster stands in contrast to the thermal stability of the pure compound which is stable to  $>250^\circ C$ . Therefore, there must be a strong support-cluster interaction which facilitates loss of  $CO$  from the adsorbed cluster.

Figure 4 shows the IR spectrum of pure cluster 1 and spectra of the cluster adsorbed on  $\gamma-Al_2O_3$ . The bridging  $CO$  band at  $1795\text{ cm}^{-1}$  is most strongly perturbed, suggesting that the cluster is bound to a Lewis acid site (e.g.  $Al^{+3}$ ) on the surface through the bridging  $CO$ , normally the most basic  $CO$  on the cluster (16). As the adsorbed cluster is heated to  $110^\circ C$ , the intensities of the  $CO$  bands diminish and finally disappear as the  $CO$  is lost. No new  $CO$  peaks are observed during the TPDE and no new  $CO$  bands appear if the decarbonylated cluster is placed in an atm. of  $CO$  at  $25^\circ C$ . Since the TPDE shows the loss of only 5 of the 8  $CO$ -groups under these conditions, the remaining 3  $CO$ 's must be either dissociatively adsorbed or must be bonded in a multi-hapto manner with very low frequency  $CO$ -stretching vibrations.

The Mössbauer parameters (Table 1) suggest that the Fe in the cluster is oxidized during TPDE from  $Fe^0$  to  $Fe^{+3}$ .

Table 1. Mössbauer Spectral Parameters ( $\text{mms}^{-1}$ )

	Pure <u>1</u>	<u>MoFeSA-01</u> *	Used Cat.
I.S.	-0.01	0.38	0.43
$\Delta E_Q$	0.78	0.84	0.84

\*1% loading of cluster 1 on  $\gamma-Al_2O_3$

#### METHANATION CATALYSIS

Clusters 1 and 3 (1% total metal loading) on  $\gamma-Al_2O_3$  were pre-treated in flowing  $H_2$  (1 atm.) at  $400^\circ C$  for 6-12 hr. The resulting catalysts are labelled MoFeSA-01 and MoCoSA-01. The methanation activity of these catalysts was determined in the temperature range  $250^\circ$ - $500^\circ C$  with total pressures from 30 psi to 300 psi. The feed stream composition was 3:1 or 1:1  $H_2:CO$ . A differential flow reactor

with GHSV  $\approx 2500 \text{ hr}^{-1}$  and CO conversions  $\leq 2\%$  was employed for kinetic measurements.

A break-in period of several hours was observed during which time the methanation activity was nearly zero. Methane then appears and the activity goes through a peak and then reaches steady state behavior which remains constant for days if the temperature is  $\geq 300^\circ\text{C}$ . At lower temperatures, a very gradual decrease in activity, presumably due to coking, was observed.

Arrhenius plots of the formal turnover frequency,  $N_f$ , vs.  $1/T$  are shown in Figure 5 ( $N_f$  is defined as moles of  $\text{CH}_4$ /mole of cluster precursor/sec). Apparent activation energies are approximately 22 kcal/mol for MoCoSA-01 and 26 kcal/mol for MoFeSA-01.

The methanation reaction over MoFeSA-01 seems to follow Langmuir-Hinshelwood kinetics with the rate expression ( $T = 300^\circ\text{C}$ ,  $P$  in psi.):

$$N_f (\text{s}^{-1}) = \frac{(4.0 \times 10^{-6}) P_{\text{H}_2} P_{\text{CO}}}{\{1 + (0.018 P_{\text{H}_2})^{1/2} + 0.143 P_{\text{CO}}\}^2}$$

This rate law is consistent with a CO dissociative mechanism in which  $\text{CH}(\text{ads.}) + \text{H}(\text{ads.}) \rightarrow \text{CH}_2(\text{ads.})$  is the rate limiting step and all previous steps are in steady-state equilibrium.

The product distributions are plotted in Figure 6 for MoFeSA-01 and MoCoSA-01 under typical conditions. Selectivity for methane ranges from 90-98% depending on the temperature and pressure. Higher temperatures and lower pressures favor methane formation. Small amounts of  $\text{C}_2$  and  $\text{C}_3$  alkanes and olefins are formed, the latter are in greater abundance with the MoCoSA-01 catalyst. At higher pressures, dimethyl ether constitutes 2-4 mole % of the product stream, but methanol has never been detected.

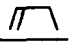



It should be pointed out that the selectivities of MoFeSA-01 and MoCoSA-01 differ from  $\text{Mo}/\text{Al}_2\text{O}_3$ ,  $\text{MoS}_2$ ,  $\text{Fe}/\text{Al}_2\text{O}_3$  or  $\text{Co}/\text{Al}_2\text{O}_3$  which all produce less  $\text{CH}_4$  and more  $\text{C}_2$ - $\text{C}_5$  hydrocarbons in a Schultz-Flory distribution. This result suggests that the clusters are not fragmenting and re-aggregating into larger metal (or metal sulfide) crystallites. After reaction, SEM and STEM also failed to reveal any particles  $>10\text{\AA}$ , the resolving power of the microscope under the conditions used. The Fe I.S. (Table 1) increases somewhat after time on stream, possibly indicating that Fe(III) is being reduced somewhat.

#### HDS CATALYSIS

The activity of MoFeSA-01 and MoCoSA-01 toward catalysis of thiophene HDS has been determined in a differential flow reactor at GHSV  $\approx 3000 \text{ hr}^{-1}$  and thiophene conversions of 1-2% (conditions: 2.8 mol % thiophene in 1 atm.  $\text{H}_2$  at  $250^\circ\text{C}$ - $350^\circ\text{C}$ ). The catalysts were reduced in  $\text{H}_2$  at  $400^\circ\text{C}$  and then presulfided with  $\text{H}_2\text{S}/\text{H}_2$  or directly with the thiophene/ $\text{H}_2$  feed stream. No difference in catalytic behavior due to the different pretreatments was observed. Catalytic activity was immediately established, in contrast to the methanation activity. Steady state selectivity was observed after 1 hr. on stream and no diminution of catalytic activity was observed after 3-4 days of operation.

Figure 7 is an Arrhenius plot of the formal turnover frequencies (moles converted/mole cluster/sec) for total thiophene conversion and for C<sub>4</sub> and C<sub>3</sub> products. Table 2 compares turnover frequencies and product slates of a clean Mo (100) surface, several cobalt molybdate catalysts with high metal loading, and the MoFeSA-01 and MoCoSA-01 (1% total metal loading) catalysts described above.

Table 2. Comparison of Activities and Selectivities of Various Catalysts for Thiophene HDS.

catalyst	N <sub>f</sub> (sec <sup>-1</sup> )	T°C	BuH				
Mo(100) <sup>a</sup>	.02-.12	340	8	53	14	19	-
Mo14-Co4 <sup>b,c</sup>	0.05	420	-	NOT GIVEN			
Mo8-Co3 <sup>d</sup>	0.03	?		"butenes"			
Mo13-Co7 <sup>e</sup>	0.05	290	10	-	29	62	-
MoCoSA-01	0.04	340	1	14	17	26	41
MoFeSA-01	0.01	340	2	13	18	25	41
				(11)	(19)	(27) <sup>f</sup>	

a) J. Catal. 1984, 88, 546. Butadiene (6%) also formed.

b) numbers refer to %Mo and %Co on γ-Al<sub>2</sub>O<sub>3</sub>.

c) J. Catal. 1984, 87, 292.

d) ibid. 1984, 85, 44.

e) ibid. 1984, 86, 55.

f) equilibrium ratios of butenes.

Two features are especially noteworthy. First, the activity of the MoCoSA-01 catalyst is comparable to catalysts with much higher metal loadings when compared on a per mol of Mo basis. This is unusual for HDS catalysts because the first few % of metal occupies tetrahedral holes in the Al<sub>2</sub>O<sub>3</sub> lattice and is not converted to sulfides during the sulfiding step in conventional HDS catalysts.

Second, the cluster catalysts produce a large fraction of propene. Thus a carbon-carbon bond has been totally cleaved by hydrogenolysis. To our knowledge, C-C bond hydrogenolysis without C=C bond hydrogenation is unprecedented. Methane and 1-5% C<sub>2</sub> hydrocarbons (mostly C<sub>2</sub>H<sub>4</sub>) are also produced, but technical difficulties have precluded our quantifying the methane. Presumably, the amount of methane is equal to the amount of propene.

## CONCLUSIONS

Sulfided bimetallic clusters of early and late transition metals have been shown to be precursors for methanation and HDS catalysts when supported on Al<sub>2</sub>O<sub>3</sub>. The activities and selectivities in CO hydrogenation closely resembles other metals in very highly dispersed states on Al<sub>2</sub>O<sub>3</sub>. Thus, stable metal clusters are not likely to be useful Fischer-Tropsch catalyst precursors.

However, these cluster species are exceptionally active in thiophene HDS and exhibit an unprecedented selectivity. Catalysts capable of simultaneously removing sulfur and cracking large molecules into smaller unsaturated fragments at relatively low temperatures could be especially useful for producing clean, low viscosity fluids from still bottoms and heavy coal liquids.

## References

1. Wen, C.-Y.; Lee, E. S. "Coal Conversion Technology", Addison-Wesley, Reading, MA, 1979.
2. Cusumano, J. A.; Dalla Betta, R. A.; Levy, R. B. "Catalysts in Coal Conversion", Academic Press, New York, NY, 1978.
3. Grange, P. Catal. Rev. **1980**, 21, 135.
4. Alstrup, I.; Chorkendorff, I.; Candia, R.; Clausen, B. S.; Topsoe, H. J. Catal. **1982**, 77, 397.
5. Boudart, M.; Arrieta, J. S.; Dalla Betta, R. A. J. Am. Chem. Soc. **1983**, 105, 6501.
6. Clausen, B. S.; Topsoe, H.; Candia, R.; Villadsen, J.; Langeler, B.; Als-Nielsen, J.; Christensen, F. J. Phys. Chem. **1981**, 85, 3868.
7. Clausen, B. S.; Langeler, B.; Candia, R.; Als-Nielsen, J.; Topsoe, H. Bull. Soc. Chim. Belg. **1981**, 90, 1249.
8. Parham, T. G.; Merrill, R. P. J. Catal. **1984**, 85, 295.
9. Chiu, N.-S.; Bauer, S. H.; Johnson, M. F. L. J. Catal. **1984**, 89, 226.
10. Clausen, B.; Topsoe, H.; Candia, R.; Langeler, B. Springer Proc. Phys. **1984**, 2, 181.
11. Boudart, M.; Dalla Betta, R. A.; Foger, K.; Loffler, D. G. Springer Proc. Phys. **1984**, 2, 187.
12. Chianelli, R. R.; Pecoraro, T. A.; Halbert, T. R.; Pan, W.-H.; Stiefel, E. I. J. Catal. **1984**, 86, 226.
13. Curtis, M. D.; Williams, P. D. Inorg. Chem. **1983**, 19, 2661.
14. Williams, P. D.; Curtis, M. D.; Duffy, D. N.; Butler, W. M. Organometallics **1983**, 2, 165.
15. Curtis, M. D.; LaBarge, W. Unpublished results, 1985.
16. Horwitz, C. P.; Shriver, F. D. Adv. Organometal. Chem. **1984**, 23, 219.



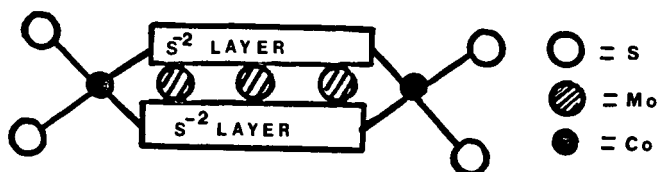


Figure 1. Proposed structure of "CoMoS" phase in promoted  $\text{MoS}_2$  HDS catalysts.

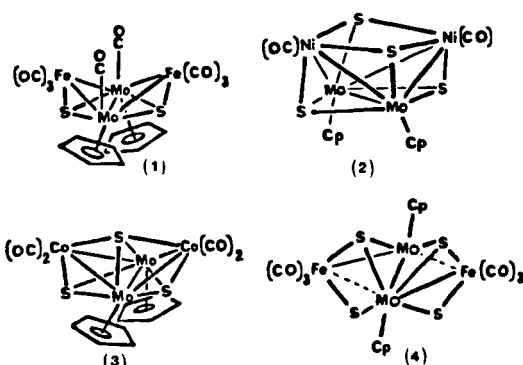


Figure 2. Structures of molecular models of promoted Mo-sulfide phases.

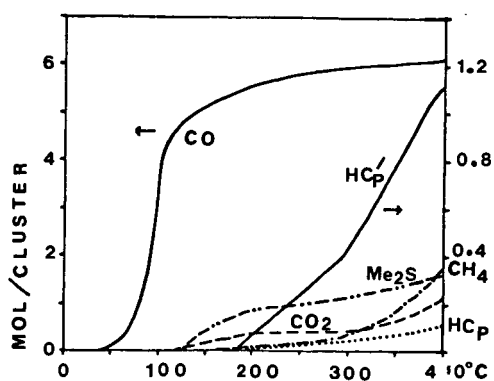


Figure 3. TPDE curves for cluster 1.

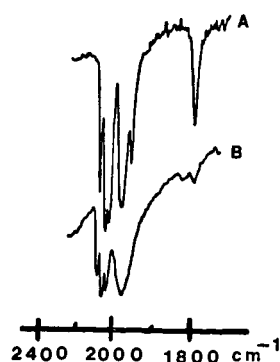


Figure 4. IR spectra of 1 in  $\text{CH}_2\text{Cl}_2$  solution (A) and on  $\text{Al}_2\text{O}_3$  (B).

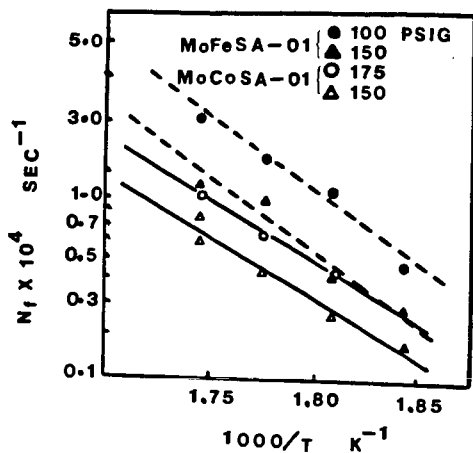


Figure 5. Arrhenius plots for CO hydrogenation with cluster catalysts.

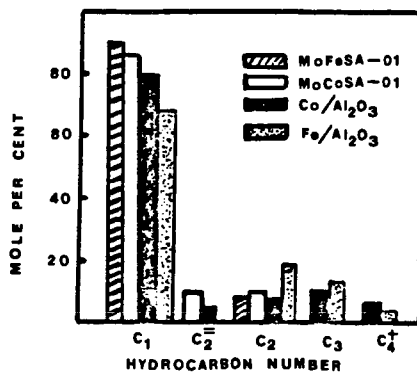


Figure 6. Product distribution in CO hydrogenation with various catalysts.

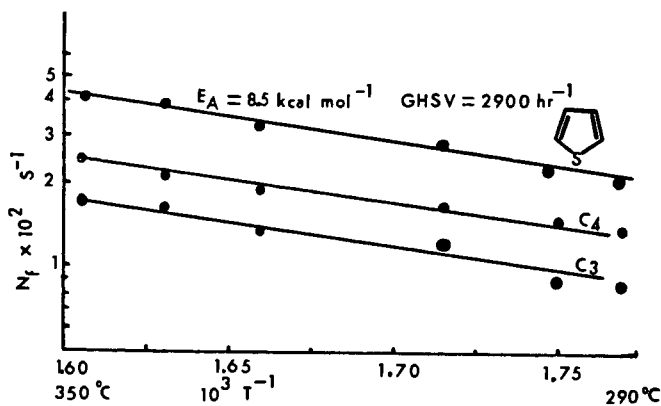


Figure 7. Arrhenius plots for thiophene HDS catalyzed by MoCoSA-01.

**PHYSICAL AND CHEMICAL PROPERTIES OF  $\text{Fe}(\text{CO})_5/\text{Al}_2\text{O}_3$   
CO-HYDROGENATION CATALYSTS.**

M. Rameswaran and C. H. Bartholomew.

BYU Catalysis Laboratory, Department of Chemical Engineering,  
Brigham Young University, Provo, UT 84602:

**Introduction**

Carbonyl-derived catalysts (CDCs), ie catalysts prepared by the decomposition of metal carbonyls on catalyst carriers, have attracted recent attention because of their unusually high dispersions (fractions exposed to the surface) and high extents of reduction [1,2] . While conventional preparation methods may lead to metal contamination with S or Cl or may result in support decoration [3,4], it may be possible to produce "clean" particles by decomposing carbonyl complexes on carefully dehydroxylated supports. Thus, effects of metal loading, and crystallite size may be investigated in the absence of these contaminants using this class of catalysts.

The objective of this study was to investigate the effects of metal loading and support dehydroxylation temperature on the physical and chemical properties of Fe CDCs.

**Experimental**

Alumina (DISPAL M,) was dehydroxylated under vacuum at 473-1073 K for 16 hours and stored in a dry box. A dehydroxylation temperature of 923 K was used in the preparation of most of the catalysts in this study. About a two fold excess of  $\text{Fe}(\text{CO})_5$  to achieve a given Fe loading was mixed with pentane. The dehydroxylated alumina was then impregnated to incipient wetness using this solution. The pentane solvent was removed by evacuation at room temperature. About 10 g of the catalyst thus prepared was reduced in flowing hydrogen and stored in a dry box and the remainder was sealed and stored in a refrigerator. Total hydrogen adsorption capacities and oxygen titration uptakes (upon oxidizing the reduced catalyst at 723 K) were measured using a volumetric apparatus and procedures described elsewhere [5]. The reactor system used for obtaining the activity/selectivity properties are described elsewhere[6].

**Results and Discussion**

Figure 1 depicts the effect of reduction temperature on the dispersion and the extent of reduction of a 4.6 %Fe/alumina catalyst. The dispersion goes through a maximum while the extent of reduction reaches 100% as the temperature of reduction is increased from 473-773 K. Garten [7] reported that in the case of Fe/alumina catalysts prepared by aqueous impregnation, up to 1.5% Fe (300

μmoles per gram catalyst) was irreducible even at very high reduction temperatures due to strong interaction of iron oxide with the support. However, the results from this study indicate that the Fe/alumina prepared via carbonyl decomposition can be easily reduced to the Fe(0) state at relatively mild reduction conditions. The significant decrease in dispersion at higher reduction temperatures suggests that the carbonyl-derived species are mobile at higher temperatures in reducing atmosphere. Since the maximum dispersion was obtained at 573 K, this temperature was used for reducing all the catalysts in this study.

Data showing the effects of metal loading on the physical properties of carbonyl-derived Fe/alumina reduced at 573 K are tabulated in Table 1. Although dispersion decreases with increasing metal loading, neither the hydrogen uptake nor the extent of reduction follow any clear trends. Nevertheless, the dispersions and extents of reduction for these catalysts are much higher than obtainable for catalysts prepared by other method with similar metal loadings.

Table 2 illustrates effects of support-dehydroxylation temperature on the physical properties of Fe/alumina CDS's. All the catalysts listed in Table 2 contain 4.0-4.8 wt.% iron. However the amount of hydrogen adsorbed per gram of catalysts varies significantly with dehydroxylation temperature. The extent of reduction and the %D for the catalyst with the support dehydroxylated at 473 K were not obtained due to the inability to measure any significant oxygen uptake by the conventional methods. Hence it can be safely assumed that the impregnated carbonyl was fully oxidized. However, the catalyst with the support dehydroxylated at 1023 K was easily reduced. Thus, it is seen that the extent of reduction (or the ease of reduction) increases with decreasing surface OH concentration. This observation is consistent with that of Brenner and Burwell [8], who proposed that the surface OH groups act as anchors for the carbonyls by causing their partial oxidation.

The activity of iron/alumina dehydroxylated at 923 K increases with decreasing metal loading or increasing dispersion. This observation is opposite to that observed for Co/alumina prepared by aqueous impregnation [9] and Ru/alumina prepared from carbonyls on partially dehydroxylated alumina [10]. However, the selectivities of these Fe/alumina CDC catalysts were independent of metal loading or dispersion (Table 3). The 1 and 1.5% Fe/alumina catalysts deactivated rapidly at temperatures above 473 K, hence accurate measurement of activation energies was not possible. Although Fu and Bartholomew [9] observed a trend of decreasing activity with decreasing metal loading or increasing dispersion for Co catalysts prepared by aqueous impregnation with cobalt nitrate, they also observed that a 3% Co/alumina CDC catalyst was at least twice as active as 3% Co/alumina prepared by impregnation. Their results suggest that the conventional impregnation method leads to crystallite decoration and thus lower activity. Hence the results

TABLE 1.  
Effects of Metal Loading on the Physical Properties of Fe/ Alumina<sup>a</sup> Catalysts.

Wt % Fe	H <sub>2</sub> uptake (μmoles/g)	% Dispersion <sup>b</sup>	Extent <sup>c</sup> of Reduction
1.0	45.1	75	33.6
1.5	31.5	40	58.6
4.6	72.6	31	55.1

a. Support dehydroxylated at 923 K under vacuum, catalyst reduced at 573 K.

b. %D=  $\frac{\text{\# of exposed atoms of Fe measured by hydrogen adsorption}}{\text{Total \# of reduced Fe atoms. (From oxygen titration and AA)}} \times 100$

c. Measured by O<sub>2</sub> titration at 673 K.

Table 2  
Effects of Support Dehydroxylation Temperature on the Physical Properties of ~4.5 Fe/Alumina<sup>a</sup>.

Dehydroxy- lation Temp. (K)	H <sub>2</sub> uptake (μmoles/g)	% Dispersion <sup>b</sup>	Extent <sup>c</sup> of Reduction
473	8.9	--d	--d
923	72.6	31	55.1
1073	55.9	16	95.4

a. Catalyst reduced at 573 K.

b. %D=  $\frac{\text{\# of exposed atoms of Fe measured by hydrogen adsorption}}{\text{Total \# of reduced Fe atoms. (From oxygen titration and AA)}} \times 100$

c. Measured by O<sub>2</sub> titration at 673 K.

d. Unable to measure oxygen uptakes.

TABLE 3.

Effects of Metal Loading on Activity/Selectivity Properties.  
( $H_2/CO = 2$ , 1 atm, 473 K)

Wt % Fe	TOF <sup>a</sup> $\times 10^{-3}$ ( $\text{sec}^{-1}$ )	% HC in <sup>b</sup> product Stream	HC Selectivity <sup>c</sup>				O/P <sup>d</sup>
			CH <sub>4</sub>	C <sub>2</sub> -C <sub>4</sub>	C <sub>5</sub> -C <sub>11</sub>	C <sub>12</sub> +	
1.0	0.36	87.2	26.2	40.8	33.0	0	1.6
1.5	0.13	83.8	28.3	42.4	29.3	0	2.5
4.6	0.05	87.2	21.7	40.1	38.1	0	2.5

a. Based on total  $H_2$  adsorption.

b. Mole percent based on carbon balance; the remainder of the C appeared as  $CO_2$ .

c. Wt.% hydrocarbon in product.

$$d. \quad O/P = \sum_{n=3}^7 C_n / C_n$$

observed for catalysts prepared by conventional methods [9] are probably due to a secondary structure-sensitivity [ie. decoration of the crystallites by support species] while the results in this study reflect either a primary structure sensitivity or changes in the electronic properties of the small metal clusters in the well-dispersed Fe/alumina. In a study by Kellner and Bell [10] of highly dispersed Ru/alumina prepared from the carbonyl, their observation of a decreasing activity with increasing dispersion may be a result of incomplete dehydroxylation of the support leading to crystallite contamination in the more highly dispersed catalysts.

The results of this study show that the support dehydroxylation temperature has a greater influence on the activity/selectivity properties than does dispersion (Table 4). The activity, selectivity for CH<sub>4</sub> and C<sub>2</sub>-C<sub>4</sub> hydrocarbons, and the O/P ratio decrease with increasing dehydroxylation temperature, while the C<sub>5</sub>-C<sub>11</sub> fraction increases. Figure 2 indicates that the activation energy also increases with increasing dehydroxylation temperature. These effects of dehydroxylation temperature may be due to changes in the concentration of surface OH groups.

### Conclusions

1. It is possible to produce highly dispersed and highly reduced catalysts by decomposing Fe(CO)<sub>5</sub> on dehydroxylated alumina.
2. The specific activity decreases with increasing metal loading (or decreasing dispersion). This effect may be due to a primary structure sensitivity on "clean" metal crystallites. The independence of selectivity with metal loading supports this hypothesis.
3. The significant changes in activity/selectivity with support dehydroxylation temperature may be a function of support hydroxyl group concentration, a significant concentration leading to support contamination of the metal surface and oxidation of the metal.

### Acknowledgments

The authors wish to acknowledge the financial support of Atlantic Richfield Company for this project. M.R. also wishes to thank ASBYU for a research grant which enabled the construction of bulk pretreatment cell.

### References.

1. Phillips, J. and Dumesic, J. A., Appl. Catal., 9(1981), 1.

TABLE 4.

Effects of Dehydroxylation Temperature on Activity/Selectivity  
 Properties of ~4.5 % Fe on  $\text{Al}_2\text{O}_3$ .  
 ( $\text{H}_2/\text{CO} = 2$ , 1 atm, 473 K)

Dehydro- xylation Temp. (K)	TOF <sup>a</sup> $\times 10^{-3}$ ( $\text{sec}^{-1}$ )	% HC in <sup>b</sup> product Stream	HC Selectivity <sup>c</sup>				O/P <sup>c</sup>
			$\text{CH}_4$	$\text{C}_2\text{-C}_4$	$\text{C}_5\text{-C}_{11}$	$\text{C}_{12+}$	
473	0.2	77.0	43.0	56.0 <sup>e</sup>	0	0	$\infty^f$
923	0.05	87.2	21.7	40.1	38.1	0	2.5
1073	0.02	87.4	21.7	39.0	39.7	0	2.3

a. Based on total  $\text{H}_2$  adsorption.

b. Mole percent based on carbon balance; the remainder of the C appeared as  $\text{CO}_2$ .

c. Wt.% hydrocarbon in product.

$$\text{d. } \text{O/P} = \sum_{n=3}^7 \frac{C_n}{C_n}$$

e.  $\text{C}_2$  and  $\text{C}_3$  only

f.  $\text{C}_2$ : no parafins;  $\text{C}_3$ :  $\text{O/P}=1.54$



2. Zwart, J. and Snell, R. J. Mol. Catal., 30(1985), 305.
3. Raupp, G. B. and Dumesic J. A., J. Catal., 95(1985), 587.
4. Bartholomew, C. H., (ed. Paal, Z. and Menon, P. G.) in press.
5. Weatherbee G.D., Rankin, J. L. and Bartholomew, C. H., Appl. Catal., 11(1984), 73.
6. Rameswaran, M. et al., paper in preparation, (1986).
7. Garten, R. L, J. Catal., 43 (1976), 18.
8. Brenner, A. and Burwell, R. L., J. Catal., 52(1978), 353.
9. Fu, L. and Bartholomew, C. H., J. Catal., 92(1985), 376..
10. Kellner, C. S. and Bell, A. T., J. Catal., 71(1981), 296.

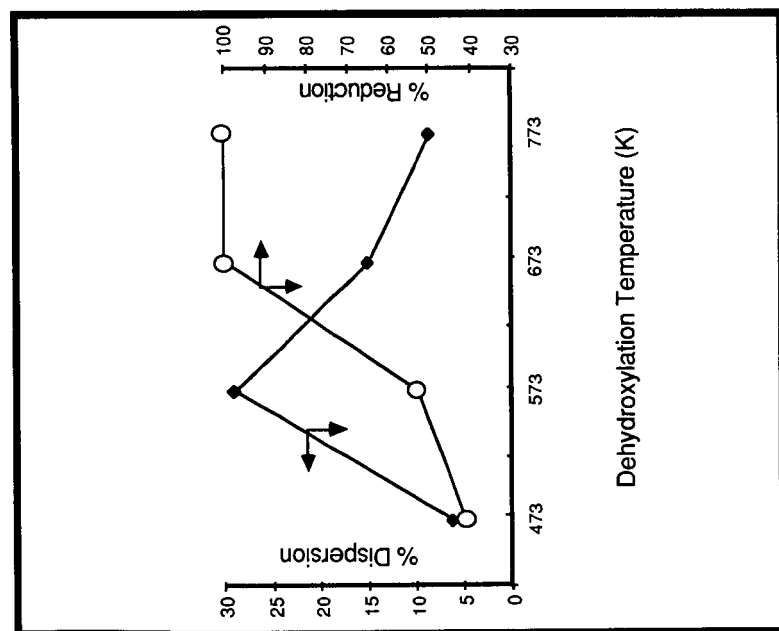


Figure 1. Reduction Temperature vs % Reduction and % Dispersion

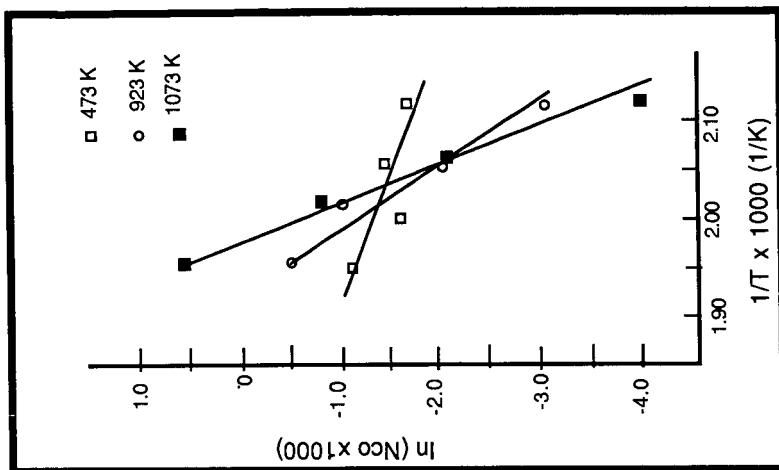


Figure 2. Effect of Dehydroxylation Temperature on Activation Energy for CO Hydrogenation

ZSM-5 SUPPORTED Fe AND Ru FROM  $\text{Fe}_3(\text{CO})_{12}$  AND  $\text{Ru}_3(\text{CO})_{12}$ : STRUCTURE-ACTIVITY  
CORRELATIONS FOR SYNTHESIS GAS CONVERSION

Ellis B. Zuckerman and Gordon A. Melson

Department of Chemistry, Virginia Commonwealth University, Richmond, VA 23284.

INTRODUCTION

The goal of improving the efficiency and product selectivity in the conversion of synthesis gas ( $\text{CO} + \text{H}_2$ ) to liquid hydrocarbons has resulted in efforts to develop bifunctional catalysts which combine a transition metal Fischer-Tropsch component with a zeolite support. This combination utilizes the carbon monoxide reduction and carbon chain propagation functions of the metal as well as the shape selectivity and dispersive effects of the zeolite. During the 1970's, workers at Mobil introduced the new synthetic zeolite ZSM-5 which possesses a unique channel structure. In its acid form H<sup>+</sup>-ZSM-5 is capable of isomerizing hydrocarbons and converting reactive species to alkylbenzenes in the gasoline range. The combination of metal oxides with ZSM-5 and the impregnation of metal salts into ZSM-5 have resulted in catalysts which produce gasoline range hydrocarbons containing a high percentage of aromatics from synthesis gas (1-4). Metal particle size and metal-support interaction also affect product selectivity. It has been argued (5) that the former, in particular, is an important factor in controlling the molecular weight distribution of hydrocarbon products from synthesis gas conversion.

During the past decade, there has been considerable interest in the development of supported metal catalysts by the incorporation of metal carbonyls (6,7). It has been demonstrated that this approach, depending on the method of preparation, is a means of rendering the metal component in the form of highly dispersed, small particles on oxide and zeolite supports (8). It thus provides an alternative to conventional aqueous impregnation of metal salts which usually results in the formation of large metal particles and low dispersion. Furthermore, the method of preparation of zeolite-supported metal catalysts affects the interaction of the metal with the Brønsted acid sites of the zeolite. It has been demonstrated (9,10) that the introduction of transition metals by aqueous methods leads to ion-exchange between metal ions and protons and results in a partial depletion of the catalytically active Brønsted acid sites. It also seems reasonable to suspect that physical blockage of the zeolite channels causes an apparent loss of acidity after calcination or reduction if the metal species initially penetrates the zeolite channels.

The present goal of the research effort is to develop supported metal catalysts which are both efficient for synthesis gas conversion and selective for the production of aromatic and branched aliphatic hydrocarbons in the gasoline range. If the metal component can be introduced onto the zeolite particle without extensive penetration of the channel structure and subsequent ion-exchange at the Brønsted acid sites, an efficient bifunctional catalyst should be produced. Such a catalyst would convert reactive intermediates and high molecular weight hydrocarbons produced by the metal component directly on the particle. This would eliminate the necessity for physical transfer of the organic products from the metal site to the zeolite site that is necessary in a mixed metal-zeolite system. Additionally, the products of synthesis gas conversion may be different by using a bifunctional catalyst from those obtained with the mixed system. In order to achieve this goal, we have

prepared bifunctional ZSM-5 supported Fe and Ru in which the catalytic functions of the metal and the support are retained. This was accomplished by using an extraction method reported earlier (8) with  $\text{Fe}_3(\text{CO})_{12}$  and  $\text{Ru}_3(\text{CO})_{12}$  as the source of the metals. It was anticipated that this method would lead initially to a high degree of dispersion of the metal and that the metal would be restricted to the external surface of the zeolite. It was also anticipated that changes in the metal particle size could be induced by subsequent pre-treatment, e.g. calcination. We report here evaluation of some Fe/ZSM-5 and Ru/ZSM-5 catalysts for their activity and product selectivity in the conversion of synthesis gas, and draw conclusions concerning catalyst structure-activity relationships.

### EXPERIMENTAL

ZSM-5 ( $\text{SiO}_2/\text{Al}_2\text{O}_3 = 32$ ) was received in the  $\text{NH}_4^+$  form and was calcined under vacuum at  $400^\circ\text{C}$  for 3 h to obtain the acid form. Ru/ZSM-5 and Fe/ZSM-5 materials were prepared by an extraction technique (8) using  $\text{Ru}_3(\text{CO})_{12}$  (Strem Chemical) and  $\text{Fe}_3(\text{CO})_{12}$  (Alfa, Ventron Division) with cyclohexane as the solvent. All of the catalysts discussed in this report have metal loadings of approximately 3% by weight. Portions of the as-prepared (AP) catalysts were calcined in air at  $400^\circ\text{C}$  (H-400) in order to induce an increase in the particle size of the metal component.

The materials have been characterized by infrared spectroscopy (IR), X-ray powder diffractometry (XRPD), X-ray photoelectron spectroscopy (XPS), ion scattering spectrometry (ISS), Mossbauer spectroscopy (for Fe), and pyridine chemisorption studies.

For catalytic evaluation, the catalysts were dispersed in silica (200-300 mesh), and reduced under flowing  $\text{H}_2$  at 20.4 atm. Fe catalysts were reduced at  $450^\circ\text{C}$  for 20 h whereas Ru catalysts were reduced at  $400^\circ\text{C}$  for 12-15 h. Following reduction, Fe catalysts underwent a carbiding step in flowing synthesis gas ( $\text{H}_2/\text{CO} = 1$ ) at 6.8 atm and  $250^\circ\text{C}$  for 20 h. Evaluation was carried out by using a fixed-bed, continuous flow microreactor. The reaction conditions consisted of a pressure of 20.4 atm of synthesis gas ( $\text{H}_2/\text{CO} = 1$ ) and reactor temperatures of  $280^\circ\text{C}$  and  $300^\circ\text{C}$ . For studies designed to determine the effects of space velocity, the flow rate was adjusted so that the WHSV was established at 990, 2085, and 3135 cc/g.h. In studies which did not involve space velocity comparisons, the WHSV was set to 2090 cc/g.h. Each evaluation at a given set of conditions was allowed to proceed for a period of 48 h during which the liquid products were collected in an ice-cooled trap which followed a heated trap ( $180^\circ\text{C}$ ) for the collection of high molecular weight products. The gaseous effluent was analyzed by using a gas chromatograph which is an integral part of the reactor system. The liquid product was separated into oil and aqueous fractions; the analysis of the oil was accomplished primarily by a quantitative infrared method described earlier (11). Additional supporting information such as the carbon number distribution and the degree of paraffin branching were obtained by capillary GC and  $^1\text{H}$  NMR spectroscopy respectively.

### RESULTS AND DISCUSSION

#### Characterization

The results of characterization studies have been reported earlier (12); however, because our objective is to enable correlations between the nature of the

catalysts and the results of catalytic evaluation to be drawn, some conclusions are presented here.

In XRPD studies of both Fe/ZSM-5/AP and Ru/ZSM-5/AP, no evidence for the presence of the metal component was detected. This suggests that the metals are highly dispersed with a particle size of  $<50 \text{ \AA}$  and/or that the metal species are non-crystalline. Calcination of the AP materials induces the formation of bulk  $\alpha\text{-Fe}_2\text{O}_3$  and  $\text{RuO}_2$ , which have been detected by XRPD. Depth profile studies of both Fe/ZSM-5/AP and Ru/ZSM-5/AP, by ISS, reveal a rather large initial M/Si ratio which rapidly decreases with sputtering. We have interpreted this observation to indicate that the metal component is restricted to the external surface of the zeolite particles (by virtue of the relative sizes of the metal clusters and the diameter of the ZSM-5 channels) and is highly dispersed, perhaps monodispersed at low loadings, on that surface. The ISS depth profiles of calcined materials consist of small initial M/Si ratios which increase slightly with sputtering time and suggest the formation of large metal oxide particles. XPS studies of Fe/ZSM-5/AP and Ru/ZSM-5/AP reveal the presence of metal oxides, but are inconclusive regarding the exact nature of the species. Calcined materials clearly contain the metals in the form of  $\text{Fe}_2\text{O}_3$  and  $\text{RuO}_2$ , and the trends observed with sputtering of AP and calcined samples parallel those observed in ISS studies. Infrared studies of chemisorbed pyridine were conducted as a probe to determine whether channel blockage and/or chemical interaction between the metal and Brønsted acid sites in the zeolite channels had occurred as a result of metal loading or subsequent calcination or reduction. No indication of such interactions was observed.

We have concluded from the results of characterization of Fe/ZSM-5 and Ru/ZSM-5 materials that both contain the metal component in a highly dispersed state on the external surface of the zeolite particles. Calcination, and to a lesser extent reduction, both induce the formation of large particles of the oxides or metals which remain excluded from the zeolite channels. The restriction of the metal to the external surface of the of the ZSM-5 particles should result in the retention of Brønsted acidity and permit access of reactants to the interior of the zeolite.

#### Catalytic Evaluation

Fe/ZSM-5/AP, Ru/ZSM-5/AP and Ru/ZSM-5/H-400 catalysts have been evaluated for their efficiency and selectivity in synthesis gas conversion. The three catalysts discussed here have been compared in order to investigate effects of the choice of transition metal and the effects which result from calcination of the Ru/ZSM-5 catalyst prior to evaluation. Furthermore, the effect of varying the space velocity at different temperatures for Fe/ZSM-5/AP and Ru/ZSM-5/AP was examined.

Comparison of the data in Tables 1 and 2 reveals a number of similarities regarding the effects of space velocity and temperature on the two catalysts. For both as-prepared catalysts, the percentages of  $\text{H}_2$  and CO conversion generally decrease at higher space velocities while increasing at higher temperature. The two catalysts exhibit a decreasing activity for the water gas shift reaction at higher space velocity and an increasing activity for the shift reaction at higher temperature. Analysis of the liquid products by a quantitative IR technique reveals an enhanced selectivity for aromatic hydrocarbons coupled with an apparent consumption of olefins and oxygenated species at higher temperature and lower space velocity. The efficiencies of synthesis gas conversion, the shift reaction, and the conversion of Fischer-Tropsch products and intermediates by the acidic and shape selective

TABLE 1. RESULTS FROM CATALYTIC EVALUATION OF A 3% Ru/ZSM-5/AP CATALYST

WHSV ( $\frac{\text{CC}}{\text{g}\cdot\text{h}}$ )	CATALYST TEMP. (°C)	% CONVERSION H <sub>2</sub> CO	REACTOR EFFLUENT DISTRIBUTION (wt. %)					HYDROCARBON PRODUCT DISTRIBUTION (wt. %)						LIQUID PRODUCT DISTRIBUTION (wt. %)			
			CO	H <sub>2</sub>	CO <sub>2</sub>	H <sub>2</sub> O	HC	CH <sub>4</sub>	C <sub>2</sub>	C <sub>3</sub>	C <sub>4</sub>	C <sub>5</sub> +	WAX	AR	OL	SAT	OX
990		92 51	54	1	4	21	20	23	5	7	13	52	0	27	7	63	3
2085	280	70 31	64	2	2	18	14	27	5	10	17	41	0	21	11	64	4
3135		49 23	71	3	2	14	10	33	7	12	13	35	0	18	12	65	5
990		89 55	47	1	15	17	20	49	11	13	10	18	0	30	3	65	2
2085	300	75 37	60	2	6	17	16	40	8	11	17	23	0	26	5	66	3
3135		69 35	62	2	4	17	15	43	8	11	10	28	0	21	6	70	3

TABLE 2. RESULTS FROM CATALYTIC EVALUATION OF A 3% Fe/ZSM-5/AP CATALYST

WHSV ( $\frac{\text{CC}}{\text{g}\cdot\text{h}}$ )	CATALYST TEMP. (°C)	% CONVERSION  H <sub>2</sub> CO	REACTOR EFFLUENT DISTRIBUTION (wt. %)					HYDROCARBON PRODUCT DISTRIBUTION (wt. %)					LIQUID PRODUCT DISTRIBUTION (wt. %)				
			CO	H <sub>2</sub>	CO <sub>2</sub>	H <sub>2</sub> O	HC	CH <sub>4</sub>	C <sub>2</sub>	C <sub>3</sub>	C <sub>4</sub>	C <sub>5</sub> +	WAX	AR	OL	SAT	OX
990		37 37	64	5	12	12	7	37	19	16	16	12	0	47	<1	51	<1
2085	280	28 17	75	5	6	7	7	33	17	21	12	17	0	26	1	72	1
3135		26 16	75	5	7	7	6	32	17	12	15	24	0	19	3	77	1
990		46 49	51	4	26	6	13	55	20	11	7	7	0	47	0	53	0
2085	300	41 31	64	4	15	6	11	43	17	9	18	13	0	48	<1	51	0
3135		42 32	62	4	16	7	11	35	17	15	12	21	0	33	1	66	0

zeolite are known to be influenced by temperature and the residence time of the reactants and products in the catalyst bed. In this respect, the trends mentioned above are not surprising.

Of greater interest is the effect of the choice of metal on the overall behavior of the catalysts. Inspection of Tables 1 and 2 reveals a number of differences in the efficiencies and product selectivities. These serve to distinguish the two catalysts on the basis of the metal component in spite of the presence of the ZSM-5 which is certainly a factor in controlling the nature of the product distribution and may also exert an influence on the properties of the metals. For example, the Ru/ZSM-5/AP catalyst showed higher activity than Fe/ZSM-5/AP for synthesis gas conversion. This observation is consistent with the results reported by Vannice (13) who demonstrated that Ru has the greatest specific activity among Group VIII metals for the conversion of CO/H<sub>2</sub> mixtures to hydrocarbons. Furthermore, Ru is well known to be the most selective of the Group VIII metals for higher molecular weight hydrocarbons, and this is also evident in the present study when the relative quantities of C<sub>5</sub>+ hydrocarbons are compared. This same selectivity, on the part of Ru, for species of higher carbon number may also account for the smaller aromatic content of the oil from Ru/ZSM-5/AP compared to that from Fe/ZSM-5/AP. The higher molecular weight products are more likely to be cracked and isomerized by the zeolite whereas lighter products such as C<sub>3</sub> and C<sub>4</sub> olefins are more favorable for conversion to aromatics. If this is the case, then the greater selectivity of Fe for lighter hydrocarbons could explain the greater aromaticity of the oil product from Fe/ZSM-5/AP. Consistent with this explanation is the fact that the normalized ratio of methyl to methylene hydrogen in the aliphatic fraction, obtained from <sup>1</sup>H NMR spectra, is large and is indicative of a significant degree of branching. This suggestion is not meant to preclude other factors which may influence the liquid product distribution. For example, we have considered the possibility that Fe might be more favorable for the formation of the correct chemical species (olefins and alcohols) for conversion to alkylbenzenes.

It should also be noted that the oil product from Ru/ZSM-5/AP contains a substantially larger fraction of olefins and oxygenates than that from Fe/ZSM-5/AP. At first glance this would appear to refute the statement above concerning correct chemical species for aromatization. However, it must be mentioned that the olefins detected in all of these oils are trans and branched  $\alpha$  olefins which, unlike normal  $\alpha$  olefins, are not considered to be primary products of synthesis gas conversion. The presence of these species may result from the activity of the zeolite. The oxygenated fraction consists of aldehydes and acids but no alcohols. Kellner and Bell (14) have reported that acetaldehyde was the only oxygenate produced over a Ru/SiO<sub>2</sub> catalyst.

Finally, it is apparent that the Fe catalyst is more active for the water gas shift reaction than the Ru catalyst. This is in agreement with the fact that the shift reaction is faster over Fe than over Ru, Co or Ni (15).

Comparison of the results of evaluation of the Ru/ZSM-5/AP and the Ru/ZSM-5/H-400 catalysts reveals some striking differences in activity and product selectivity. It should be mentioned, before further discussion, that while the activity and selectivity of the AP catalyst were stable for the 48 h duration of each evaluation period, the H-400 catalyst exhibited significant deactivation over the first 24 h at 280°C. Consequently it is unreasonable to treat the results of the

H-400 evaluation as if they were representative of a behavior which persisted for 48 h; nevertheless, some general comparisons of the two catalysts can be made.

At 280°C and a space velocity of 2090 cc/g.h the percentage conversion of CO and H<sub>2</sub> was much lower over the H-400 catalyst than over the AP catalyst. Furthermore, the selectivity for higher molecular weight hydrocarbons is greater with the H-400 catalyst. Both of these observations may be related to a metal particle size effect as a result of prior calcination. The liquid hydrocarbon product, like that produced over the AP catalyst, contained substantial aromatic and branched aliphatic fractions.

### CONCLUSIONS

Bifunctional catalysts consisting of Fe and Ru supported on ZSM-5 have been prepared by an extraction technique using metal cluster carbonyls. As anticipated, these precursors of the supported metal component were excluded from the ZSM-5 channels which have a diameter significantly smaller than that of the metal clusters. Evidence for this restriction was obtained from studies of the catalysts by ISS, XPS and pyridine chemisorption. These studies revealed that the metal was present as highly dispersed metal particles on the external surface of the ZSM-5 particles and that obstruction of the zeolite channels and extensive interaction with Bronsted acid sites did not occur. As a result, these materials were found to be efficient bifunctional catalysts for synthesis gas conversion. The metal component produces hydrocarbon and oxygenated products and intermediates which are further converted by the zeolite to mixtures containing substantial fractions of aromatic and branched hydrocarbons.

Calcination of a Ru/ZSM-5 catalyst prior to evaluation results in an increase in the average metal particle size. When evaluated, this catalyst exhibits less activity, but greater selectivity for higher molecular weight products when compared to the as-prepared catalyst. However, rapid deactivation of the calcined catalyst occurred. Although the reason for this is not clear at the time of writing, this behavior is being investigated.

The product distributions obtained by synthesis gas conversion over the above bifunctional catalysts will be compared with those obtained from catalysts consisting of the metal component dispersed on a conventional oxide support as well as from these catalysts physically mixed with ZSM-5. Correlations concerning the nature of the catalysts and differences observed among the various product distributions will be drawn, and mechanistic considerations will be presented.

### ACKNOWLEDGEMENTS

The authors wish to thank J.M. Stencel and J.R. Diehl of the U.S. Department of Energy, Pittsburgh Energy Technology Center, for assistance in obtaining some of the characterization data (XPS and ISS) and the Department of Energy for financial support.



#### REFERENCES

1. Chang, C.D., Lang, W.H. and Silvestri, A.J., J. Catal., 56, 268 (1979).
2. Caesar, P.D., Brennan, J.A., Garwood, W.E. Ciric, J., J. Catal., 56, 274 (1979).
3. Rao, V.U.S., Gormley, R.J., Hydrocarbon Process., 59 (11), 139 (1980).
4. Huang, T.J., Haag, W.O., in "Catalytic Activation of Carbon Monoxide", ACS Symposium Series, Vol. 152, Peter C. Ford (ed.), American Chemical Society, Washington, D.C., 1980.
5. Nijs, H.H. and Jacobs, P.A., J. Catal., 65, 328 (1980).
6. Zwart, J. and Snel, R., J. Mol. Catal., 30, 305 (1985), and references therein.
7. Phillips, J. and Dumesic, J.A., Applied Catal., 9, 1 (1984), and references therein.
8. Crawford, J.E., Melson, G.A., Makovsky, L.E., Brown, F.R., J. Catal., 83, 454 (1983).
9. Rhee, K.H., Brown, F.R., Finseth, D.H., Stencel, J.M., Zeolites, 3, 344 (1983).
10. Shamsi, A., Rao, V.U.S., Gormley, R.J., Obermeyer, R.T., Schehl, R.R., Stencel, J.M., Ind. Eng. Chem., Prod. Res. Dev., 23, 513 (1984).
11. Zuckerman, E.B., Melson, G.A., Finseth, D.H., 35th Southeastern Regional Meeting of the American Chemical Society, Charlotte, NC (1983).
12. Zuckerman, E.B. and Melson, G.A., Abstracts, 191st Annual Meeting of the American Chemical Society, New York, NY (1986).
13. Vannice, M.A., J. Catal., 37, 449 (1975).
14. Kellner, C.S. and Bell, A.T., J. Catal., 71, 288 (1981).
15. Anderson, R.B., "The Fischer-Tropsch Synthesis," Chapter 5. Academic Press, Orlando, 1984.

## CO HYDROGENATION ON ZEOLITE-SUPPORTED Ru: EFFECT OF NEUTRALIZING CATIONS

Rachid Oukaci, Jeffrey C.S. Wu, James G. Goodwin, Jr.

Department of Chemical & Petroleum Engineering,  
University of Pittsburgh, Pittsburgh, PA 15261

### INTRODUCTION

Previous results for zeolite-supported Ru prepared by ion exchange suggested a possible effect of the nature and concentration of the neutralizing cations in the zeolite on the catalytic properties of the metal (1). However, the interpretation of these results was complicated by the fact that a series of zeolites with different Si/Al ratios was used.

The present study was undertaken to investigate systematically the influence of the nature of alkali neutralizing cations on CO hydrogenation over ion-exchanged Y-zeolite-supported ruthenium catalysts.

### EXPERIMENTAL

A series of RuY catalysts was prepared from  $\text{NH}_4\text{Y}$ ,  $\text{LiY}$ ,  $\text{NaY}$ ,  $\text{KY}$ ,  $\text{RbY}$ , and  $\text{CsY}$  zeolites by ion-exchange with  $\text{Ru}(\text{NH}_3)_6\text{Cl}_3$ . After decomposition under vacuum and reduction in hydrogen at 673 K, the resulting Ru catalysts were characterized by atomic absorption and chemisorption of hydrogen and carbon monoxide.

CO hydrogenation was carried out in a tubular microreactor where the prereduced catalyst (0.25 g) was first rereduced in a hydrogen stream at 673 K for two hours before cooling to reaction temperature. The reaction was carried out at atmospheric pressure and 483-573 K using 1:1 mixture of  $\text{H}_2$  and CO. A sample of the effluent gas was analyzed on-line by gas chromatography after five minutes of reaction. The hydrogen bracketing technique was used to maintain a clean metallic surface.

### RESULTS AND DISCUSSION

#### Catalytic Activity and Product Distribution

Hydrogen chemisorption measurements were used to calculate the Ru dispersion (Table I) as described in (2). Based on both  $\text{H}_2$  and CO chemisorption results it was concluded that the metal dispersions were high and similar in the various Y-zeolites, except for RuHY.

Table I compares the turnover frequencies (TOF) at 523 K for CO conversion on the various catalysts, as well as the product distributions. No significant effect of the nature of the neutralizing alkali cations on TOF nor on the selectivity for  $\text{CH}_4$  and the chain growth probability were observed. Having similar metal loadings, the concentrations of the structural hydroxyl groups, formed during the reduction of the ruthenium ions in  $\text{LiY}$ ,  $\text{NaY}$ ,  $\text{KY}$ ,  $\text{RbY}$ , and  $\text{CsY}$ , should be comparable in all these catalysts.

TABLE I

CATALYTIC PROPERTIES OF ZEOLITE-SUPPORTED RU CATALYSTS AT 523 K

Catal.	Load. (wt%)	Disp. (%)	TOF ( $s^{-1} \times 10^3$ )	Selectivity (wt%)					
				$C_1$	$C_2$	$C_3$	$C_4$	$C_5$	$C_6$
RuHY	3.8	30	40.5	34.3	13.7	19.1	17.1	12.3	3.5
RuLiY	3.4	53	10.7	33.4	14.3	21.8	17.6	11.8	1.1
RuNaY	3.8	67	6.9	32.7	14.0	21.5	17.0	10.9	3.9
RuKY	3.2	52	8.0	30.7	13.7	23.5	15.8	11.0	5.2
RuRbY	3.6	49	14.1	33.5	14.4	22.0	15.3	9.7	5.1
RuCsY	3.7	56	12.4	36.1	13.2	21.6	15.1	9.8	4.2

It is generally accepted that for alkali cation zeolites, exchange of sodium ions for smaller or larger cations produces a change in the electrostatic field inside the zeolites, and hence a change in the strength of their acid sites (3-4). However one possible reason why these different acid sites have no significant effect on the catalytic properties of the metal is the "neutralization" of these sites by olefins adsorbed on them (5), thus interrupting any possible interactions that these acid sites might have with the metal particles. Such interactions have been often suggested to be responsible for the observed changes in adsorption properties of zeolite-supported metals (6-7). The higher activity observed for RuHY is probably due in large part to the fact that the Ru particles were significantly larger in this catalyst.

The apparent activation energy for CO conversion,  $E_a$ , varied with the neutralizing cation employed. A plot of  $E_a$  versus the crystal ionic radius of the initial charge balancing cations suggests that Ru is more uniformly distributed throughout the zeolite crystallites for the small cation zeolites. In the larger cation zeolites, Ru is probably preferentially distributed in the external shell of the zeolite crystallites. Although this uniform versus shell distribution, if true, does not seem to affect the % dispersion of the reduced Ru, but it affects the activation energy of reaction by introducing diffusion limitations on reactants and products for the zeolite catalysts having smaller neutralizing cations. This is further confirmed by the non-linearity of the Arrhenius plots for these catalysts.

#### Secondary Olefin Transformations

The nature of the neutralizing cations in Y-zeolites was found to have a strong influence on the olefin-to-paraffin ratios ( $C_3^-/C_3^-$ ), regardless of whether the comparison was made at constant temperature (Figure 2) or constant CO conversion. The  $C_3^-/C_3^-$  ratio was highest where the larger alkali cations had been exchanged into the zeolite and followed the sequence: Cs ~

Rb > K > Na > Li ~ H. The variation in the amount of isobutane in the C<sub>4</sub>-fraction is also included in Figure 2 as this reflects the secondary acid-catalyzed reactions which were enhanced in the order: Cs ~ Rb < K << Na < Li << H. The results listed in Table II show that at 523 K RuHY gave 53% isobutane (based on the total amount of C<sub>4</sub>). When this catalyst was exchanged after reduction with a dilute solution of K<sub>2</sub>CO<sub>3</sub>, in order to replace H<sup>+</sup> by K<sup>+</sup>, the isobutane was no longer obtained and the propene-to-propane ratio increased to 16.9. On the other hand, RuRbY yielded only very small quantities of isobutane, but, when 0.2 g of HY was added at the tail end of the reactor bed in a separate layer, the isobutane content of the C<sub>4</sub>-fraction increased to 30%, and the C<sub>3</sub><sup>-</sup>/C<sub>3</sub> ratio dropped from 6.4 to 4.1.

These results provide strong evidence that the hydrocarbon products of CO hydrogenation over supported ruthenium catalysts are mainly, if not totally, desorbed as olefins which can then undergo secondary reactions on the acid sites or to a lesser extent hydrogenation on the metal sites.

TABLE II

EFFECT OF ACIDITY ON OLEFIN AND ISOBUTANE SELECTIVITIES

Catalyst	Propene/Propene Ratio	Isobutane (wt% in C <sub>4</sub> )
RuHY	1.1	53.0
RuHY(K) (a)	16.9	0.0
RuRbY	6.4	1.4
RuRbY+HY (b)	4.1	30.6

(a) RuHY treated in 0.1 N K<sub>2</sub>CO<sub>3</sub> solution after reduction.

(b) RuRbY and HY in separate layers.

The most important acid-catalyzed reactions of olefins are isomerization, oligomerization, disproportionation, hydrogenation by hydride transfer, and coke formation. The rate of these reactions are influenced by the concentration and the acid strength of the hydroxyl groups present in the zeolite (8). The decrease of the olefin-to-paraffin ratio with decreasing cation radius, paralleled by an increasing acidity strength, may be partly explained by the enhancement of hydrogen transfer reactions catalyzed by acid sites. Several studies (8-10) of acid-catalyzed olefin reactions have demonstrated that the interaction of acidic hydroxyl groups with adsorbed olefins is accompanied by olefin oligomerization. At temperatures higher than 370 K, the olefin oligomers decompose by a disproportionation mechanism to produce gaseous paraffins and some polyene species which remain on the zeolite (8). The primary olefinic products may be hydrogenated on the acid sites, not only by hydrogen resulting from the oligomer decomposition, but also by hydrogen supplied by spillover from the metal to the support. However, the effect of mass transfer

limitations on the propene-to-propane ratio due to a uniform versus shell distribution of Ru in the zeolite cannot be ruled out. The increase in residence time of olefins following their formation may result in an increased probability for readsorption on the metal sites and hydrogenation.

It has also been shown that the higher the concentration and strength of the acid sites in a zeolite, the more branched the olefin oligomers (8). Thus, decomposition of the oligomers formed on the more acidic zeolites would result in the formation of more isoparaffins. The trend in selectivity for isobutane suggests that the nature of the alkali cations modify the strength of the acid sites. A possible effect of diffusion and steric factors may also account for this trend in selectivity for isobutane.

#### CONCLUSION

The nature of the charge balancing cations in zeolites can have a marked effect on the catalytic properties of ruthenium for CO hydrogenation in ion-exchanged zeolite-supported Ru catalysts. Although it has hardly any influence on the specific activity of the catalysts or on the overall chain growth probability, the nature of the neutralizing cations has a pronounced effect on the selectivities for olefins and branched hydrocarbons. Variations in the strength of the acid sites with the nature of these cations as well as mass transfer limitations apparently play a major role in shaping the olefin and isoparaffin selectivities.

#### LITERATURE CITED

- (1) Chen, Y.W., Wang, H.T., and Goodwin, J.G., Jr., *J. Catal.* **85**, 499 (1984).
- (2) Goodwin, J.G., Jr., *J. Catal.* **68**, 227 (1981).
- (3) Barthomeuf, D., in "Catalysis by Zeolites", (B. Imelik et al. eds.), p.55, Elsevier Sci. Publ. Co., Amsterdam, 1980.
- (4) Ward, J.W., *J. Catal.* **10**, 34 (1968).
- (5) Romannikov, V.N., Ione, K.G., and Pedersen, L.A., *J. Catal.* **66**, 121 (1980).
- (6) Arai, H., *Nippon Kagaku Kaishi* **192** (1982), *Chem. Abstr.* **96**, 125964f (1982).
- (7) Blackmond, D.G., and Goodwin, J.G., Jr., *J. Chem. Soc., Chem. Comm.*, 125 (1981).
- (8) Datka, J., in "Catalysis by Zeolites", (B. Imelik et al. eds.) p. 121, Elsevier Sci. Publ. Co., Amsterdam, 1980.
- (9) Venuto, P.B., Hamilton, L.A., and Landis, P.S., *J. Catal.* **5**, 484, (1966).
- (10) Langner, B.E. *J. Catal.* **65**, 416 (1980).

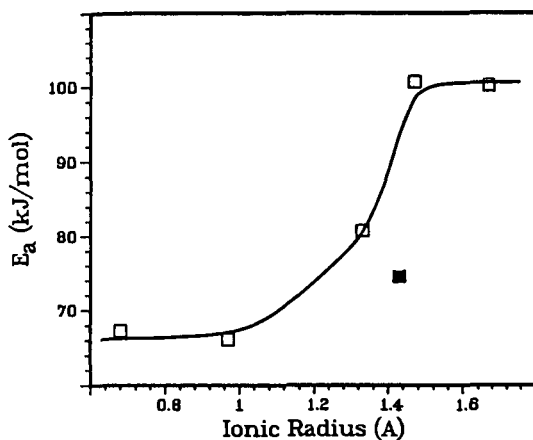


Figure 1. Variation in  $E_a$  with neutralizing cation radius; (■) RuHY.

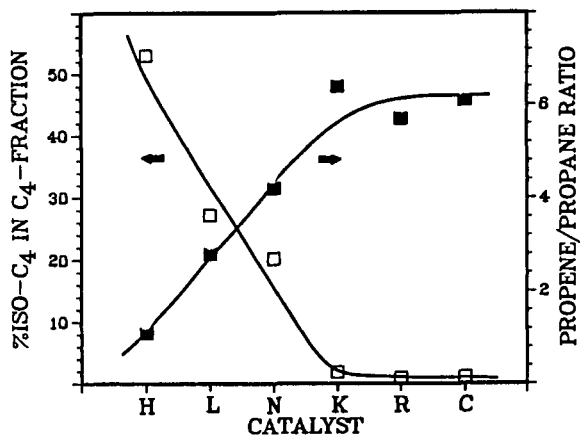


Figure 2. Effect of neutralizing cation on olefin fraction and isobutane formation; Catalysts: (H) RuHY, (L) RuLiY, (N) RuNaY, (K) RuKY, (R) RuRbY, (C) RuCsY.

## Synthesis and CO Hydrogenation Activity of Ruthenium Zeolite A

Joseph A. Rossin and Mark E. Davis

Department of Chemical Engineering  
Virginia Polytechnic Institute and State University  
Blacksburg, Virginia 24061

Ruthenium zeolite A was synthesized by several techniques from either  $\text{RuCl}_3$  or  $[\text{Ru}(\text{NH}_3)_5\text{Cl}]\text{Cl}_2$ . An example of our synthesis procedure with  $\text{RuCl}_3$  is described below.<sup>3</sup> First, zeolite A is synthesized in the presence of  $\text{RuCl}_3$  by simple addition of the ruthenium salt to a standard zeolite A synthesis gel. The resulting ruthenium-zeolite A was crystallized in approximately 2 hours under autogeneous pressure at  $95^\circ\text{C}$ . Next, a portion of the ruthenium-zeolite A was added to another zeolite A synthesis gel to serve as a "carrier" of ruthenium and as a "seed" for the synthesis. Ruthenium-zeolite A was recovered from the "seeded" synthesis and exchanged with  $\text{CaCl}_2$  for the two reasons: (1) to remove exchangeable ruthenium from the surface of the zeolite (intrazeolitic ruthenium will be too large to exchange out of the  $\alpha$ -cage), and (2) to place the zeolite A in its most stable form (the calcium form of zeolite A is more stable than NaA to attack by water at elevated temperatures). This RuCaA will be denoted catalyst B. For comparison, a CaA was ion exchanged with aqueous  $\text{RuCl}_3$  and this RuCaA will be denoted catalyst A.

Table 1 shows the X.P.S. and bulk chemical analysis (C.A.) data for catalysts A and B. Notice that the X.P.S./C.A. ratio for ion exchanged RuCaA is 14.7 while that of our synthesized RuCaA is 0.22. Since the X.P.S./C.A. ratio gives an indication of the amount of ruthenium in the superficial region relative to that in the bulk, it is obvious that catalyst B contains intrazeolitic ruthenium.

Catalyst B was tested for CO hydrogenation activity. The catalyst was heated to  $150^\circ\text{C}$  in flowing He for several hours to partially dehydrate the zeolite before reduction. Next, this material was exposed to flowing  $\text{H}_2$  at  $275^\circ\text{C}$ , 2.25 atm. in order to reduce the ruthenium. Finally, 1:1  $\text{CO}:\text{H}_2$  was contacted with the catalyst at  $255^\circ\text{C}$ , 2 atm. (2.1 g catalyst,  $F = 6.5 \text{ ml/min}$ ).

Figure 1 shows the start-up behavior of catalyst B. Notice that the production of all hydrocarbons other than  $\text{C}_2$  proceeds through a maximum. Also, these maxima do not occur at the same time. Figure 2 illustrates the hydrocarbon product distribution for over 10 hours of contact with syngas. In no case were branched hydrocarbons or hydrocarbons of  $\text{C}_8$  (only traces of  $\text{C}_6$  and  $\text{C}_7$ ) or greater observed in the product stream (see Table 2 for an example of an exact product distribution).

X-ray diffraction analysis of catalyst B following reaction showed no loss in crystallinity, however, a 22% loss in pore volume (by  $\text{O}_2$  adsorption) was observed. The loss in pore volume could be due to adsorbed hydrocarbons, structural rearrangements of the zeolite, or a combination of both factors. The FTIR spectrum of catalyst B after exposure to reaction conditions did show new bands in the zeolite framework region. These alterations suggest that changes in the zeolite have occurred over the course of the reaction. X.P.S. analyses of catalyst B: (i) as synthesized, (ii) after  $\text{H}_2$  exposure, and (iii) after reaction show that the ruthenium was reduced by the  $\text{H}_2$  and that during the course of the reaction the ruthenium did not migrate to the surface of the zeolite.

Table 1  
XPS and Chemical Analysis Data for RuCaA

<u>Catalyst</u>	<u>wt.%Ru</u>	<u>Ru/Si</u>		<u>XPS/CA</u>	<u>Preparation</u>
		<u>XPS</u>	<u>CA</u>		
A	1.98	0.534	0.0363	14.7	exchange
B	1.53	0.006	0.0276	0.22	synthesis

Table 2  
Product Distribution for RuCaA (Catalyst B).  
T = 255°C, P = 2 atm, CO:H<sub>2</sub> (1:1), t = 3.5 h

<u>Hydrocarbon</u>	<u>Mole Percent</u>	<u>Weight Percent</u>
Methane	66.09	36.17
Ethane	2.00	2.19
Ethylene	2.00	2.19
Propane/Propylene	13.30	21.84
1-Butene	0.43	0.95
n-Butane	2.98	6.52
t-2-Butene	7.08	15.15
c-2-Butene	3.65	7.80
n-Pentane	2.48	6.80



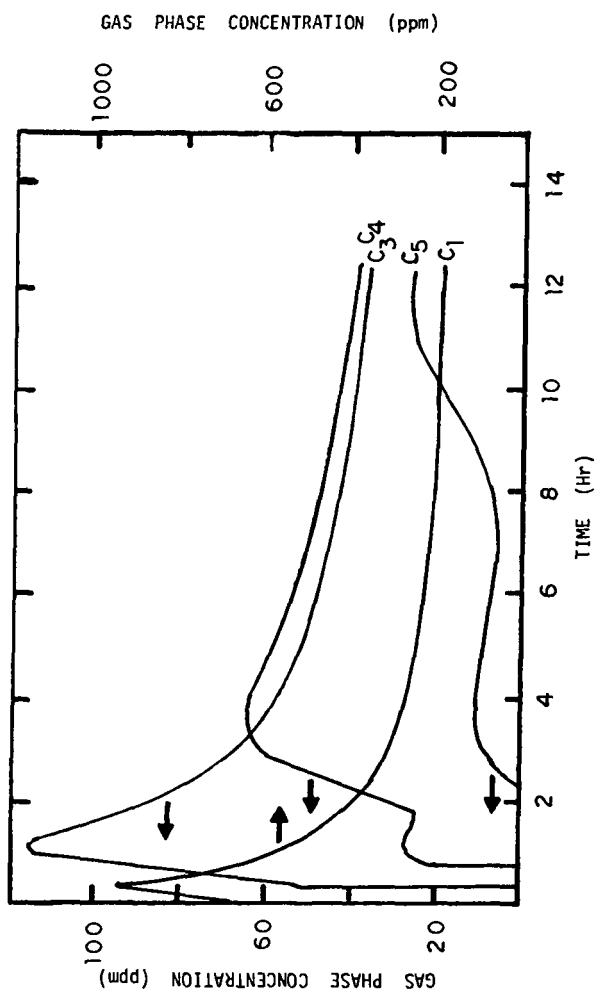


Figure 1: Hydrocarbon Product Start-up Behavior for Catalyst B at 255 C.  
All hydrocarbons were linear.

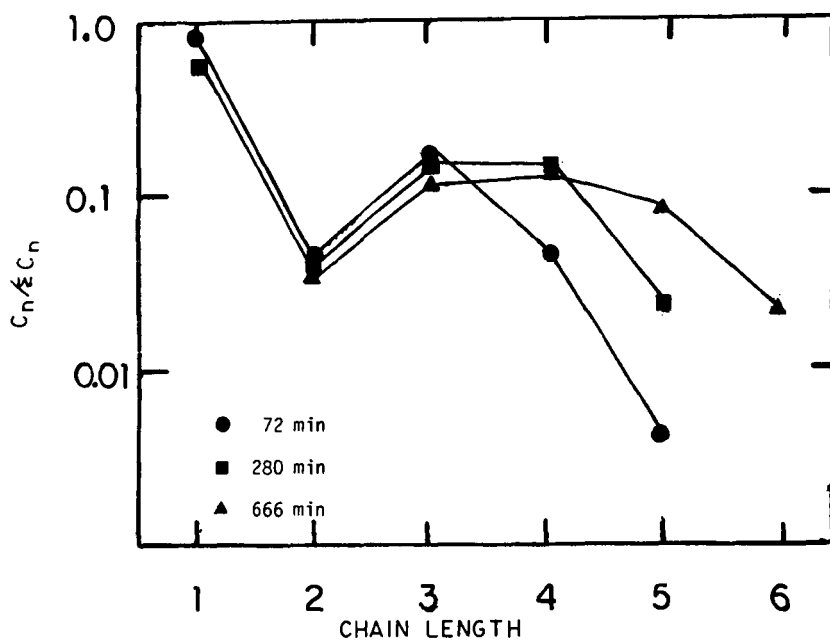


Figure 2: Hydrocarbon Product Distribution for Catalyst B at 255 C. All hydrocarbons were linear.

## CATALYTIC CONVERSION OF SYN GAS WITH PEROVSKITES

J. A. Broussard and L. E. Wade

Celanese Research Company, Summit, NJ, 07901

### INTRODUCTION

Perovskites, mixed metal oxides of the general formula  $ABO_3$ , have been examined as catalysts for conversion of syn gas to oxygenated organic chemicals. Several of these perovskites have been found to provide moderate to high selectivities to oxygenated organics, particularly methanol and C2OX (acetic acid, acetaldehyde, and ethanol).

### RESULTS AND DISCUSSION

#### CATALYST EVALUATIONS

The perovskites were prepared by co-precipitation with subsequent calcination in air to form pure crystalline phases. The resulting powders (pelleted with  $SiO_2$ ) were evaluated in a U-tube vapor phase reactor. Catalysts were evaluated with 2:1  $H_2:CO$  at 1000 psig. Conclusions are based on results obtained in the CO conversion range of 1-20% (usually 1-10%). Results of catalyst evaluations are presented in Tables I-III.

Perovskites of La with late transition metals and other closely related perovskites were evaluated as syn gas conversion catalysts. The maximum oxygenate selectivities obtained with  $LaCoO_3$ ,  $LaNiO_3$ , and  $LaFeO_3$  were in the range of 24-33%. No oxygenated products were observed with  $LaMnO_3$ .  $LaCoO_3$  and  $LaNiO_3$  underwent runaway methanation, but  $LaFeO_3$  and  $LaMnO_3$  did not. Co, Ni, and Fe are best known as catalysts for producing hydrocarbons (1, 2).

Six substituted derivatives of the above ternary perovskites were evaluated in hopes of finding positive synergism.  $LaNi_{0.5}Fe_{0.5}O_3$  and  $LaMn_{0.5}Ni_{0.5}O_3$  exhibited positive synergism (i. e. higher oxygenate selectivity than the average for the related ternary perovskites).  $LaNi_{0.5}Co_{0.5}O_3$ ,  $LaFe_{0.5}Co_{0.5}O_3$ ,  $LaMn_{0.5}Co_{0.5}O_3$ , and  $LaMn_{0.5}Fe_{0.5}O_3$  exhibited either no synergism or negative synergism when compared to the related ternary perovskites.

Partial substitution of La with Ce and Sr was examined as a means of modifying the catalytic behavior of  $LaCoO_3$ . The maximum oxygenate selectivities obtained with  $La_{0.8}Ce_{0.2}CoO_3$  and  $La_{0.8}Sr_{0.2}CoO_3$  (7-8%) were much lower than the results obtained with the parent system.

$LaCo_{0.5}Ru_{0.5}O_3$ ,  $LaNi_{0.5}Ru_{0.5}O_3$ , and  $LaFe_{0.5}Ru_{0.5}O_3$  were evaluated to determine the effect of partial substitution of Ru for Co, Ni, and Fe and the selectivity patterns typical of Ru in these perovskite lattices. The maximum oxygenate selectivities obtained with these materials (3-14%) are much lower than those obtained with related ternary perovskites. Ru is apparently a poor catalyst for converting syn gas to oxygenates which is consistent with reports that Ru is used in Fischer Tropsch synthesis for producing higher hydrocarbons (2).

$LaNi_{0.5}Ti_{0.5}O_3$  and  $LaFe_{0.5}Ti_{0.5}O_3$  were evaluated to determine the catalytic effects of partial substitution of the B cations by Ti(IV). Both of these materials provided significantly lower oxygenate

selectivities than the related ternary perovskites.

$\text{LaCu}_{0.5}\text{Ti}_{0.5}\text{O}_3$  and  $\text{LaCu}_{0.5}\text{Mn}_{0.5}\text{O}_3$  were evaluated to determine the catalytic behavior of Cu in a perovskite lattice. Both materials exhibited high methanol selectivities (37-38%, maximum). These results suggest that Cu is the catalytic metal in these systems, probably in reduced form. Cu is used in commercial methanol synthesis catalysts.

$\text{NdNiO}_3$ ,  $\text{NdFeO}_3$ , and  $\text{NdCoO}_3$  were evaluated to determine the catalytic effects of replacing La with closely related Nd. The maximum oxygenate selectivities obtained with these perovskites (0-10%) are much lower than those obtained with the analogous La perovskites (24-33%).

Perovskites of barium with platinum group metals were also evaluated as catalysts for syn gas conversion. These materials were prepared by Professor B. L. Chamberland (U. Conn.). Materials prepared by low temperature calcination ( $< 400^\circ\text{C}$ ) were amorphous by XRPD. Materials prepared by re-calcination at higher temperatures ( $\geq 600^\circ\text{C}$ ) were pure crystalline phases by XRPD.

High oxygenate selectivities (almost exclusively methanol) were obtained with  $\text{BaRhO}_3$  and  $\text{BaPtO}_3$  (maximum, 62% and 54%, respectively). Maximum oxygenate selectivities obtained with  $\text{BaIrO}_3$  and  $\text{BaRuO}_3$  were 39% and 14%, respectively. High methanol selectivities have been reported for the related  $\text{LaRhO}_3$  by Bartley (3) and by Watson and Samorjai (4). Supported-Pt catalysts have been reported to be selective catalysts for methanol synthesis (2). Supported Ir has been reported as catalysts for both methanol and hydrocarbon synthesis (2). Ru Fischer Tropsch catalysts (2) and our own La-Ru perovskites are mainly hydrocarbon producing catalysts.

#### CATALYST CHARACTERIZATION

Catalysts were characterized to determine the crystalline phase purity of starting materials, to determine if perovskite phases were preserved or decomposed (by reduction) under reaction conditions, and to determine the nature of catalytic sites in these materials. Catalyst samples were characterized by XRPD, EXAFS, XANES, AND ESCA. Results are presented in Table IV.

The "A" cations in these perovskites ( $\text{La(III)}$ ,  $\text{Nd(III)}$ , and  $\text{Ba(II)}$ ) are stable to reduction and catalytically inactive under these conditions. Therefore, the stability of these crystalline lattices to reductive decomposition and the catalytic activity of these materials depends on the late transition metal "B" cations.

The ternary perovskites of La with Co, Ni, Fe, and Mn were pure crystalline phases prior to catalyst testing. EXAFS and XANES results indicated the expected +3 bulk oxidation state for the "B" metals. ESCA analysis of surface "B" atoms indicated oxidation states  $> 0$ , but specific oxidation state (i. e. +2 or +3) could not be assigned.

Recovered materials exhibited a consistent trend. Perovskite lattices of materials not exposed to runaway methanation were preserved. Ni and Co perovskites not exposed to runaway methanation appeared to have been partially reduced (ca. one electron) to form oxide deficient perovskite lattices. Fe and Mn perovskites were unaffected. The oxidation state of surface "B" cations in all of these recovered

catalysts was  $> 0$ .

Perovskite lattices of materials exposed to runaway methanation were destroyed by reduction. During runaway methanation catalyst bed temperatures exceed  $500^{\circ}\text{C}$ . After exposure to runaway methanation the perovskite lattices of  $\text{LaCoO}_3$  and  $\text{LaNiO}_3$  were destroyed. Ni was reduced from +3 to a mixture of +1 and 0, and Co was probably comparably reduced. These results parallel those of Hall and coworkers who reported that hydrogen reduces  $\text{LaCoO}_3$  by one electron at  $400^{\circ}\text{C}$  and by three electrons at  $500^{\circ}\text{C}$  (5). The Fe and Mn perovskites did not undergo runaway methanation under the conditions employed.

Based on these data it appears that the catalytic sites for these materials are higher valent ( $> 0$ ), late transition metal, surface "B" cations in a perovskite or perovskite-like lattices, so long as runaway methanation does not occur. This conclusion applies also to substituted perovskites of La and Nd with Mn, Fe, Co, and Ni.

Six perovskites of the general formula  $\text{LaM}_{0.5}\text{M}'_{0.5}\text{O}_3$  ( $\text{M} \neq \text{M}' = \text{Mn, Fe, Co, and Ni}$ ) were characterized after catalyst testing.  $\text{LaNi}_{0.5}\text{Co}_{0.5}\text{O}_3$  was exposed to runaway methanation and its crystalline lattice was decomposed. The other materials were not exposed to runaway methanation, and their crystalline lattices were preserved.

$\text{La}_{0.8}\text{Ce}_{0.2}\text{CoO}_3$  and  $\text{La}_{0.8}\text{Sr}_{0.2}\text{CoO}_3$  were exposed to runaway methanation, and the crystalline lattices of both materials were destroyed.

$\text{LaCo}_{0.5}\text{Ru}_{0.5}\text{O}_3$  was not exposed to runaway methanation, but  $\text{LaNi}_{0.5}\text{Ru}_{0.5}\text{O}_3$  and  $\text{LaFe}_{0.5}\text{Ru}_{0.5}\text{O}_3$  were. Yet, the perovskite lattices of all three materials were preserved. This contrasts with the behavior of  $\text{LaNiO}_3$ , which underwent lattice decomposition under these conditions. Ru apparently confers added stability to these lattices.

$\text{LaNi}_{0.5}\text{Ti}_{0.5}\text{O}_3$  and  $\text{LaFe}_{0.5}\text{Ti}_{0.5}\text{O}_3$  were not exposed to runaway methanation. As expected, the perovskite lattices were preserved. The catalytic sites for these materials appear to be higher valent surface cations of Ni and Fe in perovskite lattices.

Neither of the Cu containing perovskites were exposed to runaway methanation. The perovskite structures of both materials were preserved, albeit, with partial reduction. The stability of these lattices is probably due to the reductive stability of Ti(IV) and Mn(IV). The catalytic sites for these materials appear to be lower valent surface atoms of Cu in a perovskite or perovskite-like lattice.

$\text{NdNiO}_3$ ,  $\text{NdCoO}_3$ , and  $\text{NdFeO}_3$  all underwent runaway methanation. Like the analogous La compounds, the Ni and Co perovskite structures were destroyed, but the perovskite structure of  $\text{NdFeO}_3$  was preserved.

The crystalline barium platinum metal perovskites were all pure crystalline phases prior to catalyst testing. The bulk oxidation states of the platinum metals were the expected +4. However, all of these materials except  $\text{BaRuO}_3$  contained surface platinum metal cations in lower oxidation states instead of, or in addition to the +4 state.

Both crystalline and amorphous barium platinum metal perovskites are unstable to syn gas and its products. Platinum metals were reduced to the elemental state, and Ba was converted to  $\text{BaCO}_3$ . It appears that these materials after an induction period are transformed to zero valent platinum metal crystallites on  $\text{BaCO}_3$ .

## CONCLUSIONS

Seven base metal lanthanum perovskites that provide 20-40% selectivity to oxygenates have been found. All of the lanthanum metal perovskites are stable to reductive decomposition if not exposed to runaway methanation and some are stable even if exposed to runaway conditions. The catalytic sites in these materials are thought to be late transition metal surface "B" atoms in higher oxidation states ( $> 0$ ) and in perovskite or perovskite-like lattices. Two platinum metal barium perovskites that provide  $> 50\%$  selectivity to oxygenates (mainly methanol) have also been found. These materials are unstable under reaction conditions and are converted to elemental platinum metals and  $\text{BaCO}_3$ . After an induction period, the catalytic sites for these materials are thought to be the mainly zero valent platinum metal crystallites on  $\text{BaCO}_3$ .

## ACKNOWLEDGMENTS

The authors wish to acknowledge the contributions of several of their co-workers to this study. Messrs. R. Sgrignoli and G. Abaskaron prepared catalysts and performed catalyst evaluation experiments. Dr. D. Karim performed and interpreted EXAFS and XANES experiments. Dr. E. Prack performed and interpreted ESCA experiments. Dr. J. Stamatoff and Dr. C. Saw performed and interpreted XRPD experiments. The authors also want to thank the Celanese Research Company for supporting this research and permitting presentation of this paper.

## REFERENCES

1. Kalfadelis, C. D., and H. Shaw, in "Encyclopedia of Chemical Technology", John Wiley and Sons, New York, NY, 1980.
2. Anderson, R. B., "The Fischer-Tropsch Synthesis", Academic Press, New York, NY, 1984.
3. Bartley, W. J. (Union Carbide), United States Patent 4,312,955, January 26, 1982.
4. Watson, P. R. and G. A. Samorjai, *J. Catal.* **74**, 282-95, 1982.
5. Crespin, M. and W. K. Hall, *J. Catal.* **69**, 359-70, 1

TABLE I  
CATALYTIC EVALUATION OF PEROVSKITES FOR SYN GAS CONVERSION (a)

PEROVSKITE	GHSV 1/HR	TEMP °C	CO CONV		CO SELECTIVITY, %				STY, G/L.HR	
			%	MeOH	C2OX	HiOX	HC	CO2	OXY	TOTAL
LaCoO3	3944	280	2.3	12.5	10.0	10.6	62.4	4.4	2.1	14.6
	300	300	9.2	10.3	15.7	0.7	37.9	35.4	9.4	21.5
	320	320	100.	3.7	3.3		64.5	28.4	91.5	1120.
LaNiO3	2471	320	4.1	20.8	4.7	1.6	55.6	17.3	8.2	24.9
	2434	340	8.7	10.6	2.9	0.9	62.2	23.5	10.1	59.1
	360	360	100.				67.4	32.6		748.
LaFeO3	3000	280	3.9	6.4	15.0	2.5	66.5	9.6	7.8	25.0
	300	300	10.4	4.5	14.0	2.3	66.3	12.8	16.7	63.6
	320	320	22.8	3.7	8.2	2.1	70.3	15.6	24.7	142.5
LaMnO3	3054	340	4.3				64.3	35.7		33.2
		360	6.2				61.9	38.1		50.0
		380	8.3				62.4	37.6		74.6
LaNi0.5Fe0.5O3	3487	340	9.5	0.9	31.3		54.6	13.1	33.1	55.1
		360	15.2	0.6	16.0		66.7	16.8	28.6	111.7
		380	26.4		8.7		73.3	17.9	26.1	212.8
LaMn0.5Ni0.5O3	3504	320	2.6		26.6		61.5	11.9	6.5	15.8
		340	4.5	0.8	15.6		69.3	14.4	6.9	31.3
		360	6.5	0.6	10.8		71.5	17.1	6.9	48.8
LaNi0.5Co0.5O3	3529	280	2.72		1.0	0.4	93.6	5.0	0.3	18.3
		300	7.4	1.4	13.9	0.4	73.1	11.3	11.6	50.1
		320	100.				73.2	26.8		1013.
LaFe0.5Co0.5O3	3529	320	13.6		19.0		73.5	7.5	28.4	80.0
		340	30.2	0.5	8.1		79.4	12.0	26.4	213.2
		360	34.0		6.8		77.6	15.5	26.0	266.5
LaMn0.5Co0.5O3	2958	380	40.6		5.1	0.1	76.3	18.4	24.5	346.9
		320	3.3		0.3	3.0	76.3	20.4	0.6	20.8
		340	19.3	3.4	0.3	0.2	82.8	13.3	4.2	71.8
LaMn0.5Fe0.5O3	3769	360	22.6	2.0	0.3	0.1	79.9	17.6	4.6	137.
		340	10.4	5.3	4.6	4.0	69.5	16.7	18.6	115.
		360	15.9	3.9	3.7	2.0	69.4	20.9	18.6	170.
		380	19.1	3.3	3.2	1.3	68.8	23.4	19.8	223.

a. Pressure = 970-1000 psig, GHSV = gas hourly space velocity, TEMP = temperature, CO CONV = CO conversion, STY = space time yield, MeOH = methanol, C2OX = ethanol + acetaldehyde + acetic acid, HiOX = C3-C6 alcohols, HC = hydrocarbons, OXY = oxygenated organics.

TABLE II

## CATALYTIC EVALUATION OF PEROVSKITES FOR SYN GAS CONVERSION (a)

PEROVSKITE	GHSV 1/HR	TEMP °C	CO CONV		CO SELECTIVITY, %				STY, G/L.HR	
			%	MEOH	C2OX	HiOX	HC	CO2	OXY	TOTAL
La0.8Ce0.2CoO3	3250	280	2.9		1.3	1.6	88.5	8.6	0.7	22.
		300	7.8		1.2	2.7	83.1	8.9	6.9	62.
		320	40.2	4.1	1.2	1.6	84.5	12.0	12.7	308.
La0.8Sr0.2CoO3	3803	280	2.8	0.7	6.9		80.9	12.2	2.1	27.
		300	95.9		0.7	1.0	74.9	23.5	14.1	966.
LaCo0.5Ru0.5O3	2615	320	1.7				94.0	6.0		9.4
		340	5.2				96.9	3.1		26.9
		360	28.3		2.6	0.3	83.7	13.4	5.8	171.4
LaNi0.5Ru0.5O3	3015	320	10.0		6.9	.5	87.6	5.0	6.0	57.
		340	19.6	6.7	3.7	.4	82.6	6.7	6.6	130.
		360	52.1		1.3	.5	89.5	8.6	7.9	355.
LaFe0.5Ru0.5O3	2658	300	5.7		12.6	0.9	81.3	5.2	5.5	26.1
		320	11.0		8.5	0.7	79.1	11.7	7.0	59.6
		340	21.7		4.5	1.0	81.9	9.7	8.5	123.
LaNi0.5Ti0.5O3	3337	360	60.7	0.1	1.5	8.5	67.4	22.6	14.7	132.
		360	1.2				69.7	30.3		9.6
		380	1.9				69.7	30.3		15.5
LaFe0.5Ti0.5O3	3189	340	11.4	6.9	10.1	1.3	60.2	21.5		95.5
		360	16.5	4.9	4.7	0.6	64.0	26.9	15.9	143.
		380	20.3	3.1	3.3	0.2	60.5	32.8	12.9	189.
LaCu0.5Ti0.5O3	3323	320	2.9	38.0		0.9	28.7	32.4	13.8	35.6
		340	5.0	32.3		1.6	32.6	33.6	20.7	60.6
		360	7.6	24.1		2.0	35.4	36.8	23.3	88.3
LaCu0.5Mn0.5O3	3361	320	3.4	37.0			29.0	34.0	14.2	38.2
		340	6.5	28.9		.6	36.3	34.2	21.2	69.4
		360	12.4	20.5		1.3	48.8	29.4	30.0	121.5
NdNiO3	3561	260	2.4				92.8	7.2		15.1
		280	7.0		9.8		90.2		6.0	43.3
		300	73.		0.7		79.6	19.7	3.8	549.
NdFeO3	3060	300	3.3				70.6	29.4		29.6
		320	36.8		2.1	0.7	68.4	28.8	8.3	335
		260	.68				86.2	13.8		5.6
NdCoO3	3494	280	6.1				95.8	4.2		39.7
		300	92.1		0.3		77.3	22.3	3.2	892.

a. Pressure = 970-1000 psig, GHSV = gas hourly space velocity, TEMP = temperature, CO CONV = CO conversion, STY = space time yield, MeOH = methanol, C2OX = ethanol + acetaldehyde + acetic acid, HiOX = C3-C6 alcohols, HC = hydrocarbons, OXY = oxygenated organics.



TABLE III

CATALYTIC EVALUATION OF PEROVSKITES FOR SYN GAS CONVERSION (a)

PEROVSKITE	GHSV 1/HR	TEMP °C	CO CONV %	CO SELECTIVITY, %				STY, G/L.HR	
				MeOH	C2OX	HIOX	HC	CO2	TOTAL
BaRuO <sub>3</sub> , Amorph	2381	280	3.5		2.6	3.6	83	10.9	1.2
		300	9.6		4.3	3.8	81.5	10.4	4.6
		320	34.4		3.2	3.5	83.1	10.2	12.8
BaRuO <sub>3</sub> , Cryst	3564	340	80.9	0.2	0.3	0.2	79.9	19.4	4.1
		260	6.6	1.5	12.1	0.6	66.6	19.2	7.5
		280	13.4		8.7	1.1	66.9	23.3	8.9
BaRhO <sub>3</sub> , Amorph	2556	300	100.		0.4		71.4	28.2	3.9
		240	1.1	54.3	2.4	0.9	27.5	14.9	6.9
		260	2.5	36.6	8.4	1.5	29.8	23.6	11.7
BaRhO <sub>3</sub> , Cryst	2483	280	6.7		10.2	3.1	38.8	25.4	22.2
		300	16.7	13.4	10.3	3.2	44.3	28.9	39.2
		260	1.7	62.3	2.2	0.5	22.2	12.8	11.6
BaIrO <sub>3</sub> , Amorph	2576	280	3.9	46.8	5.0	1.0	28.2	19	19.9
		300	7.9	29.7	5.9	1.3	36.9	26.2	28.3
		320	19.0	15.5	6.4	1.6	43.2	33.2	40.8
BaPtO <sub>3</sub> , Amorph	2540	340	49.6	4.7	5.3	1.5	51.5	37	49.1
		280	2.9	29.3	7.7	2.2	43.1	17.6	10.8
		300	8.7	20.4	5.8	2.1	51.0	20.6	23.1
BaPtO <sub>3</sub> , Cryst	2550	320	21.4	17.1	5.1	1.4	47.6	28.7	43.7
		340	22.0	8.8	6.2	1.0	61.2	22.8	30.7
		360	34.0	5.1	3	0.9	61.4	29.5	25.6
BaPtO <sub>3</sub> , Amorph	2540	360	4.3	0.2	1.2	0.9	59.8	37.9	0.8
		380	10.0	4.6	0.9	0.9	56.3	37.6	5.9
		280	5.7	38.6	4.8	2.2	26.4	28	25
BaPtO <sub>3</sub> , Cryst	2860	300	8.4	48.1	3.4	6.2	19.6	22.6	44.5
		320	10.6	53.8	4.3	0.4	19.8	21.6	59.5
		340	12.7	49.6	1.9	0.2	25.2	23	63.1
BaPtO <sub>3</sub> , Cryst	2860	360	13.3	39.8	1.9	0.2	31.5	26.6	52.2
		320	2.6	46	1.5		24.2	28.4	14.6
		340	4.4	49.1	1.2	0.2	23.6	25.9	25.5
BaPtO <sub>3</sub> , Cryst	2860	360	6.7	43.8	8.1	0.3	24.2	23.6	38.7
		380	6.5	37.1	1.8	0.3	32.0	28.9	30.6

a. Pressure = 970-1000 psig, GHSV = gas hourly space velocity, TEMP = temperature, CO CONV = CO conversion, STY = space time yield, MeOH = methanol, C2OX = ethanol + acetaldehyde + acetic acid, HIOX = C3-C6 alcohols, HC = hydrocarbons, OXY = oxygenated organics, Amorph = amorphous by XRPD, Cryst = crystalline by XRPD.

# CHARACTERIZATION OF PEROVSKITES RECOVERED AFTER CATALYST EVALUATION

PEROVSKITE (a)	MAX RXN TEMP, °C (b)	XRPD(c) STRUCTURE PRESERVED	OTHER PHASES	EXAFS/XANES, BULK OXID STATE		ESCA, SURFACE OXID STATE	
				FRESH	USED	FRESH	USED
LaCoO <sub>3</sub>	RUNAWAY	NO					
LaCoO <sub>3</sub>	300	YES, (PR)		+ 3	+ 2	+ 0	> 0
LaNiO <sub>3</sub>	RUNAWAY	NO		+ 3	+ 1, 0		
LaNiO <sub>3</sub>	340	YES, (PR)					
LaFeO <sub>3</sub>	320	YES		+ 3	+ 3	> 0	> 0
LaFeO <sub>3</sub>	360	YES					
LaFeO <sub>3</sub>	380	YES		+ 3	+ 3	> 0	> 0
LaMnO <sub>3</sub>	380	YES					
LaFeO <sub>0.5</sub> Co <sub>0.5</sub> O <sub>3</sub>	380	YES					
LaNiO <sub>0.5</sub> Co <sub>0.5</sub> O <sub>3</sub>	RUNAWAY	NO					
LaNiO <sub>0.5</sub> Fe <sub>0.5</sub> O <sub>3</sub>	380	YES					
LaMnO <sub>0.5</sub> Co <sub>0.5</sub> O <sub>3</sub>	380	YES					
LaMnO <sub>0.5</sub> Ni <sub>0.5</sub> O <sub>3</sub>	380	YES					
LaMnO <sub>0.5</sub> Fe <sub>0.5</sub> O <sub>3</sub>	380	YES					
LaO <sub>0.8</sub> Ce <sub>0.2</sub> CoO <sub>3</sub>	RUNAWAY	NO					
LaO <sub>0.8</sub> Si <sub>0.2</sub> CoO <sub>3</sub>	RUNAWAY	NO					
LaCoO <sub>0.5</sub> Ru <sub>0.5</sub> O <sub>3</sub>	360	YES					
LaNiO <sub>0.5</sub> Ru <sub>0.5</sub> O <sub>3</sub>	RUNAWAY	YES					
LaFeO <sub>0.5</sub> Ru <sub>0.5</sub> O <sub>3</sub>	RUNAWAY	YES					
LaNiO <sub>0.5</sub> Ti <sub>0.5</sub> O <sub>3</sub>	380	YES					
LaFeO <sub>0.5</sub> Ti <sub>0.5</sub> O <sub>3</sub>	380	YES					
LaCuO <sub>0.5</sub> Ti <sub>0.5</sub> O <sub>3</sub>	380	YES, (PR)					
LaCuO <sub>0.5</sub> Mn <sub>0.5</sub> O <sub>3</sub>	380	YES, (PR)					
LaCuO <sub>0.5</sub> Ni <sub>0.5</sub> O <sub>3</sub>	RUNAWAY	NO					
LaCuO <sub>0.5</sub> FeO <sub>3</sub>	RUNAWAY	YES					
LaCuO <sub>0.5</sub> CoO <sub>3</sub>	RUNAWAY	NO					
BaRuO <sub>3</sub> , Amorph	360	NO	BaCO <sub>3</sub> , Ru(0)	+ 4	0	+ 4	+ 4, 0
BaRuO <sub>3</sub> , Cryst	RUNAWAY	NO	BaCO <sub>3</sub> , Ru(0)				
BaRhO <sub>3</sub> , Amorph	RUNAWAY	NO	BaCO <sub>3</sub> , Rh(0)	+ 4	0	+ 3	0
BaRhO <sub>3</sub> , Cryst	RUNAWAY	NO	BaCO <sub>3</sub> , Rh(0)				
BaIrO <sub>3</sub> , Amorph	380	NO	BaCO <sub>3</sub> , Ir(0)	+ 4	0	+ 4, + 3	+ 3
BaIrO <sub>3</sub> , Cryst	380	NO	BaCO <sub>3</sub> , Ir(0)				
BaPtO <sub>3</sub> , Amorph	380	NO	BaCO <sub>3</sub> , Pt(0)	+ 4	0	+ 4, + 2	+ 2, 0
BaPtO <sub>3</sub> , Cryst	380	NO	BaCO <sub>3</sub> , Pt(0)				

(a) Amorph = amorphous by XRPD, Cryst = crystalline by XRPD.

(a) Amorphous by xrd, crystalline by xrd.  
(b) Runaway indicates that the catalyst bed temperature has exceeded 500°C.

runaway indicates that the catalyst bed temperature has exceeded 500°C. (c) PR indicates that the perovskite structure has apparently been partially reduced through the formation of oxide vacancies, but the lattice has been essentially preserved.

FISCHER-TROPSCH SLURRY CATALYSTS FOR SELECTIVE  
TRANSPORTATION FUEL PRODUCTION

W. E. Carroll, N. Cilen, H. P. Withers, Jr.

AIR PRODUCTS AND CHEMICALS, INC.  
P. O. Box 538, Allentown, PA 18105

©Air Products and Chemicals, Inc., 1986

### Introduction

The future use of coal as a source of conventional transportation fuel will depend on the development of an economical and energy efficient liquefaction process. Technologies that have been commercially proven or that are close to commercialization include the fixed- and fluidized-bed Fischer-Tropsch (FT) synthesis, methanol synthesis (fixed-bed and slurry-phase) and the Mobil methanol-to-gasoline process. Of these technologies, the Fischer-Tropsch hydrocarbon synthesis produces the widest slate of products and has been in operation for the longest period.

The FT reaction produces hydrocarbons with a broad spectrum of molecular weights ranging from methane to paraffin waxes. This broad product distribution significantly limits the maximum yield of transportation fuel fraction and creates the need for further downstream processing such as hydrocracking and light olefin oligomerization to increase such yields. Research has shown that selectivity is controlled mainly by catalyst composition and process conditions. In order to improve the economics of the FT process, a catalyst should display high activity and minimize the formation of both light hydrocarbons ( $C_1$ - $C_4$ ) and waxes ( $C_{24}^+$ ), while producing the bulk of the product fraction in either the gasoline ( $C_5$ - $C_{11}$ ) or diesel ( $C_{12}$ - $C_{18}$ ) ranges. Product selectivity, however, has been more successfully controlled by manipulating process conditions. Since the FT reaction is exothermic, control of the reaction heat plays a major role in controlling product selectivity. The slurry-phase process offers the best means of heat transfer and temperature control and has been shown to improve liquid product selectivity mainly by lowering the light gas yield(1). The amount of data from slurry-phase operation, however, is limited to only a few studies and significant differences have been reported in yields, catalyst life and ease of operation(1-4). More research is needed to fully determine the potential of slurry-phase FT processing, and we will describe our efforts in developing new slurry-phase FT catalyst systems.

Under an earlier contract with the Department of Energy, Air Products and Chemicals, Inc. developed several new slurry-phase FT catalysts that enhanced selectivity to liquid fuel products(5). One group of catalysts included supported metal carbonyl clusters modified by promoters. To further develop and improve these catalyst systems, Air Products has begun a program to thoroughly investigate the preparation, characterization and performance of metal carbonyl cluster-based catalysts for use in slurry phase FT technology. Our overall objectives focused predominately on increasing catalyst activity, improving product selectivity for liquid fuels, reducing the yield of methane, developing catalyst systems active at high  $CO/H_2$  ratios and incorporating water-gas shift activity. Catalysts were evaluated by a combination of tests in stirred and fixed-bed reactors. In addition, catalysts were characterized by surface techniques and bulk analyses.

### Experimental

Catalyst Preparation: Catalyst precursors and supports were purchased from commercial sources. The following supports were used after a calcining treatment at 500°C for 3 hr in air:  $\gamma$ - $Al_2O_3$  (Catapal® SB, 217 m<sup>2</sup>/g),  $SiO_2$  (Davison 952, 339

m<sup>2</sup>/g), MgO·3.6 SiO<sub>2</sub> (Florisil®, 298 m<sup>2</sup>/g) and TiO<sub>2</sub> (Degussa P-25, 50 m<sup>2</sup>/g). The catalysts and precursors were protected from air and moisture using standard Schlenk techniques(6) and a Vacuum Atmospheres dry box. All solvents were reagent grade and distilled from sodium benzophenone ketyl in a nitrogen atmosphere. Immediately prior to use, the supports were further dried in vacuo at 110°C for 1-2 hr. Catalysts were prepared by impregnation (to incipient wetness) of the supports with separate solutions containing the promoter and metal carbonyl. Several promoters were evaluated, with one being particularly effective. All catalysts discussed in this report made use of this promoter (designated "Prom"). This method was used for the following catalysts that were prepared from metal carbonyls:

- 3.8% Co/6.8% Prom on Al<sub>2</sub>O<sub>3</sub>
  - 2.8% Ru/4.9% Prom on Al<sub>2</sub>O<sub>3</sub>
  - 4.7 Co on Al<sub>2</sub>O<sub>3</sub> (no promoter)
  - 5.1% Co/4.4% Prom on Al<sub>2</sub>O<sub>3</sub>
  - 4.0% Co/6.4% Prom on Al<sub>2</sub>O<sub>3</sub>
  - 10.8% Co/8.5% Prom on Al<sub>2</sub>O<sub>3</sub>
  - 3.5% Co/6.6% Prom on SiO<sub>2</sub>
  - 3.7% Co/7.2% Prom on MgO·3.6 SiO<sub>2</sub>
  - 3.5% Co on TiO<sub>2</sub> (no promoter)
- } basecase catalysts

Two catalysts were also prepared using Co(NO<sub>3</sub>)<sub>2</sub> as the cobalt source. The method was slightly modified, in that after addition of the promoter and removal of the solvent, the material was exposed to air. An aqueous solution of Co(NO<sub>3</sub>)<sub>2</sub> was then used to impregnate the support, the material was dried at 110°C and calcined at 300°C in air for 5-6 hr. The two catalysts and their analyses are as follows:

- 4.2% Co/7.1% Prom on γ-Al<sub>2</sub>O<sub>3</sub>
- 4.6% Co/7.5% Prom on SiO<sub>2</sub>

Gas Phase Tests: Prior to slurry-phase testing, gas-phase tests were conducted to screen catalyst activity. Those catalysts with gas-phase activities greater than 20 mol of syngas converted/kg of catalyst/hr were selected for further slurry-phase testing.

The gas phase reactor was a fixed-bed, 316 SS tubular unit with downflow configuration and 10 cc bed volume. All gas-phase tests used a CO/H<sub>2</sub> feed ratio of 1 at 300 psig and nearly all were conducted at 1000 GHSV (v/v). Temperature was varied in the range of 220 to 280°C. For the gas-phase tests, the catalyst was activated with H<sub>2</sub>.

Slurry Phase Tests: Two continuous, stirred, 1 liter autoclave reactors were used for slurry tests. Figure 1 shows a schematic diagram of one of these units. For the slurry phase tests, catalysts were activated in a separate, 150 cc fixed bed tubular unit using either pure H<sub>2</sub> or 20% syngas in N<sub>2</sub>. Activated catalyst was slurried in deoxygenated paraffin oil (Fisher #0-122) in the dry box and transferred to the slurry autoclave reactor under a N<sub>2</sub> blanket.

Slurry tests were performed continuously for up to 21 days, except for the test of basecase Co on promoted alumina, which was run for 55 days. Inlet CO/H<sub>2</sub> ratios were 2, 1.5, and 0.5, with emphasis on CO-rich feeds. Space velocities were 1 and 2 NL/g of catalyst/hr. Operating pressures and temperatures ranged from 300 to 600 psig and 220 to 280°C, respectively. The solids content of the slurry was 15 to 25 wt%.

Because of the complexity of the Fischer-Tropsch product, equilibration of the reactor and the product collection systems, and a flexible quantitative analysis scheme incorporating all products including waxes were required to produce good carbon and hydrogen material balances, which were in the range of 95-105%. The details of the analytical and data handling system have been published(7). The method, illustrated schematically in Figure 2, consisted of four separate gas

chromatographs linked via a Perkin-Elmer Sigma 15 computing integrator/controller to a Tektronix 4052 microcomputer equipped with a 1.9-megabyte disk system.

**Catalyst Characterization:** Catalyst supports were characterized by B.E.T. surface area measurements, mercury intrusion porosimetry, helium pycnometry, and particle size distribution. Freshly prepared catalysts and reduced catalysts were characterized by B.E.T. surface area measurements and hydrogen chemisorption. Metal loadings were determined in-house and at Schwarzkopf Microanalytical Laboratories. Some of the catalysts were also studied using X-ray photoelectron spectroscopy and X-ray diffraction.

## Results and Discussion

The type of activation used for "conventional" FT catalysts has been shown by several researchers to affect performance(8). Dry detailed the effects of activation on the performance of precipitated and fused iron catalysts(9) and indicated that pure  $H_2$  was preferred. Another recent study of catalyst performance vs. degree of reduction for  $Co(NO_3)_2$  on alumina used only  $H_2$  reduction(10). The activation of supported metal carbonyl catalysts has generally been done by thermal decomposition under vacuum or inert atmosphere(11). The effect of reducing gases such as  $H_2$  and syngas on supported metal carbonyls has not been well established, but these gases should improve the degree of metal reduction since the metals are initially oxidized by the support.

Our study of activation conditions compared pure  $H_2$  activation with syngas ( $CO/H_2 = 1$ ) activation using the 4% Co on promoted alumina catalyst. Hydrogen activation significantly improved both activity and liquid fuel selectivity in the slurry tests. Figure 3 compares syngas conversion following both types of activation as a function of temperature and space velocity. At comparable reaction conditions,  $H_2$  activation converted 30 to 40% more syngas in the 220 to 260°C range, but at 280°C, the difference was less. For  $H_2$ -activated catalyst at lower space velocity, the syngas conversion appeared to be independent of temperature between 240 and 280°C.

Table 1 shows that  $H_2$  activation increased the  $C_{5-23}$  selectivity by 25 relative percent, from 57 to 71 wt% and decreased both the  $CH_4$  and wax selectivity. The increased activity probably resulted from a higher degree of Co reduction but the reason for the enhanced liquid fuel selectivity is less clear. Perhaps the degree of reduction and metal particle sizes which both depend on activation conditions together affect chain growth probability. However, we did not examine or compare the catalysts from different activation procedures for these two properties. Since a major objective of our research was to study the use of metal carbonyls as catalyst

Table 1. Effect of syngas vs. hydrogen activation on hydrocarbon selectivity.

4% CO ON PROMOTED - $Al_2O_3$		
	SYNGAS	$H_2$
SPACE VELOCITY, NL/g cat/hr.	1.8	2.0
$CO/H_2$	1.5	1.5
PRESSURE, PSIG	300	300
TEMPERATURE, °C	250	256
WT%		
$C_1$	11.5	7.2
$C_{2-4}$	10.4	10.6
$C_{6-11}$	28.2	34.1
$C_{12-18}$	15.3	27.9
$C_{19-23}$	12.5	8.5
$C_{24}^*$	21.1	11.4
$C_{6-23}$	67.0	70.8

precursors, a comparison to conventionally prepared catalysts was necessary. This was done by examining catalysts prepared from cobalt nitrate using the same support and promoter as the cobalt carbonyl-based catalysts. The activity and selectivity of the two catalysts in the slurry-phase reactor are compared in Table 2. Both

catalysts had similar cobalt and promoter loadings. Again, performance differences were larger at lower temperatures. At 240°C, bulk activity of the carbonyl catalyst was more than twice that of the nitrate catalyst, while specific activity was three times higher. At 260°C, the carbonyl catalyst still outperformed the nitrate catalyst in both bulk activity (29% increase) and specific activity (52% increase). The carbonyl-prepared catalyst also provided better liquid fuel selectivity at both temperatures, producing less methane but more light hydrocarbons ( $C_{2-4}$ ). The major difference was in the production of heavier hydrocarbons, with the nitrate-derived catalyst giving significantly higher  $C_{7+}$  selectivity. These differences are likely related to metal particle sizes and work is in progress toward characterizing and comparing these catalysts.

Table 2. Effect of Co source on activity and selectivity.

4% Co ON PROMOTED $Al_2O_3$ ( $CO/H_2 = 1.0$ , 2.0 NL/hr-g cat, 300 psig)				
COBALT SOURCE	CARBONYL		NITRATE	
	240°C	260°C	240°C	260°C
BULK ACTIVITY, mol SYNGAS/kg cat/hr	35.3	36.5	15.8	29.9
SPECIFIC ACTIVITY, mol CO/mol Co/min	0.29	0.32	0.09	0.21
SELECTIVITY, WT%				
$C_1$	7.9	10.4	10.9	16.5
$C_{2-4}$	13.7	15.0	6.5	11.1
$C_{5-11}$	37.0	44.5	12.9	26.5
$C_{12-18}$	23.4	25.8	19.6	23.8
$C_{19-23}$	6.9	2.0	21.9	10.6
$C_{24+}$	9.1	2.3	28.0	11.5
TOTAL FUELS $C_{5-23}$	69.3	72.3	54.6	60.9

Several other parameters were examined using the carbonyl-based catalysts. The effect of cobalt to promoter ratio on activity was examined with alumina-supported catalysts. Figure 4 plots specific activity vs. cobalt/promoter ratio for slurry-phase tests at similar reaction conditions and different activation procedures. Catalyst that had undergone syngas activation showed a decrease in specific activity as the Co/promoter ratio increased. The specific activity of the  $H_2$ -activated catalyst, however, was independent of this ratio. One possible explanation involves the interaction of cobalt with the support and its subsequent reducibility. As the amount of promoter decreases, the cobalt interacts more strongly with the support and becomes more difficult to reduce. This decreased reducibility is especially evident when the catalyst is activated with syngas; the cobalt is not sufficiently reduced, resulting in lower activity. Hydrogen, on the other hand, provides sufficient reducing power to activate cobalt that is more strongly associated with the support.

The effect of cobalt loading on bulk activity of the cobalt carbonyl-promoted alumina catalyst was examined in the slurry reactor at 240 and 260°C (Figure 5). Higher loading gave lower bulk activities at both temperatures. Since the catalyst having the higher cobalt loading also had a higher metal dispersion, these results agree with the general trend of increasing activity with decreasing dispersion reported in the literature.

The type of support also had a major influence on catalyst activity, as shown in Figure 6. These catalysts all had similar cobalt and promoter loadings, except for the  $TiO_2$ -supported catalyst, which had no promoter. The silica-supported catalyst was approximately twice as active as all the others. This may be due to the low reactivity between cobalt carbonyl and silica as opposed to the high reactivity of the other supports towards metal carbonyls. A surface area effect is being checked by using a lower surface area silica.

We also studied the effects of operating parameters such as temperature and  $CO/H_2$  feed ratio on catalyst performance. As expected, increasing the reaction temperature increased the bulk activity of both  $Al_2O_3$ - and  $SiO_2$ -supported Co catalysts, as shown

in Figure 7. The  $\text{SiO}_2$ -supported catalyst activity was independent of temperature at 240°C and 260°C, but increased at 280°C. The activity of the  $\text{Al}_2\text{O}_3$ -supported catalyst began to level off at higher temperatures.

The ratio of carbon monoxide to hydrogen in the feed strongly affected catalyst activity, as shown in Figure 8 for promoted cobalt on silica. The catalyst performed best with  $\text{H}_2$ -rich feed; when the feed was stoichiometric with respect to hydrocarbon ( $-\text{CH}_2-$ ) formation ( $\text{CO}/\text{H}_2 = 0.5$ ), the syngas conversion was highest at 60%. Conversion dropped dramatically to only 25% when the  $\text{CO}/\text{H}_2$  ratio was increased to 1.5.

This poor performance with CO-rich feeds reflects the low activity for the water-gas shift reaction. Figure 9 further illustrates this by comparing  $\text{CO}/\text{H}_2$  usage ratios with feed ratios for the supported cobalt and ruthenium catalysts, as well as, a precipitated iron catalyst, all in the slurry reactor. The cobalt catalyst showed the poorest CO usage at all feed levels, usage ratios never exceeded 0.60. The ruthenium catalyst offered some improvement with a usage ratio nearly matched to a  $\text{CO}/\text{H}_2$  feed ratio of 1.0. The usage ratio, however, never improved above 1.0 as the feed ratio was increased. The slight improvement in shift activity for ruthenium correlates with its observed shift activity in homogeneous systems(12). Neither catalyst showed the excellent shift activity that is exhibited by precipitated or fused iron catalysts.

In an effort to improve the shift activity of the promoted Co on alumina catalyst, a commercially available, low temperature shift catalyst ( $\text{Cu}/\text{Zn}/\text{Al}_2\text{O}_3$ ) was physically mixed with it and tested in the gas phase reactor. The results are summarized in Table 3 along with results in which no shift catalyst was added. The added shift catalyst caused a drop in activity with no indication of enhanced shift activity. There was an increase in oxygenate production, especially of ethanol and higher alcohols. A second gas-phase test of the mixed catalysts, this time using preactivated shift catalyst, still gave lower activity than without shift catalyst, but shift activity increased slightly. Upon increasing the feed ratio from 1.0 to 1.9, however, shift activity declined as the usage ratio dropped to 0.35.

Table 3. Addition of  $\text{Cu}/\text{Zn}/\text{Al}$  water-gas shift catalyst to  $\text{Co}/\text{Prom}/\text{Al}_2\text{O}_3$  FT catalyst.

Catalyst <sup>(1)</sup>	$\text{CO}/\text{H}_2$	Usage Ratio ( $\text{CO}/\text{H}_2$ )	% Conversion, $\text{CO} + \text{H}_2$	Bulk Activity, (mol syngas/kg cat/hr)
90% F-T + 10% SHIFT	1.0	0.53	36	16.8
90% F-T + 10% SHIFT (Preactivated)	1.0	0.55	44	21.6
BASECASE F-T	1.9	0.35	16	8.6
	1.0	0.59	55	27.0

<sup>(1)</sup> CONDITIONS: 240°C, 300 psig, 1000 GHSV

Another important objective of this study was catalyst characterization and its correlation to catalyst performance. X-ray photoelectron spectroscopy (XPS) was used to examine cobalt oxidation states; three spectra are shown in Figure 10. The lower spectrum is that for oxidized Co on promoted  $\text{Al}_2\text{O}_3$  prepared from  $\text{Co}(\text{NO}_3)_2$ . The binding energy for Co 2p electrons of 781 eV corresponds to established values for Co(II) and Co(III). The strong interaction of cobalt with alumina was evident from the XPS data on fresh catalyst prepared from zero-oxidation-state  $\text{Co}_2(\text{CO})_8$ . This data, shown as the middle spectrum, indicates that most of the cobalt is oxidized to 2+ and 3+. Only a shoulder corresponding to a binding energy less than 780 eV suggests the presence of a small amount of zero valent cobalt. Finally, upon activation in pure  $\text{H}_2$  at 300°C, the top spectrum was obtained, indicating the presence of a only oxidized cobalt. This is further evidence for a strong

metal-support interaction. That supported cobalt is difficult to reduce, especially at low loadings, is well established(10). Hall and coworkers have used XPS to show that after  $H_2$  reduction at 250°C, alumina-supported  $Co_4(CO)_{12}$  had only 25% of its cobalt as zero valence(13).

Hydrogen chemisorption was used to determine active cobalt surface area and percent dispersion. These results, presented in Table 4, are consistent with the XPS data, showing only small amounts of metallic cobalt. Hydrogen chemisorption was low, especially at room temperature and low loadings. This activated adsorption has been reported by Reuel and Bartholomew(14) and is possibly due to some metal support

Table 4. Catalyst properties.

Catalyst	B.E.T. Surface Area	Total $H_2$ Uptake	Active Metal Surface Area	% Dispersion
4% Co/Prom/ $Al_2O_3$	209 $m^2/g$	5.6 $\mu mol/g$ at 55°C	0.4 $m^2/g$	1.2
10.8% Co/Prom/ $Al_2O_3$	N.A.	101.2 at 100°C	5.4	9.7
3.5% Co/Prom/ $SiO_2$	318	39.8 at 100°C	3.0	10
3% Co/ $SiO_2$ <sup>(1)</sup>	N.A.	20	N.A.	11
3% Co/ $Al_2O_3$ <sup>(1)</sup>	N.A.	8.6	N.A.	10
22% Co/0.5% Ru/Th/ $Al_2O_3$ <sup>(2)</sup>	150-225	150-200	N.A.	N.A.

<sup>(1)</sup> C. H. Bartholomew (1985) <sup>(2)</sup> U.S. Patent 4,413,064 to Gulf (11/1/83).

interaction. Comparison shows our data are consistent with those of Bartholomew. Furthermore, a 22% Co/0.5% Ru/Th/ $Al_2O_3$  catalyst described in a U.S. Patent to Gulf showed high  $H_2$  chemisorption, probably because reduction occurs more readily as metal loading is increased.

Finally, we compared the activity of our supported cobalt catalysts with other supported cobalt catalysts (see Table 5). All of the data, except one, are from fixed-bed reactors. Our bulk activities fall near that of the Gulf catalyst, but are somewhat lower than that of the Shell catalyst. Note though that our data were not obtained at the optimum  $H_2/CO$  feed ratio of 2.0, at which the other catalysts were tested. Turnover frequencies, based on  $H_2$  chemisorption data, are quite good for our catalysts.

Table 5. Catalyst activity comparisons, fixed-bed reactors.

Catalyst	Temp. (°C)	Press. (psig)	Feed $H_2/CO$	Bulk Activity (mol syngas/kg cat/hr)	Turnover Frequency (molecules CO/site-sec) $\times 10^3$
3.5% Co/Prom/ $SiO_2$	220	300	1.0	31	50
3.5% Co/Prom/ $SiO_2$ (Slurry)	240	300	1.0	36	41
10.8% Co/Prom/ $Al_2O_3$	220	300	1.0	18	14
17% Co/Zr/ $SiO_2$ (Shell)	220	300	2.0	91	N.D.
22% Co/0.5% Ru/Th/ $Al_2O_3$ (Gulf)	215	15	2.0	34	9
3% Co/ $SiO_2$ (Bartholomew)	225	15	2.0	N.D.	6

### Acknowledgments

We would like to acknowledge the U.S. Department of Energy (Contract No. DE-AC22-84PC70030) and Air Products and Chemicals, Inc. for supporting this work. The skilled technical assistance of P. A. Dotta, G. W. Long, M. Louie, V. A. Monk and L. E. Schaffer, is greatly appreciated, as well as the contributions of S. A. Motika and D. A. Bohling.



## References

1. H. Kolbel and M. Ralek, Catal. Rev. Sci. Eng., **21**, 225 (1980).
2. M. L. Poutsma, "Assessment of Advanced Process Concepts for the Liquefaction of Low  $H_2/CO$  Ratio Synthesis Gas", ORNL-5635 (1980).
3. W.-D. Deckwer, Y. Serpeman, M. Ralek and B. Schmidt, Ind. Eng. Chem. Proc. Des. Dev., **21**, 222 and 231 (1982).
4. C. N. Satterfield, G. A. Huff and J. P. Longwell, Ind. Eng. Chem. Proc. Des. Dev., **21**, 465 (1982).
5. (a) R. Pierantozzi, E. G. Valagene, A. F. Nordquist and P. N. Dyer J. Mol. Catal., **21**, 189 (1983).  
(b) J. V. Bauer, B. W. Brian, S. A. Butter, P. N. Dyer, R. L. Parsons, and R. Pierantozzi in "Catalytic Conversions of Synthesis Gas and Alcohols to Chemicals", R. G. herman, ed., Plenum, New York (1984), pp. 129-149.
6. "The Manipulation of Air-Sensitive Compounds", D. F. Shriver, McGraw-Hill, New York (1969).
7. J. V. Bauer and P. N. Dyer, Chem. Eng. Prog., **78** (9), 51 (1982).
8. C. N. Satterfield and H. G. Stenger, Ind. Eng. Chem. Proc. Des. Dev., **23**, 849 (1984).
9. M. E. Dry in "Catalysis - Science and Technology", J. R. Anderson and M. Boudart, eds., Vol. 1, Springer-Verlag, New York (1981) p. 159.
10. S. H. Moon and K. E. Yoon, Applied Catalysis, **16**, 289 (1985).
11. J. Zwart and R. Snel, J. Mol. Catal., **30**, 305 (1985).
12. P. C. Ford, C. Ungermann, V. Landis, S. A. Moya, R. C. Rinker and R. M. Laine, "Advances in Chemistry Series, No. 173: Inorganic Compounds with Unusual Properties-II", R. B. King, ed., American Chem. Soc. (1979).
13. G. F. Meyers and M. B. Hall, Inorg. Chem., **23**, 124 (1984).
14. (a) R. C. Reuel and C. H. Bartholomew, J. Catal., **85**, 78 (1984).  
(b) R. C. Reuel and C. H. Bartholomew, J. Catal., **85**, 63 (1984).

FIGURE 1

**CONTINUOUS, AUTOMATED FISCHER-TROPSCH SLURRY REACTOR**

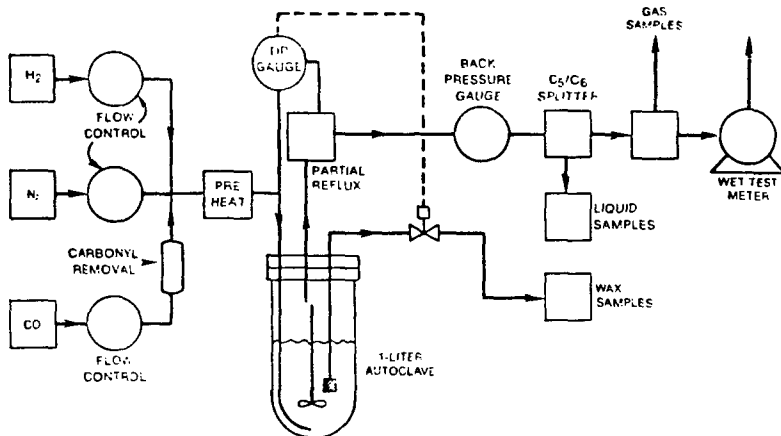


FIGURE 2

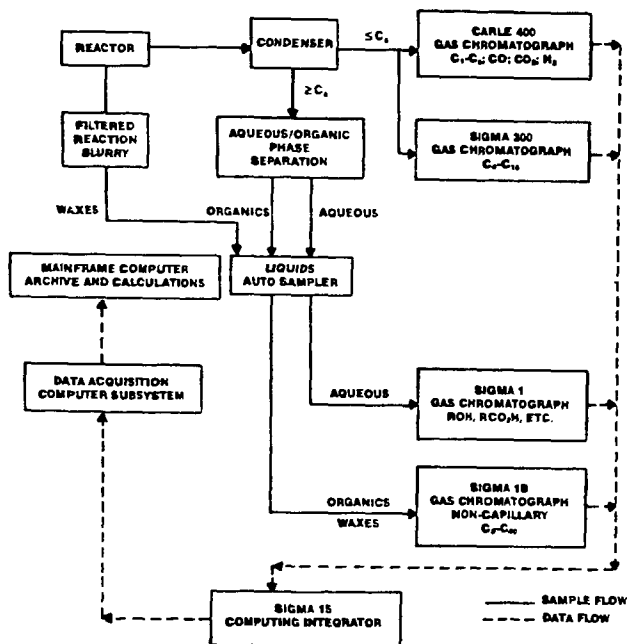


FIGURE 3

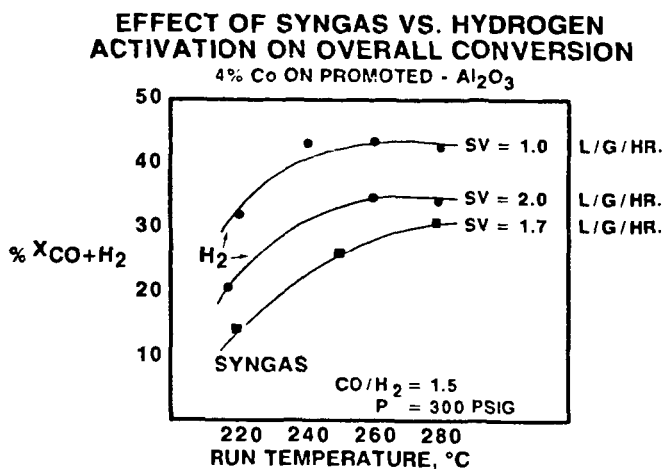


FIGURE 4

**Co/PROMOTER RATIO EFFECT ON ACTIVITY**  
Co ON PROMOTED -  $\text{Al}_2\text{O}_3$

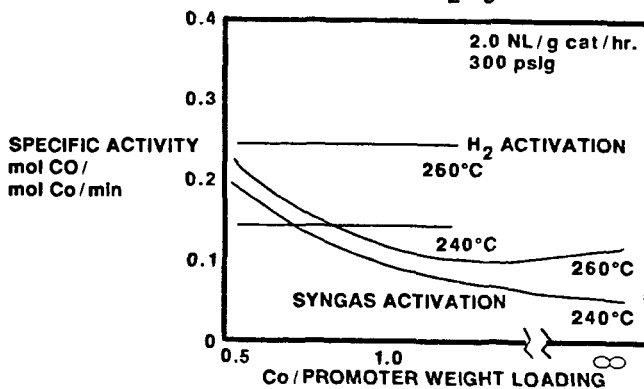


FIGURE 5

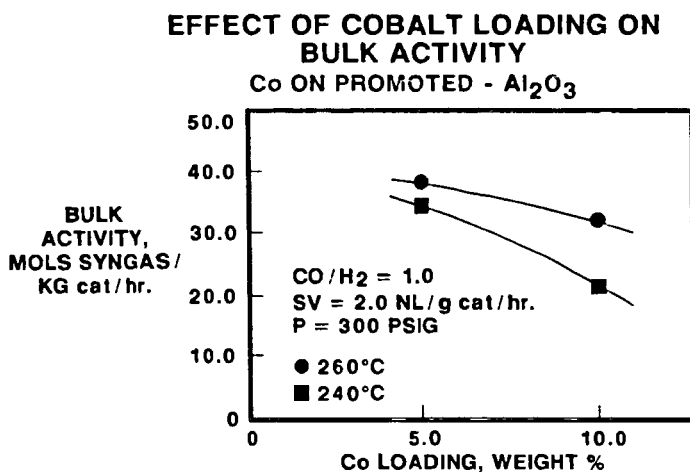


FIGURE 6

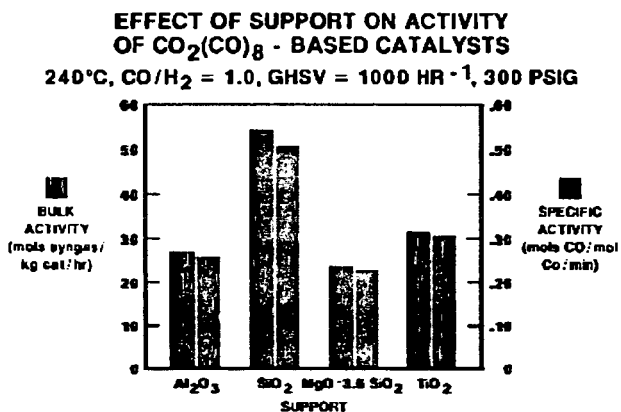


FIGURE 7

**BULK ACTIVITY DEPENDENCY ON TEMPERATURE  
Co CATALYSTS**

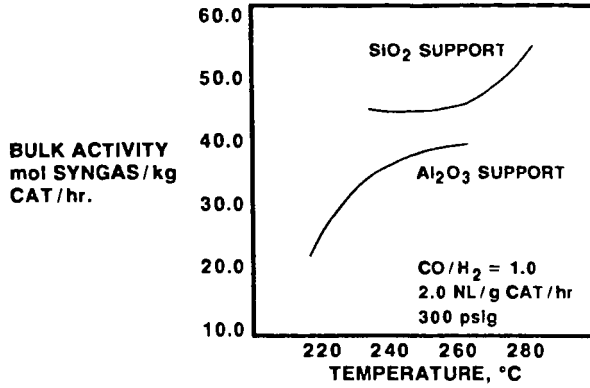


FIGURE 8

**CONVERSION DEPENDENCY ON  
 $\text{CO}/\text{H}_2$  FEED  
3.5% Co ON PROMOTED -  $\text{SiO}_2$**

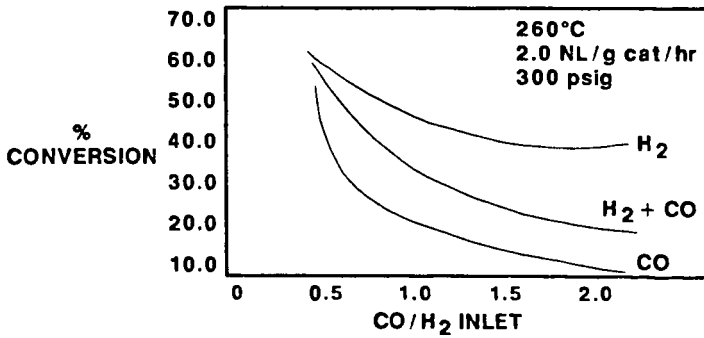


FIGURE 9

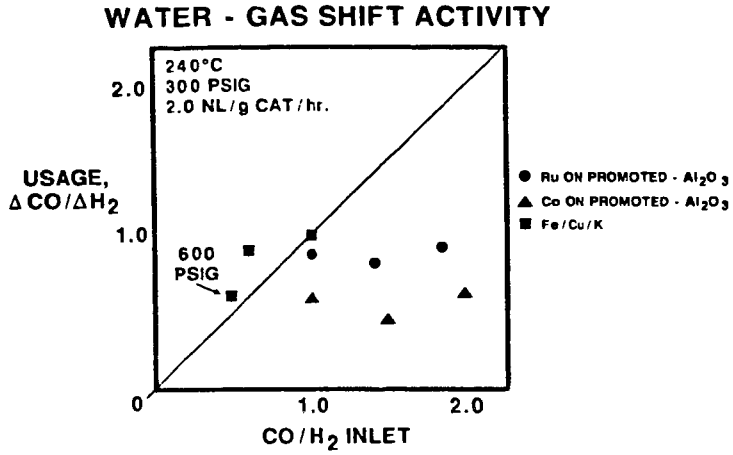
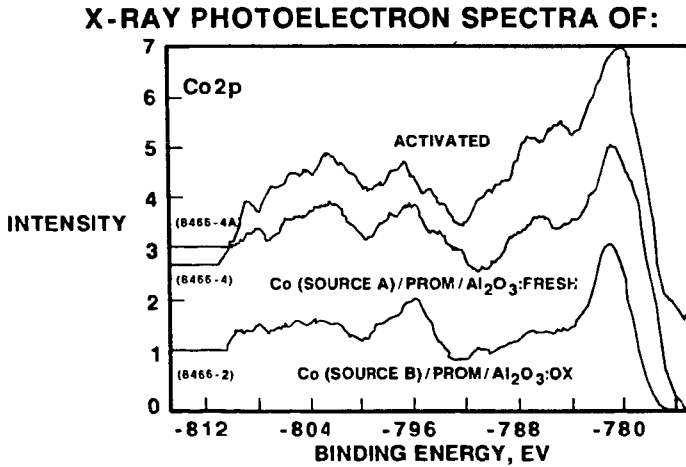


FIGURE 10



## THE HYDROGENATION OF CARBON MONOXIDE OVER RANEY IRON-MANGANESE CATALYSTS

K. R. Chen, F. V. Hanson, N. K. Nag and A. G. Oblad

Department of Fuels Engineering  
University of Utah  
Salt Lake City, UT 84112-1183

### INTRODUCTION

The hydrogenation of carbon monoxide for the synthesis of hydrocarbons was extensively investigated in Germany beginning in the 1920s<sup>(1)</sup> and in the United States during the 1950s.<sup>(2)</sup> These early studies focused on the production of liquid hydrocarbons and methane and very little attention was paid to the synthesis of low-molecular weight hydrocarbons such as ethane, ethylene, propane, butane and butylenes.

Coprecipitated iron-manganese catalysts<sup>(3)</sup> gave favorable selectivity for low molecular weight olefins. This preliminary investigation<sup>(3)</sup> was extended to include process variable and reactor studies using coprecipitated iron-manganese catalysts.<sup>(4-6)</sup>

Raney alloy catalysts, first developed by Raney<sup>(7)</sup>, have been used in applications where high activity and selectivity were required in hydrogenation reactions.<sup>(7)</sup> Raney iron-manganese catalysts have recently been studied to determine their selectivity towards low molecular weight  $C_2$ - $C_4$  olefins.<sup>(8)</sup>

The objective of this investigation was to determine the optimum operating conditions for the production of low-molecular weight olefins over Raney iron-manganese catalysts.

### EXPERIMENTAL APPARATUS AND PROCEDURES

#### Raney Alloy Preparation

The individual metal components; aluminum, iron and manganese were weighed in the appropriate proportions: Al/Fe/Mn = 59/38/3 parts by weight, were thoroughly mixed and transferred to a carbon crucible, which was placed inside a ceramic crucible and heated by an electric furnace at 1523 K for 24 hours in flowing argon. The resulting melt was quenched to room temperature. Specific details regarding the preparation procedures have been reported elsewhere.<sup>(8,9)</sup>

#### Raney Catalyst Activation

Fifty grams of the alloy (25-50 mesh) were added in 5 gram aliquots to a well-stirred tank reactor which contained a 25-weight percent solution of sodium hydroxide at 3-minute intervals to avoid a significant temperature rise in the solution. The reaction temperature was controlled at  $363 \pm 5$  K. After all the alloy had been added to the reactor it was maintained at the leaching temperature for an additional 90 minutes in order to complete the leaching of the aluminum. The catalyst was washed with distilled

water until the pH of the decanted solution was  $7.0 \pm 0.3$ . It was then washed three times with 95% alcohol, followed by three times with 100% alcohol. The catalyst was stored under 100% ethyl alcohol in a refrigerator for subsequent characterization and evaluation.

#### Catalyst Evaluation Apparatus

A fixed-bed flow reactor was used to evaluate the catalysts. The flow rates of  $H_2$  and CO gases were controlled by mass flow meters (Union Carbide Model FM 4550) which were calibrated at different operating pressures for a variety of flow rates. A Grove loader was used as a back pressure control valve to maintain the reactor system pressure constant. Downstream from the Grove loader, the pressure dropped to the ambient pressure. A condenser at the ambient temperature and pressure was used to collect the liquid products. The condensable vapor-free product gas flow was measured with a wet test meter.

#### Catalyst Evaluation Unit and Operating Procedure

Approximately, 2 grams of dried catalyst was mixed with an appropriate amount of inert Denstone, wetted with water and loaded into the reactor. A hydrogen flow ( $600 \text{ cm}^3/\text{min}$ ) was established through the catalyst bed at the ambient temperature and pressure and was maintained for 1 hour to evaporate any water from the catalyst surface. The temperature of the system was then raised to 648 K in flowing hydrogen and the catalyst was reduced for 6 hours. At the desired temperature, the reactant gas (a mixture of  $H_2/CO$ ) was passed through the system and the pressure was slowly increased to the desired value. The stabilization period for a typical experiment with the Raney iron-manganese catalyst was 6 to 15 hours. When necessary, the system operating variables were changed and after the system stabilized at the new conditions (30 to 45 minutes) the product stream was sampled after an additional 10 minutes. The gas products were analyzed by a gas chromatograph (HP 5830A). A thermal conductivity detector (TCD) was used for carbon dioxide, carbon monoxide and water and a flame ionization detector (FID) was used for the hydrocarbon products up to heptanes. A Chromosorb 102 (80-100 mesh 6.1 meters) column which was capable of resolving methane through the heptanes (saturates and unsaturates), was used.

#### Catalyst Stability Test

The stability of Raney iron-manganese catalyst was determined in an experiment which lasted 36-40 hours. The global heat transfer problem associated with exothermic reactions in fixed-bed reactors was alleviated by loading inert Denstone with the catalyst. The density of Raney catalyst is approximately equal to  $2 \text{ g/cm}^3$ , and 2 grams of it were used in each experiment. The amounts of Denstone diluent loaded with the catalyst in the three experiments were 1, 2, and  $4 \text{ cm}^3$ , respectively. Thus, the volume ratios used in the stability tests were 1, 2 and 4.



### Process Variable Investigation

A statistical design<sup>(9)</sup> method was used in the process variable investigation with the Raney iron-manganese catalyst system. Four variables, namely, temperature, pressure,  $H_2/CO$  ratio and space velocity were selected for study. Each process operating variable was assigned five different levels: -2, -1, 0, 1 and 2. The selection of the range of operating variables was based on preliminary experimental data and on experimental design theory. The process operating conditions are listed in Table 1.

### RESULTS AND DISCUSSION

#### Catalyst Loading and Stability Tests

The loading and stability tests were conducted to determine the range of operating conditions for the process variable investigation and to determine the effect of on-stream time on the activity, selectivity and stability of Raney iron-manganese catalysts. The carbon monoxide conversion as a function of run time at different inert diluent to catalyst ratios at 1470 KPa, 443 K, sv of  $4.2 \text{ cm}^3 \text{ g}^{-1} \text{ s}^{-1}$  and  $H_2/CO$  ratio of two is presented in Figure 1. It was determined that the induction period for the catalysts at three different diluent/catalyst ratios was about 15 hours. The two diluted bed experiments gave the same carbon monoxide conversions 2.8%, after 15 hours on stream. The effect of reaction temperature on the product selectivity for two different diluent/catalyst ratios at 1470 KPa, sv of  $4.2 \text{ cm}^3 \text{ g}^{-1} \text{ s}^{-1}$  and  $H_2/CO$  ratio of two are presented in Figures 2 and 3. The temperature had almost no effect on the yields of all products except carbon dioxide in both cases. The carbon dioxide selectivity increased as the temperature increased and the rate of increase was almost the same for both the dense and the diluted bed modes of operation; however, at a given temperature, the carbon dioxide yield for the diluted bed mode was lower than that for the dense bed mode. It was concluded from the higher operating temperature and lower carbon dioxide yields in the diluted bed mode that the surface temperature of the catalyst in dense bed mode was higher than the catalyst surface temperature in the diluted bed. Poor heat transfer in the dense bed caused a higher temperature gradient. The results of the loading and the stability test indicated that the preferred diluent to catalyst ratio was four to one.

#### Process Variable Investigation: $C_2-C_4$ Olefin Yield Response Equation

A statistical design model was used to optimize the  $C_2-C_4$  olefin production. The second order response equation for a four variable system is written as follows:

$$Y_1 = B_0 + B_1X_1 + B_2X_2 + B_3X_3 + B_4X_4 + B_{11}X_1^2 + B_{22}X_2^2 + B_{33}X_3^2 + B_{44}X_4^2 + B_{12}X_1X_2 + B_{13}X_1X_3 + B_{14}X_1X_4 + B_{23}X_2X_3 + B_{24}X_2X_4 + B_{34}X_3X_4$$

where  $Y_1$  is the  $C_2-C_4$  olefin to paraffin ratio response factor,  $X_1$  is the pressure,  $X_2$  is the temperature,  $X_3$  is the reactant gas space velocity, and  $X_4$  is the  $H_2/CO$  molar ratio.

The operating variables, carbon monoxide conversions and the product distributions for 25 design experiments are listed in Table 2. The carbon dioxide yield, the carbon monoxide conversion, the  $C_2$ - $C_4$  hydrocarbon yield, the olefin to paraffin ratio in the  $C_2$ - $C_4$  hydrocarbon fraction and the  $C_5^+$  hydrocarbon yield were used as independent variables in the statistical design computations. The selectivities, as reflected by the olefin to paraffin ratios for the  $C_2$ ,  $C_3$ ,  $C_4$  and  $C_2$ - $C_4$  hydrocarbon fractions, are listed in Table 3. The computed response surface correlation coefficients are listed in Table 4. The F-test technique was used to determine the significance of each coefficient. Those coefficients which were determined not to be significant were eliminated. The reduced set of response surface correlation coefficients from the process variable study are listed in Table 5. The  $C_2$ - $C_4$  olefin to paraffin ratio,  $Y_1$ , can be expressed as a response surface equation from the data as follows:

$$Y_1 = 3.406 - 0.243 X_1 + 0.319 X_2 - 0.884 X_4 + 0.026 X_1^2 - 0.003 X_2^2 + 0.111 X_4^2 + 0.164 X_1 X_4 - 0.233 X_2 X_4$$

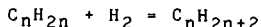
where  $Y_1$ ,  $X_1$ ,  $X_2$ ,  $X_3$  and  $X_4$  have been defined previously.

This equation can be used to quantitatively predict the  $C_2$ - $C_4$  olefin to paraffin ratio for the range of operating variables investigated. The response surface equations for other independent variables can also be constructed using the same technique and the coefficients are presented in Table 5. In this study, the  $H_2/CO$  ratio appeared to be the most significant operating variable. The response factor for the  $C_2$ - $C_4$  olefin to paraffin ratio changed by a factor of unity when the  $H_2/CO$  ratio was changed by a factor of -0.884 and thus the  $H_2/CO$  ratio was judged to be the most significant operating variable while the space velocity was the least significant operating variable influencing the olefin to paraffin ratio. Thus, the space velocity ( $X_3$ ) was eliminated from the response surface equation. The first-order coefficients for the pressure and temperature terms ( $X_1$  and  $X_2$ , respectively) were  $B_1 = -0.243$  and  $B_2 = 0.319$ , respectively. Since the magnitude of each is less than the magnitude of the first order coefficient for the  $H_2/CO$  ratio ( $X_4$ ),  $B_4 = -0.884$ , the temperature and pressure are less significant with regard to the  $C_2$ - $C_4$  olefin-to-paraffin ratio than the  $H_2/CO$  ratio. The first and second order coefficients for the  $C_2$ - $C_4$  and  $C_5^+$  hydrocarbon yields are considerably smaller than their respective zero order coefficients, which indicates that the yield of  $C_2$ - $C_4$  and  $C_5^+$  hydrocarbons is somewhat insensitive to the operating conditions in the range of process variables investigated.

#### Effect of Pressure on Product Distribution and Olefin Selectivity

The carbon monoxide conversion decreased as the pressure decreased. At a temperature of 463 K, a space velocity of  $9 \text{ cm}^3 \text{ g}^{-1} \text{ s}^{-1}$  and a  $H_2/CO$  ratio of one, the carbon monoxide conversion decreased from 4% at 4230 KPa to 2.8% at 1470 KPa. At a temperature of 473 K, a space velocity of  $12 \text{ cm}^3 \text{ g}^{-1} \text{ s}^{-1}$  and  $H_2/CO$  ratio of two, the carbon monoxide conversion decreased from 6.3% at 3540 KPa to 5.7% at 2160 KPa. This decrease may be due to a change in the carbon monoxide surface coverage brought about by the pressure

decrease. The  $C_2$ - $C_4$  olefin to paraffin ratio decreased from 3.8 at 1470 KPa to 2.7 at 4230 KPa. The carbon dioxide,  $C_2$ - $C_4$  hydrocarbons, and  $C_5^+$  hydrocarbon yields remained almost constant in the pressure range from 1470 to 4230 KPa. The olefin to paraffin ratios for the  $C_2$ ,  $C_3$ ,  $C_4$  and  $C_2$ - $C_4$  hydrocarbon fractions also decreased as the pressure increased. The olefin to paraffin ratios for the  $C_2$  and  $C_3$  hydrocarbon fractions were consistently higher than that of the  $C_4$  hydrocarbon fraction in the pressure range investigated: 1470 KPa to 4230 KPa. At a reaction temperature of 453 K, a space velocity of  $9 \text{ cm}^3 \text{ g}^{-1} \text{ s}^{-1}$  and a  $H_2/CO$  ratio of 1, the olefin to paraffin ratios for the  $C_2$ ,  $C_3$ ,  $C_4$  fraction increased from 3.7, 2.8 and 2.1 at 4230 KPa to 4.2, 3.7 and 3.8 at 1470 KPa, respectively. It is obvious from the stoichiometric equation for the olefin hydrogenation reaction:



that the olefinic products are favored at lower pressure.

#### Effect of Temperature on Product Distribution and Olefin Selectivity

The carbon monoxide conversion increased as the temperature increased at a reaction pressure of 3540 KPa, a space velocity of  $12 \text{ cm}^3 \text{ g}^{-1} \text{ s}^{-1}$  and a  $H_2/CO$  of two; that is, the carbon monoxide conversion increased from 5.4% at 453 K to 6.3% at 473 K. The  $C_2$ - $C_4$  olefin to paraffin ratio increased from 2.8 to 3.7 as the temperatures increased from 443 to 483 K. The olefin to paraffin ratios of the  $C_3$  and  $C_4$  fraction increased as the temperature increased, whereas the olefin to paraffin ratio of the  $C_2$  to  $C_3$  hydrocarbon fractions was consistently higher than that of the  $C_4$  hydrocarbon fraction in the temperature range investigated, 443 to 483 K. At a pressure of 2850 KPa, a space velocity of  $9 \text{ cm}^3 \text{ g}^{-1} \text{ s}^{-1}$  and a  $H_2/CO$  ratio of 1, the olefin to paraffin ratios of  $C_2$ ,  $C_3$  and  $C_4$  increased from 4.1, 2.5 and 1.9 at 443 K to 4.3, 3.8 and 3.3 at 483 K, respectively. The carbon dioxide selectivity increased as the temperature increased. This is consistent with the observations made in connection with the catalyst loading and stability tests.

#### Effect of Reactant Gas Space Velocity on Product Distribution and Olefin Selectivity

The carbon monoxide conversion decreased as the space velocity increased (Table 2). At higher space velocities, the contact time between reactant species and the catalyst surface was reduced. The shorter contact time resulted in lower carbon monoxide conversion. At a pressure of 3540 KPa, a temperature of 453 K and a  $H_2/CO$  ratio of two, the carbon monoxide conversion increased from 3.6% to 5.4% as the space velocity decreased from  $12 \text{ cm}^3 \text{ g}^{-1} \text{ s}^{-1}$  to  $6 \text{ cm}^3 \text{ g}^{-1} \text{ s}^{-1}$ . The olefin to paraffin ratios of  $C_2$ ,  $C_3$ ,  $C_4$ , and  $C_2$ - $C_4$  hydrocarbon fractions remained constant in the range of space velocities from 3 to  $15 \text{ cm}^3 \text{ g}^{-1} \text{ s}^{-1}$ . The olefin to paraffin ratios of the  $C_2$  and  $C_3$  hydrocarbon fractions were consistently higher than that of the  $C_4$  hydrocarbon fraction in the range of space velocities from 3 to  $15 \text{ cm}^3 \text{ g}^{-1} \text{ s}^{-1}$ . At other operating conditions, the olefin to paraffin ratios were the same at space velocities of 6 and  $12 \text{ cm}^3 \text{ g}^{-1} \text{ s}^{-1}$ . The yields of the  $C_2$ - $C_4$  and  $C_5$  hydrocarbon yields were independent of space velocity. The carbon dioxide yield decreased from 50% at a

space velocity of  $3 \text{ cm}^3 \text{ g}^{-1} \text{ s}^{-1}$  to 27% at a space velocity of  $15 \text{ cm}^3 \text{ g}^{-1} \text{ s}^{-1}$ . As mentioned in the stability test section, the high space velocity suppresses the Boudouard and water gas shift reactions, thus leading to a decrease in carbon dioxide production.

#### Effect of Hydrogen to Carbon Monoxide Ratio on Product Distribution and Olefin Selectivity

The carbon monoxide conversion decreased as the  $\text{H}_2/\text{CO}$  ratio decreased (Table 2). At a pressure of 2850 KPa, a temperature of 463 K and a space velocity of  $9 \text{ cm}^3 \text{ g}^{-1} \text{ s}^{-1}$  the carbon monoxide conversion decreased sharply from 14.5 % at a  $\text{H}_2/\text{CO}$  ratio of 5 to 0.9 % at a  $\text{H}_2/\text{CO}$  ratio of 0.2. The olefin to paraffin ratios of the  $\text{C}_2$ ,  $\text{C}_3$ ,  $\text{C}_4$ , and  $\text{C}_2\text{-C}_4$  hydrocarbon fractions were very sensitive to the  $\text{H}_2/\text{CO}$  ratio (Table 3). At a constant total pressure a reduction in the hydrogen to carbon monoxide ratio reduces the hydrogen partial pressure in the reactor thus favoring the formation of olefins. The carbon dioxide yield also increased to some extent at the hydrogen to carbon monoxide ratio decreased indicating the rate of the Boudouard reaction increased with lower hydrogen to carbon monoxide ratio.

#### Interaction of Process Variable

The  $\text{C}_2\text{-C}_4$  olefin to paraffin ratios were influenced by the process variables: temperature, pressure and  $\text{H}_2/\text{CO}$  ratio. The coefficient  $B_{14}$  represents the interaction between the pressure and the  $\text{H}_2/\text{CO}$  ratio and was equal to 0.164. Thus, whenever the total pressure or the  $\text{H}_2/\text{CO}$  ratio was changed by one level, the olefin to paraffin ratio in the  $\text{C}_2\text{-C}_4$  hydrocarbon fraction changed by an amount corresponding to a value of 0.164. The coefficient  $B_{24}$  represents the interaction between temperature and the  $\text{H}_2/\text{CO}$  ratio and was equal to -0.223. Thus, whenever the reactor temperature or the  $\text{H}_2/\text{CO}$  ratio is changed one level, the olefin to paraffin ratio in the  $\text{C}_2\text{-C}_4$  hydrocarbon fraction changes by an amount corresponding to a value of 0.223. The retention of interactive terms  $B_{14}$  and  $B_{24}$ , after the analysis of the coefficients is probably related to the influence of pressure, temperature and  $\text{H}_2/\text{CO}$  ratio on the fraction of the surface covered by the reacting species, hydrogen and carbon monoxide and on the ratio of the fraction of the surface covered by each.

#### Statistical Model

The  $\text{C}_2\text{-C}_4$  olefin to paraffin ratio, displayed as a function of process variables, taken two at a time, predicted from the statistical design are presented in Figures 4 and 5. These figures were prepared using a commercial (Golden Graphics) software package (11) on an IBM PC AT. The inverse distance squared algorithm was selected for the grid calculation. (12) the calculation conditions: grid size 21, smooth factor 0.95, view angle 60 degrees, rotation angle 225 degrees, and height/width ratio of one were selected to better display the response surfaces. The variable dependence can be understood by comparing the slopes of the two lines AB and AC in Figure 4. The rate of change of AC as a function of the  $\text{H}_2/\text{CO}$  ratio is greater than that of AB as a function of pressure. The smooth response surface obtained from the correlation

at least indicates that the reaction conditions used in this investigation are reasonable and the predicted model can be extended to other process variables.

#### Optimum Process Operating Conditions

The process operating conditions required to produce the optimal  $C_2$ - $C_4$  hydrocarbon fraction, olefin to paraffin ratio, were computed using the calculated coefficients for the response surface as the input data. As discussed, a lower  $H_2/CO$  ratio, a higher temperature and a lower pressure would be expected to produce a higher olefin to paraffin ratio in the  $C_2$ - $C_4$  hydrocarbon fraction. The  $H_2/CO$  ratio is limited to a minimum value of 0.5 in the experiment to avoid excessive carbon deposition on the catalyst. The optimal operating conditions and the  $C_2$ - $C_4$  olefin to paraffin ratios predicted from the response surface equation were: a pressure of 1470 KPa, a temperature of 473 K, a space velocity of  $12 \text{ cm}^3 \text{ g}^{-1} \text{ s}^{-1}$ , a  $H_2/CO$  ratio of 0.5 and an olefin to paraffin ratio of 5.4. At the predicted optimal operating conditions, an olefin to paraffin ratio of 6.4 was obtained, which was higher than expected. At the optimal operating conditions, the olefin to paraffin ratios for the  $C_2$ ,  $C_3$  and  $C_4$  hydrocarbon fractions were as follows: the ethylene to ethane ratio was 5, the propylene to propane ratio of 9.3 and the butylenes to butanes was 5.2.

#### CONCLUSIONS

1. The activity as reflected by carbon monoxide conversion and the selectivity as reflected by the  $C_2$ - $C_4$  olefin to paraffin ratio of the Raney iron-manganese catalyst were constant up to 40 hours on stream.
2. The most influential operating variable in determining the olefin selectivity is the  $H_2/CO$  ratio.
3. The optimal operating conditions for the maximization of low molecular weight olefins were: a temperature of 473 K, a sv of  $12 \text{ cm}^3 \text{ g}^{-1} \text{ s}^{-1}$ , a  $H_2/CO$  ratio of 0.5 and a pressure of 1470 KPa. The olefin to paraffin ratio at these conditions is 6.4.

#### ACKNOWLEDGEMENT

The financial assistance provided by the Mobil Research and Development Corporation through the Industrial Affiliates Program of the Laboratory of Coal Science, Synthetic Fuels and Catalysis is gratefully acknowledged.

#### REFERENCES

1. Storch, H. H., Couloumbic, N. and Anderson, R. B., The Fischer-Tropsch and Related Synthesis, Wiley, New York, 1951.
2. Gryson, M., Demeter, J. J., Schkesinger, M. D., Johnson, G. E., and Myers, J. W., Synthesis of Methane," Report of Investigations 5137, Bureau of Mines, 1955.

3. Yang, C. H., "Catalytic Synthesis of Light Hydrocarbons from Carbon Monoxide and Hydrogen over Metal Catalysts," Ph.D. Dissertation, University of Utah, Department of Mining and Fuels Engineering, 1979.
4. Tsai, Y. S., "The Hydrogenation of Carbon Monoxide over Unsupported Iron/Manganese Catalysts to Produce Low Molecular Weight Olefins," Master Thesis, University of Utah, Department of Mining and Fuels Engineering, 1980.
5. Tai, W. P., "The Hydrogenation of Carbon Monoxide over Coprecipitated Iron/Manganese Catalyst in a Pseudo Slurry Reactor," Ph.D. Dissertation, University of Utah, Department of Mining and Fuels Engineering, 1983.
6. Tsai, Y.S., "The Synthesis of Low Molecular Weight Olefins over Co-Precipitated Iron/Manganese Catalysts", Ph.D. Dissertation, Univ. of Utah, Dept. of Fuels Engineering (1985).
7. Raney, M., "Catalysts from Alloys," Ind. Eng. Chem., 1940, 32, 1199.
8. Kim, C. S., "The Hydrogenation of Carbon Monoxide over Raney Iron-Manganese Catalysts," Ph.D. Dissertation, University of Utah, Department of Fuels Engineering, 1983.
9. Chen, K. R., "The Hydrogenation of Carbon Monoxide over Raney Iron/Manganese Catalysts: Process Variable Investigation", M.S. Thesis, University of Utah, Department of Fuels Engineering (1985).
10. Box, G. E. P. and Wilson, K. B., "On the Experimental Attainment of Optimum Conditions," J. of the Royal Stat. Soc. (series B), 1951, 13, 1.
11. Golden Graphics System Version 2. Golden Software, Inc., Colorado, 1985.
12. Ripley, B. D., Spatial Statistics, Wiley, New York, 1981.

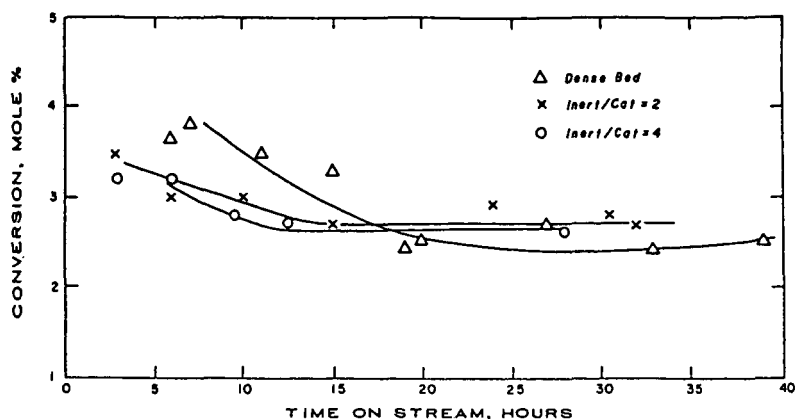


Figure 1 Catalyst Stability Test: Carbon Monoxide Conversion  
 Raney Fe/Mn Catalyst;  $T = 443 \text{ K}$ ;  $P = 1470 \text{ KPa}$ ;  
 $\text{H}_2/\text{CO} = 2/1$ ; Space Velocity =  $4.2 \text{ cm}^3 \text{ g}^{-1} \text{ s}^{-1}$

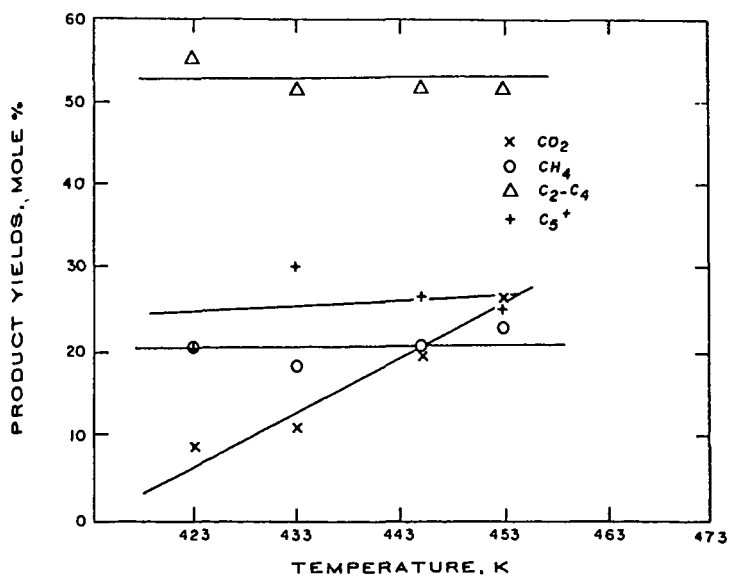


Figure 2 Effect of Temperature on Product Distribution  
 Raney Fe/Mn Catalyst;  $P = 1470 \text{ KPa}$ ,  $\text{H}_2/\text{CO} = 2/1$   
 Space Velocity =  $4.2 \text{ cm}^3 \text{ g}^{-1} \text{ s}^{-1}$ ; Diluent/Catalyst  
 Ratio = 0/1

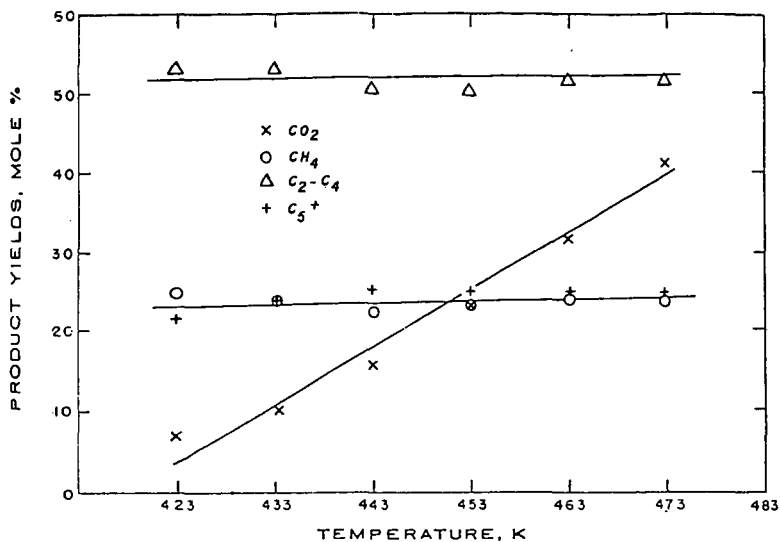


Figure 3 Effect of Temperature on Product Distribution  
 Raney Fe/Mn Catalyst,  $P = 1470$  KPa,  $\text{H}_2/\text{CO} = 2/1$   
 Space Velocity =  $4.2 \text{ cm}^3 \text{ g}^{-1} \text{ s}^{-1}$ ; Diluent/Catalyst  
 Ratio = 4/1

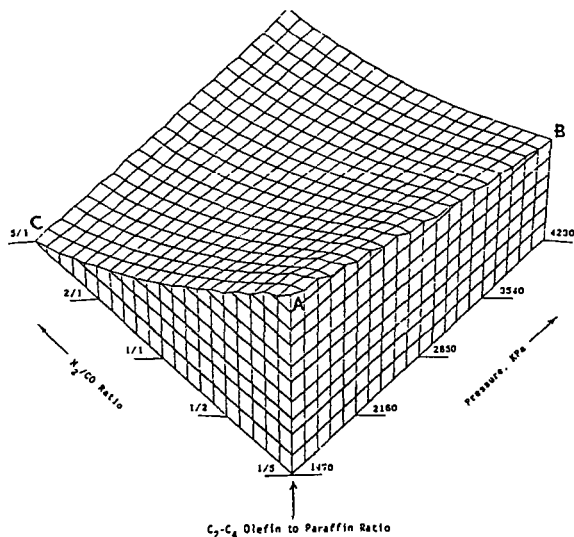


Figure 4  $\text{C}_2\text{-C}_4$  Olefin to Paraffin Ratio as a Function of  
 $\text{H}_2/\text{CO}$  Ratio and Pressure at 463 K



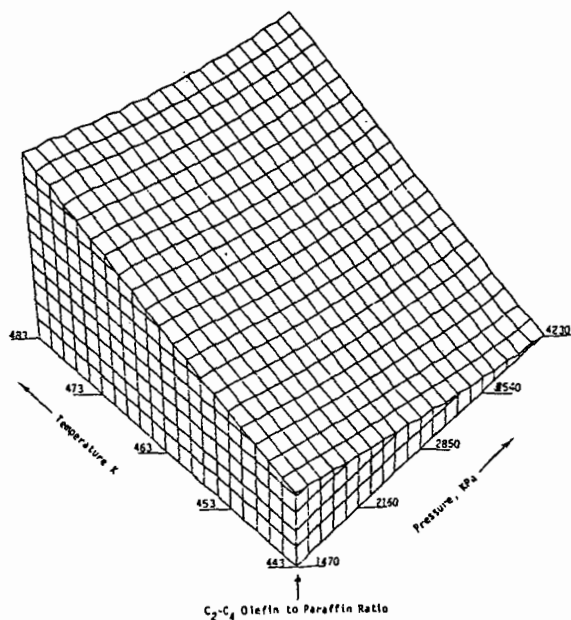


Figure 5 C<sub>2</sub>-C<sub>4</sub> Olefin to Paraffin Ratio as a Function of Temperature and Pressure at a H<sub>2</sub>/CO Ratio of Unity

Table 1

Range of Process Operating Conditions for  
Process Variable Study

Variable Level	-2	-1	0	1	2	Range <sup>(1)</sup>
Temperature, K	443	453	463	473	483	10
Pressure, KPa	1470	2160	2850	3540	4230	690
Hydrogen to Carbon Monoxide Ratio	5/1	2/1	1/1	1/2	1/5	1/2
Space Velocity, cm <sup>3</sup> g <sup>-1</sup> s <sup>-1</sup>	3	6	9	12	15	3

(1) Range =  $\frac{\text{Condition}(2) - \text{Condition}(1)}{4}$

Table 2

Carbon Monoxide Conversion and Product Distribution  
Process Variable Investigation

Raney Iron/Manganese (16/1) Catalyst

Run No.	Pressure (KPa)	Temperature (K)	Space Velocity ( $\text{cm}^3\text{g}^{-1}\text{s}^{-1}$ )	Hydrogen/Carbon Monoxide Ratio	Carbon Monoxide Conversion (mol %)	Product Distribution (mol %)			
						C <sub>1</sub>	C <sub>2</sub> -C <sub>4</sub>	C <sub>5</sub> <sup>+</sup>	CO <sub>2</sub>
1	3540	473	12	2/1	6.3	0.19	0.53	0.27	0.18
2	3540	473	12	1/2	2.2	0.15	0.54	0.31	0.27
3	3540	473	6	2/1	13.3	0.18	0.53	0.28	0.22
4	3540	473	6	1/2	5.7	0.14	0.55	0.30	0.51
5	3540	453	12	2/1	3.6	0.19	0.55	0.26	0.15
6	3540	453	12	1/2	1.2	0.17	0.49	0.29	0.38
7	3540	453	6	2/1	5.4	0.20	0.53	0.26	0.11
8	3540	453	6	1/2	1.8	0.15	0.50	0.31	0.30
9	2160	473	12	2/1	5.8	0.22	0.52	0.26	0.24
10	2160	473	12	1/2	1.8	0.17	0.51	0.32	0.32
11	2160	473	6	2/1	11.2	0.21	0.52	0.26	0.29
12	2160	473	6	1/2	2.5	0.16	0.53	0.31	0.23
13	2160	453	12	2/1	2.7	0.23	0.53	0.24	0.12
14	2160	453	12	1/2	1.1	0.19	0.45	0.31	0.44
15	2160	453	6	2/1	4.6	0.22	0.52	0.26	0.15
16	2160	453	6	1/2	1.5	0.17	0.49	0.29	0.29
17	4230	463	9	1/1	4.0	0.16	0.56	0.27	0.32
18	1470	463	9	1/1	2.8	0.20	0.50	0.29	0.31
19	2850	483	9	1/1	11.9	0.17	0.55	0.28	0.52
20	2840	443	9	1/1	0.9	0.20	0.49	0.25	0.09
21	2850	463	15	1/1	2.5	0.18	0.49	0.29	0.27
22	2850	453	3	1/1	13.6	0.16	0.56	0.27	0.51
23	2850	463	9	5/1	14.5	0.27	0.50	0.22	0.15
24	2850	463	9	1/5	0.9	0.19	0.53	0.28	0.61
25	2850	463	9	1/1	3.0	0.18	0.53	0.30	0.33

Table 3

C<sub>2</sub>, C<sub>3</sub>, C<sub>4</sub> and C<sub>2</sub>-C<sub>4</sub> Olefin Selectivity  
Process Variable Investigation

Raney Iron/Manganese (16/1) Catalyst

Run No.	Pressure (KPa)	Temperature (K)	Space Velocity (cm <sup>3</sup> g <sup>-1</sup> s <sup>-1</sup> )	Hydrogen/Carbon Monoxide Ratio	Carbon Monoxide Conversion (mol %)	Olefin to Paraffin Ratio			
						C <sub>2</sub>	C <sub>3</sub>	C <sub>4</sub>	C <sub>2</sub> -C <sub>4</sub>
1	3540	473	12	2/1	6.3	1.9	2.8	2.1	2.3
2	3540	473	12	1/2	2.2	5.0	4.3	3.5	4.0
3	3540	473	6	2/1	13.3	1.9	2.9	2.7	2.5
4	3540	473	6	1/2	5.7	5.0	4.3	3.2	4.0
5	3540	453	12	2/1	3.6	2.4	2.3	1.8	2.1
6	3540	453	12	1/2	1.2	4.8	3.2	2.3	3.1
7	3540	453	6	2/1	5.4	2.1	2.3	1.7	2.0
8	3540	453	6	1/2	1.8	4.6	3.1	2.3	3.1
9	2160	473	12	2/1	5.8	1.5	3.4	2.5	2.4
10	2160	473	12	1/2	1.8	5.4	5.6	4.3	5.1
11	2160	473	6	2/1	11.2	1.5	3.5	2.6	2.5
12	2160	473	6	1/2	2.5	5.2	5.6	4.1	4.9
13	2160	453	12	2/1	2.7	2.2	2.8	2.1	2.4
14	2160	453	12	1/2	1.1	5.6	3.8	2.8	3.7
15	2160	453	6	2/1	4.7	2.0	2.7	2.0	2.4
16	2160	453	6	1/2	1.5	5.4	3.8	2.8	3.7
17	4230	463	9	1/1	4.0	3.7	2.8	2.1	2.7
18	1470	463	9	1/1	2.8	4.1	4.2	3.7	3.8
19	2850	443	9	1/1	11.9	4.3	3.8	3.3	3.8
20	2840	443	9	1/1	0.9	4.1	2.5	1.9	2.6
21	2850	463	15	1/1	2.5	3.9	3.1	2.4	3.0
22	2850	451	3	1/1	13.6	3.3	3.4	2.3	3.0
23	2850	463	9	5/1	14.5	0.9	2.3	1.7	1.6
24	2850	463	9	1/5	0.9	7.1	5.9	4.4	5.6
25	2850	463	9	1/1	3.3	3.5	3.6	2.8	3.3

Table 4  
Correlation Coefficients from the Process Variable Investigation

$\beta_i^{(1)}$	$C_2-C_4$ Olefin/Paraffin Ratio	Product Yields			
		$C_1$	$C_2-C_4$	$C_5^+$ Hydrocarbons	Carbon Dioxide
$\beta_0$	3.310	0.180	0.530	0.300	0.380
$\beta_1$	-2.43	-0.012	0.011	-0.001	0.003
$\beta_2$	0.319	-0.007	0.012	0.006	0.049
$\beta_3$	-0.007	0.006	-0.010	0.001	-0.023
$\beta_4$	-0.884	0.021	0.004	-0.019	-0.092
$\beta_{11}$	-0.034	-0.001	-0.001	-0.002	-0.030
$\beta_{22}$	-0.057	0.000	-0.003	-0.006	-0.033
$\beta_{33}$	-0.093	-0.004	-0.002	-0.002	-0.002
$\beta_{44}$	0.051	0.011	-0.004	-0.010	-0.014
$\beta_{12}$	-0.019	0.000	0.001	0.000	0.010
$\beta_{13}$	-0.033	0.000	0.001	-0.001	-0.025
$\beta_{14}$	0.164	-0.003	-0.002	0.004	-0.020
$\beta_{23}$	-0.223	0.001	-0.014	0.000	0.030
$\beta_{34}$	-0.031	-0.001	0.005	0.004	-0.015

(1)  $\beta_1$ : pressure,  $\beta_2$ : temperature,  $\beta_3$ : space velocity  
 $\beta_4$ : hydrogen to carbon monoxide ratio

Table 5  
Reduced Correlation Coefficients from the  
Process Variable Investigation

$\beta_i^{(1)}$	$C_2-C_4$ Olefin/Paraffin Ratio	Product Yields			
		$C_1$	$C_2-C_4$	$C_5^+$ Hydrocarbons	Carbon Dioxide
$\beta_0$	3.047	0.180	0.520	2.910	0.308
$\beta_1$	-0.243	-0.012	0.011	.....	.....
$\beta_2$	0.319	0.07	0.012	0.006	0.048
$\beta_3$	.....	0.006	-0.010	.....	-0.023
$\beta_4$	-0.884	0.021	.....	-0.019	-0.092
$\beta_{11}$	0.026	.....	.....	.....	.....
$\beta_{22}$	0.003	.....	.....	-0.004	-0.016
$\beta_{33}$	.....	.....	.....	.....	.....
$\beta_{44}$	0.111	0.011	.....	-0.008	0.002
$\beta_{12}$	.....	.....	.....	.....	.....
$\beta_{13}$	.....	.....	.....	.....	.....
$\beta_{14}$	0.164	.....	.....	.....	.....
$\beta_{23}$	.....	.....	.....	.....	.....
$\beta_{24}$	-0.223	-0.014	.....	.....	.....
$\beta_{34}$	.....	.....	.....	.....	.....

(1)  $\beta_1$ : pressure,  $\beta_2$ : temperature,  $\beta_3$ : space velocity  
 $\beta_4$ : hydrogen to carbon monoxide ratio

SELECTIVE PRODUCTION OF ALPHA OLEFINS FROM SYNTHESIS  
GAS OVER ZnO SUPPORTED Pd-Fe BIMETALLICS

Bruce L. Gustafson and Paul S. Wehner

Research Laboratories, Eastman Chemicals Division,  
Eastman Kodak Company, Kingsport, Tennessee 37662

INTRODUCTION

Olefins are basic raw materials for a wide variety of commercial processes within the chemical industry. A synthesis-gas-based route to low molecular weight  $\alpha$ -olefins would provide the chemical industry with an alternative route to raw materials in the advent of future petroleum shortages or price increases.

The catalytic production of  $\alpha$ -olefins from synthesis gas has been the subject of many investigations over the past 50 years.(1,2) It has been established that, in some systems, olefin selectivity can be enhanced through the addition of various promoters such as K, Mn, Ti, or Zn.(1,3-7) Olefin selectivity can also be dependent on process parameters such as temperature, pressure, conversion levels, or feed compositions.

Recent reports in the literature indicate that supported Fe-containing bimetallics may also be selective for the production of olefins from synthesis gas.(8) This study reports the use of Pd-Fe bimetallics supported on ZnO for the selective production of olefins from synthesis gas.

EXPERIMENTAL

Catalyst Preparation

The majority of catalysts used in this study were prepared by using aqueous co-impregnation with excess solvent. The nitrate salts of the desired metals ( $\text{Pd}(\text{NO}_3)_2$ , Alpha Products or  $\text{Fe}(\text{NO}_3)_3$ , Mallinckrodt) were dissolved in excess  $\text{H}_2\text{O}$  at room temperature. It was noted that if acetate salts were used for the metal source or if acetate impurities were present on the support material, the samples which resulted were totally inactive under the conditions employed in this study. For Mössbauer studies, isotopically enriched  $^{57}\text{Fe}$  was obtained from Oak Ridge National Laboratory as  $\text{Fe}_2\text{O}_3$ . This material was added to a  $\text{HNO}_3$  solution, the solution was evaporated to near dryness twice, and then the residue was dissolved in  $\text{H}_2\text{O}$ . A sufficient amount of this solution was added to the impregnation solution to achieve approximately 50% enrichment in  $^{57}\text{Fe}$ .

The solution containing the metals for impregnation was added to the ZnO support (Alpha Products, BET S.A.  $7 \text{ m}^2\text{g}^{-1}$ ) at ambient temperature, and then the excess  $\text{H}_2\text{O}$  was removed by gentle heating in air. The samples were frequently stirred to ensure uniform impregnation. Following impregnation, the samples were calcined at 200-300°C for 3 hours to decompose residual nitrates. Metal loading levels were determined by using atomic absorption spectroscopy.

XPS measurements were made by using a PHI Model 550 ESCA/SAM spectrometer with a base pressure of  $2 \times 10^{-10}$  torr. All data were obtained at room temperature by utilizing unmonochromatized Mg K $\alpha$  radiation ( $h\nu = 1253.6 \text{ eV}$ ) and an analyzer resolution of 0.3 eV. The  $\text{Zn } 2p_{3/2}$  peak was used as an internal standard for the determination of binding energies. In previous studies, this peak was found to have a binding energy of 1021.8 eV.(9)

Mössbauer spectra were obtained by using a Ranger Scientific MS-900 spectrometer equipped with a  $^{57}\text{Co}$ -Rh source. All isomer shifts were measured relative to this source. The spectrometer was operated in the constant acceleration-flyback

mode so that only a single spectrum was recorded per scan. The velocity scale was calibrated by using an NBS-calibrated Fe foil absorber.

#### Catalyst Evaluation

All catalyst evaluations were conducted in a high-pressure-plug-flow reactor system. For a typical run, 1 mL of sample (14X40 standard mesh) was loaded into a reactor tube that was constructed from standard 1/4" stainless steel, high-pressure tubing. Prior to catalytic evaluation, the samples were reduced at 100 psig and at 300°C for 1 hour in a flow of H<sub>2</sub> or H<sub>2</sub>/CO (Matheson Gas Ultra High Purity H<sub>2</sub>, Matheson Purity CO). The feed gas was passed through an activated carbon bed at 130°C to remove metal-carbonyl impurities. Feed compositions were controlled by using Brooks mass flow controllers capable of operation up to 1500 psig. Reaction products were analyzed by using an on-line gas chromatograph fitted with a Chromosorb 102 (TM) column. Periodically, samples were analyzed off-line by GC-MS to verify product assignments. To ensure accurate rate measurements, space velocities were adjusted to keep CO conversion levels below 5%.

### RESULTS AND DISCUSSION

Following an initial prereduction, the Fe/ZnO and Pd, Fe/ZnO samples were active catalysts at 300°C and at 100 psig for the conversion of synthesis gas to hydrocarbons in the C<sub>1</sub>-C<sub>5</sub> range. The olefin fraction was typically in excess of 50 wt% of the observed products for the unpromoted catalysts. In the C<sub>2</sub>-C<sub>5</sub> range, propene was the major component, with typical propene/propane ratios of 8-10. The influence of pretreatment conditions, metal loading levels, temperature, and H<sub>2</sub>/CO ratio on catalytic activity and selectivity to olefins was investigated. The results of these studies are summarized below.

#### Catalyst Pretreatment

The catalytic activity of a 1% Pd, 0.3% Fe/ZnO sample was dependent on the nature of the pretreatment procedure. Samples reduced in a 1:1 H<sub>2</sub>/CO feed at 100 psig and at 220°C for 1 hour were inactive for the conversion of synthesis gas. However, reduction in H<sub>2</sub>/CO at 100 psig and at 260°C for 1 hour was sufficient for catalyst activation. Furthermore, after reduction at 260°C, the catalysts were active for the conversion of synthesis gas at 220°C.

Reduction at 220°C and at 100 psig in H<sub>2</sub> was comparable to reduction in H<sub>2</sub>/CO at 260°C. Pretreatment above 300°C resulted in irreversible catalyst deactivation.

XPS spectra were obtained following reduction at various pretreatment temperatures. The results of this study are summarized in Table 1. Following reduction, the Pd 3d<sub>5/2</sub> peak shifted to 336.0 eV, a value approximately 1 eV higher in binding energy than that of Pd metal.<sup>(10)</sup> This shift in Pd binding energy has been observed in the absence of Fe and can be attributed to a strong interaction between Pd and reduced ZnO.<sup>(10)</sup> As in a previous study on Pd/ZnO (ref. 10), a shoulder was observed on the Zn Auger peak which indicated that some reduction of the ZnO surface occurred with the possible formation of a Pd-Zn bimetallic particle. Similar shifts in the Pd and Zn peaks were observed following reduction under the various conditions.

In contrast to the Pd spectra, shifts in the Fe 2p<sub>3/2</sub> peak were sensitive to the pretreatment conditions. At reduction temperatures above 250°C, a significant level of zero-valent Fe (Fe<sup>0</sup>) was observed by XPS.

Preliminary Mössbauer studies were conducted with the Pd, Fe/ZnO system to determine if the oxidation state of Fe could be correlated with catalytic

activity. The spectrum obtained for the 1% Pd, 0.3% Fe/ZnO catalyst following reduction at 350°C is given in Figure 1. The best fit obtained for this data indicated the presence of two forms of iron ( $\text{Fe}^0$  and  $\text{Fe}^{3+}$ ). At lower reduction temperatures (200°C),  $\text{Fe}^{2+}$  and  $\text{Fe}^{3+}$  were the only Mössbauer observable forms of Fe present. Given the low loading levels of Fe and low transmission levels encountered with ZnO in the Mössbauer experiment, the presence of  $\text{Fe}^0$  at lower temperatures is not precluded. The absence of observable  $\text{Fe}^0$  may be a qualitative indication as to the relative amount of  $\text{Fe}^0$  formed at 350°C compared to the amount formed at a lower reduction temperature. In contrast to other Pd-Fe systems, no significant amount of Pd-Fe bimetallic was observed by Mössbauer spectroscopy under any of the reduction conditions employed in this study.

STEM studies on these samples indicate that the average particle size increased from approximately 40 Å to more than 120 Å when pretreatment temperature was raised from 260 to 350°C. Coupled with the observations discussed previously, the decrease in activity observed following reduction above 300°C may be due to a decrease in the amount of  $\text{Fe}^{2+}$  present in these samples and a sintering of the metallic components.

#### Pd, Fe Ratio

Whereas a variety of metal loadings levels were employed for this study, the results reported here were all obtained by using a constant 1 wt% Pd loading level. As shown in Table II, increasing the Fe loading resulted in a corresponding increase in catalytic activity. In all cases, the olefin/paraffin ratio was greater than unity. It is also apparent from Table II that the addition of 1 wt% Pd to the supported Fe catalysts did not significantly alter the product distribution, but did result in increased catalytic activity. This behavior is in contrast to Pd, Fe/SiO<sub>2</sub> samples evaluated in our laboratory where Pd addition resulted in a tremendous decrease in olefin to paraffin ratio.

Although Pd/ZnO is a good methanol synthesis catalyst (Table II), it should be noted that very little methanol was observed over the Pd, Fe/ZnO samples. The only apparent effect of Pd addition is to increase the overall catalytic activity of the Fe-based catalyst.

The promotional effect of Pd exhibited in this system may involve increasing the Fe dispersion. High Fe dispersions are difficult to obtain on most supports.(11) In some supported Fe-containing bimetallic systems, the metal particle surface is thought to be enriched in Fe.(12,13) It is conceivable that, in the Pd, Fe/ZnO samples, the bimetallic particles consist of a Pd-rich center covered by an Fe-rich coating. Such a model would explain the apparent lack of methanol production by the Pd component.

Because the product distribution was essentially identical for the Fe/ZnO and Pd, Fe/ZnO catalysts, significant changes in oxidation state of the Fe component were probably not responsible for the increased activity following Pd addition. In fact, the XPS and Mössbauer studies mentioned previously indicate that an increase in the Fe reduction was accompanied by catalyst deactivation.

Chemisorption and microscopy experiments were undertaken in an attempt to further characterize the Pd, Fe/ZnO catalyst. Unfortunately, because of the strong Pd-Zn interaction discussed above, chemisorption results were ambiguous and are not reported here. STEM experiments were also inconclusive, primarily due to difficulties in observing Fe on ZnO.

#### Temperature and H<sub>2</sub>/CO ratio

The apparent activation energies which were measured for the 1% Pd, 0.3% Fe/ZnO

sample between 250-300°C are shown in Table III. For comparison, the activation energies for the 0.3% Fe/ZnO are also given. While the olefin/paraffin ratio decreased slightly with increasing temperature, the olefinic fraction remained above 50 mol% of all products over this temperature range.

The fact that the apparent activation energies for the C<sub>1</sub>, C<sub>2</sub>, C<sub>3</sub>, and C<sub>4</sub> fractions are equivalent implies that formation of a common intermediate, such as CH<sub>2</sub>, is the rate-determining step for both CH<sub>4</sub> formation and chain growth to higher molecular weight products.

It is also evident from Table III that the apparent activation energies for the 0.3% Fe/ZnO catalyst were 5-6 Kcal/Mol higher than those measured for the Pd-containing catalyst. If hydrogenation is involved in the rate-determining step, this result indicates that Pd may assist in the activation of H<sub>2</sub> in this catalyst system. This conclusion is supported by the observed H<sub>2</sub> partial pressure dependency (Table IV) for the two separate systems. Addition of Pd to the Fe catalyst resulted in a decrease in reaction order with respect to H<sub>2</sub>.

#### CONCLUSIONS

The addition of Pd to Fe supported on ZnO results in a significant increase in catalytic activity for the conversion of synthesis gas. At the same time, selectivity to olefins remains high over these catalysts. One possible role of Pd addition is to increase the dispersion of the Fe component. Kinetic studies indicate that Pd may also assist in the activation of H<sub>2</sub>.

#### REFERENCES

1. (a) Storch, H. H., Galombic, N., and Anderson, R. B., "The Fischer Tröspch Synthesis," John Wiley & Sons, 1951.  
(b) Anderson, R. B., "The Fischer Tröspch Synthesis", Academic Press, Inc., 1984.
2. Caldwell, L., Council for Scientific and Industrial Research Report CENG 330, Pretoria, South Africa, June, 1980.
3. Kobel, H., Tillmetz, K. D., U. S. Patent #4,177,203, 1979.
4. McVicher, G. B., Vannice, M. A., U. S. Patent #4,192,777, 1980 and references therein.
5. Papadopoulos, M., Kieffer, R., and Deluz Arche, A., Bull. Soc. Chim., Fr., 1(3), 109, 1982.
6. Yang, C. H., Oblad, A. G., Preprints, Div. Pet. Chem., ACS Meeting, Anaheim, CA, 1978.
7. Yang, C. H., Ph.D. Dissertation, University of Utah, 1979.
8. Vannice, M. A., Lam, Y. L., Garten, R. L., Adv. Chem. Ser., 178, 25, 1979.
9. Wehner, P. S., Apai, G. A., Mercer, P. N., J. Catal., 84, 244, 1983.
10. Wehner, P. S., Tustin, G. C., Gustafson, B. L., J. Catal., 88, 246, 1984.
11. Brenner, A., J.C.S., Chem. Comm., 251, 1979.
12. Ott, G. L., Delgass, N. N., Winograd, N., Baitinger, W. E., J. Catal., 56, 174, 1979.
13. Schay, Z., Gucci, L., J.C.S. Faraday Trans. I, 78, 1911, 1982.



Table I

XPS Results For 1% Pd, 0.3% Fe/ZnO

<u>Reduction Conditions</u>	<u>Binding Energy, eV*</u>	
	<u>Pd 3d<sub>5/2</sub></u>	<u>Fe 2p<sub>3/2</sub></u>
Fresh	336.9 ± 0.1	710.7 ± 0.3
H <sub>2</sub> , 250°C	335.9	710.1
H <sub>2</sub> , 350°C	336.0	710.3/ 707.0
H <sub>2</sub> /CO, 260°C	336.0	710.3/ 707.0
CO, 260°C	336.0	710.5

\*- Referenced to the Zn 2p<sub>3/2</sub> peak assigned to be 1021.8 eV

Table II

Effect Of Fe Loading Level On Catalytic Performance  
For ZnO Supported Samples

T= 300°C, P= 100 psig, H<sub>2</sub>/CO = 1

<u>Metal Loading</u>		<u>Rate (Umoles G<sup>-1</sup> S<sup>-1</sup>) X 10<sup>2</sup></u>										
<u>% Pd</u>	<u>% Fe</u>	<u>CH<sub>4</sub></u>	<u>C<sub>2</sub><sup>=</sup></u>	<u>C<sub>2</sub><sup>-</sup></u>	<u>C<sub>3</sub><sup>=</sup></u>	<u>C<sub>3</sub><sup>-</sup></u>	<u>C<sub>4</sub><sup>=</sup></u>	<u>C<sub>4</sub><sup>-</sup></u>	<u>C<sub>5</sub><sup>=</sup></u>	<u>C<sub>5</sub><sup>-</sup></u>	<u>CH<sub>3</sub>OH</u>	
0.0	0.3	2.5	.65	.42	.78	.10	.37	.11	.23	.15	.31	
1.0	0.3	11.	2.9	1.5	3.3	.43	1.7	.48	.93	.45	.86	
0.0	1.0	13.	3.3	1.8	4.8	.48	2.5	.66	1.7	.87		
1.0	1.0	46.	7.4	12.	15.	3.4	6.6	4.0	3.8	4.8		
0.0	2.5	16.	4.9	2.4	6.9	.67	3.9	.83	2.5	1.1	1.2	
1.0	2.5	48.	9.0	11.	16.	3.0	7.1	3.3	4.3	4.1		
1.0	0.0	---	.01	---	---	---	---	---	---	---	7.18	

C<sub>n</sub><sup>=</sup> denotes olefin fraction, C<sub>n</sub><sup>-</sup> denotes paraffin fraction

Table III

Apparent Activation Energies For ZnO Supported Catalysts

$$\text{Rate} = A e^{-E_a/RT}$$

$$(P_{CO} = P_{H_2} = 50 \text{ psig, } T = 250-300^\circ\text{C})$$

Carbon No.	E <sub>a</sub> , Kcal/Mol	
	1% Pd, 0.3% Fe	0.3% Fe
1	25	30
2	25	31
3	25	31
4	25	30

Table IV

Reaction Orders For ZnO Supported Catalysts

$$\text{Rate} = k P_{CO}^N P_{H_2}^M$$

$$(T = 300^\circ\text{C})$$

Carbon No.	1 % Pd, 0.3 % Fe		0.3% Fe	
	N	M	N	M
1	0.1	0.7	0.8	1.5
2	0.1	0.5	0.9	1.1
3	0.1	0.0	---	---
4	-0.6	-1.5	---	---

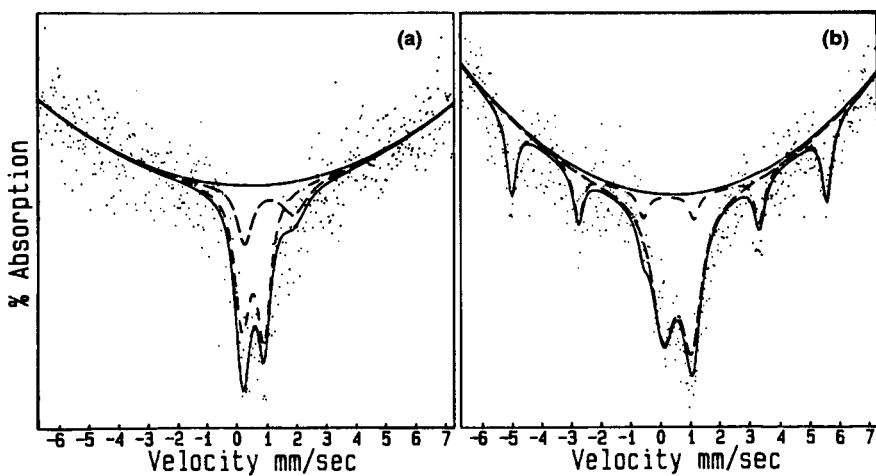


Figure 1. (a) 1% Pd, 0.3% Fe/ZnO Treated in  $H_2$  at 200°C  
(b) 1% Pd, 0.3% Fe/ZnO Treated in  $H_2$  at 350°C

CATALYTIC CONVERSION OF BIOMASS DERIVED  
SYNTHESIS GAS TO DIESEL FUEL IN A SLURRY REACTOR

William H. Zimmerman  
Charles N. Campbell  
James L. Kuester

Dept. of Chemical Engineering  
Arizona State University  
Tempe, Arizona 85287

INTRODUCTION

A project has been under investigation for several years at Arizona State University (ASU) with the objective of producing transportation grade liquid hydrocarbon fuel from a wide variety of biomass type feedstocks. The intended product is the equivalent of that derived from petroleum. Thus a renewable and/or waste feedstock is to be utilized to produce a high quality product that is compatible with the existing distribution system and engine designs.

The fundamental characteristics of biomass (as compared with coal) are given in Table 1. As indicated, biomass contains a higher hydrogen/carbon and oxygen/carbon ratio but lower sulfur and ash content. The heating value for biomass is lower (due to the oxygen content) but the volatile matter content is higher. Thus, except for the oxygen content, biomass exhibits more attractive characteristics than coal for producing a liquid hydrocarbon fuel (less hydrogen source addition, less sulfur and ash removal, milder operating conditions). To address the oxygen problem, an indirect liquefaction approach was chosen for study at ASU. The basic steps are: (1) gasification of the biomass in a circulating solid fluidized bed system to a synthesis gas containing primarily hydrogen, carbon monoxide, ethylene, methane and carbon dioxide, and (2) conversion of the synthesis gas to a liquid hydrocarbon fuel in a catalytic reactor. The oxygen in the biomass is thus converted to carbon monoxide, carbon dioxide and some water in the gasification step. In the liquefaction step, the carbon monoxide is converted to paraffinic hydrocarbons, water and normal propanol via the following possible reactions:

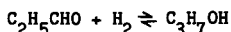
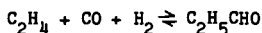
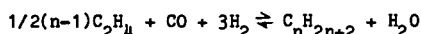
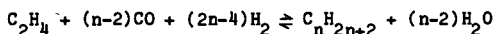


Table 1. COAL AND BIOMASS COMPOSITION (WEIGHT %)

	<u>Coal</u>	<u>Biomass</u>
C	70-80	35-55
H	4-6	4-6
O	5-20	25-50
N	0.5-2	<0.5
S	1-5	<0.5
ash	5-30	0-10
<hr/>		
Heating values (Btu/lb) (dry basis)	9500-15000	6500-9500
Volatile matter, wt. %	30-50	60-90

With proper manipulation of the above reactions, the oxygen in the biomass will end up in water, carbon dioxide and normal propanol. Carbon dioxide and water will be vented from the gasification system regenerator and an immiscible alcohol-water phase will be separated from an oxygen free paraffinic hydrocarbon phase. Past and present efforts on the project have been aimed at optimizing the implementation of this scheme via feedstock assessment, factor studies and operational reliability/control improvements. The individual steps have been studied as well as the integrated system. This paper will address recent studies on the liquefaction system. A range of synthesis gas composition produced in the laboratory in the gasification step (for approximately 100 different feedstocks and a range of operating conditions) is as follows (mole%):

hydrogen	10-45
carbon monoxide	15-60
ethylene	5-40
methane	10-45
ethane	1-5
carbon dioxide	0-15

To a certain extent, the synthesis gas composition is feedstock dependent. However control is possible with operating condition manipulation in the gasification step with the major factors being temperature, steam/biomass ratio and choice of solid in the fluidized bed system. Details on the gasification step can be found elsewhere (1,2).

#### LIQUEFACTION SYSTEM

The catalyst candidates chosen for study fall into two categories: (1) iron, and (2) cobalt. Iron is the traditional active ingredient when performing conversion studies with a synthesis gas dominated by carbon monoxide and hydrogen (3). However biomass offers the opportunity to produce a significant amount of unsaturated gases (primarily ethylene). For this case, cobalt based catalysts are attractive candidates due to the relatively high activity for olefin conversion (as opposed to the relatively inert behavior of iron). Initial liquefaction studies at ASU were performed in a fluidized bed mode. However, primarily motivated by the control complexity of operating fluidized beds in series, a slurry phase system was selected for study as an alternative. In addition to residence time (velocity control) flexibility, the slurry reactor offered the following potential advantages:

- superior temperature control
- longer catalyst life
- catalyst configuration flexibility
- superior gas distribution

The potential disadvantages were increased process complexity (slurry liquid storage and distribution) and possible slurry liquid composition stability problems.

The catalyst and liquid candidates selected for study are listed in Tables 2 and 3. Selection was based on literature guidance, physical and chemical property considerations and system compatibility. All work was performed in a bubble column reactor configuration. Reaction system details and operating procedures are described elsewhere (4,5). The experimental strategy is depicted in Figure 1.

#### RESULTS

Base operating condition screening runs resulted in the selection of following catalyst/slurry liquid combinations for additional study: (1) 25 Co/175 Al<sub>2</sub>O<sub>3</sub> in Fisher paraffin oil, and (2) 48 Fe/4.8 Cu/47.2 kieselguhr in Chevron Refined Wax 143.

Results of fractional factorial experiments to study the effect of reactor operating conditions on product yields for the cobalt study are given in Table 4. Iron catalyst factorial experiment results are shown in Table 5. Note that the feed composition did not include ethylene for the iron study since olefins are essentially inert in the presence of iron. Factor choice and levels were guided by the literature and ASU laboratory experience. Example product compositions for the two studies are shown in Figures 2 & 3. Data was obtained over a sufficient period of time (>8hrs) to insure steady state operation. Base point replication indicated an experimental error<sup>1</sup> of 2% for the cobalt study and 5% for the iron study. Mass balance closures (mass out/mass in x 100) were in the 95-105% range for the two studies.

---

Table 2  
Catalyst Candidates

Cobalt/Alumina  
Cobalt Oxide Powder  
Cobalt Oxide Precipitate  
Cobalt-Potassium/Alumina  
Iron-Copper-Potassium Precipitate  
Girdler C-73-1 (Iron Based Ammonia Synthesis Catalyst)  
Iron-Copper/Kieselguhr  
Iron-Copper/Alumina  
Iron-Copper-Potassium/Alumina  
Iron-Copper Precipitate

---

Table 3  
Slurry Liquid Candidates

Product Liquid  
Commercial No. 2 Diesel  
Mineral Oil/Paraffin Oil  
Chevron 143 Refined Wax  
Synthetic Motor Oil (Mobil One)  
Tetralin  
Tetraethylene Glycol  
Dimethyl Naphthalene  
Hexadecane  
Triethylene Glycol  
1-Octadecene  
Diethyl Phthalate  
Dow 210H  
Dow Syltherm 800  
Alpha Eicosane  
Revco Mineral Motor Oil

---

Mathematical models were fitted to the experimental data for each study, optimized and experimentally verified. Verification of predicted optimums were mixed, dependent on the particular problem posed. Thus close agreement was achieved in some cases while other problems resulted in deviations in both high and low directions. Additional product analyses were performed (eg, heating value, cetane index, API gravity, average molecular weight, most abundant carbon number, grouped composition, Schulz-Flory analysis). Also equilibrium calculations were performed. Composition analysis on the slurry liquids did not indicate any appreciable degradation in the presence of the catalysts although total operating time length was not extensive. Catalyst activity was also stable for the prescribed run lengths.

---

<sup>1</sup> exp. error =  $\frac{\text{base point product yield range}}{\text{factorial product yield range}} \times 100$

---

Table 4  
Cobalt Study Results<sup>1</sup>

Factors		Feed Gas Comp(mole%) <sup>2</sup>			Responses			
T, °C	P, psia	H <sub>2</sub>	C <sub>2</sub> H <sub>4</sub>	CO	Gas Conversions		Product Yield	
Factorial Pts:					H <sub>2</sub>	C <sub>2</sub> H <sub>4</sub>	CO (mg/gcat/hr)	
310	95	20	5	20	55.8	87.2	36.1	9.7
210	95	40	5	40	28.6	46.6	7.6	2.9
210	95	20	25	40	22.7	13.6	3.4	3.7
310	95	40	25	20	61.7	89.0	37.6	27.0
210	295	40	25	20	28.2	39.6	12.8	82.0
310	295	20	25	40	75.9	80.6	6.4	166.0
310	295	40	5	40	68.8	87.9	39.3	85.0
210	295	20	5	20	13.0	38.6	5.2	11.0
Base Pt.								
260	195	30	15	30	42.0	62.6	13.7	53.0
260	195	30	15	30	50.1	68.0	15.8	50.0
260	195	30	15	30	51.3	69.5	18.3	53.0

- <sup>1</sup> experiment: 2<sup>5-2</sup> (2 level, 5 factor)  
fractional factorial with base point replication.  
Superficial gas velocity = ~ 1.0 cm/sec at T,P  
<sup>2</sup> balance of gas = carbon dioxide + methane

Table 5  
Iron Study Results<sup>1</sup>

Factors		H <sub>2</sub> /CO		Catalyst Amount		Responses	
T, °C	P, psia	(molar)	(wt. frac.)			Gas Conversions	
Factorial Pts:						H <sub>2</sub>	CO (mg/goat)/hr
220	120	0.5	0.05			5.2	0.10
300	120	0.5	0.05			66.4	44.4
220	200	0.5	0.05			1.1	1.1
300	200	0.5	0.05			71.0	46.9
220	120	2.5	0.05			1.2	3.6
300	120	2.5	0.05			32.2	76.7
220	200	2.5	0.05			1.5	5.1
300	200	2.5	0.05			43.3	88.5
220	120	0.5	0.20			2.4	10.0
300	120	0.5	0.20			68.4	24.2
220	200	0.5	0.20			5.4	1.0
300	200	0.5	0.20			54.1	54.9
220	120	2.5	0.20			11.3	18.7
300	120	2.5	0.20			26.6	50.5
220	200	2.5	0.20			9.0	19.7
300	200	2.5	0.20			45.7	49.8
Base Pts:							
260	160	1.5	0.125			41.0	77.0
260	160	1.5	0.125			56.0	81.0
260	160	1.5	0.125			38.1	87.9

- <sup>1</sup> experiment: 2<sup>4</sup> (2 level, 4 factor)  
full factorial with base point replication.  
Superficial gas velocity = ~ 1.0 cm/sec at T,P  
<sup>2</sup> balance of gas = CO<sub>2</sub> + methane (H<sub>2</sub> + CO = 50 mole %)

## SUMMARY AND CONCLUSIONS

The following assessment of the results presented in the preceeding section is offered:

- (1) For the cobalt study, the order of importance of the factors studied with regard to effect on product yield is as follows (via analysis of variance): temperature, pressure, ethylene, hydrogen, carbon monoxide. For the iron study, the order of importance of the factors is as follows: temperature,  $H_2/CO$ , catalyst amount, pressure.
- (2) Product compositions and properties are attractive and potentially competitive with commercial fuels such as No. 2 diesel and aviation fuels. Product composition is relatively insensitive to operating condition changes with a fixed catalyst.
- (3) Cobalt based catalysts are preferred if a significant amount of olefins are present in the synthesis gas. Without significant olefins, iron catalysts should be considered.
- (4) Product yield improvement potential is considerable via adjustment of catalyst, slurry liquid and reactor operating variable factors via optimization studies.
- (5) The slurry reactor is an advantageous system with regard to temperature control, residence time flexibility and possibly catalyst life. A major disadvantage is the complexity of an additional ingredient in the system (if the product liquid is not utilized).
- (6) Catalyst and liquid life endurance testing need to be performed on the catalyst/liquid systems reported in this paper.

## ACKNOWLEDGEMENTS

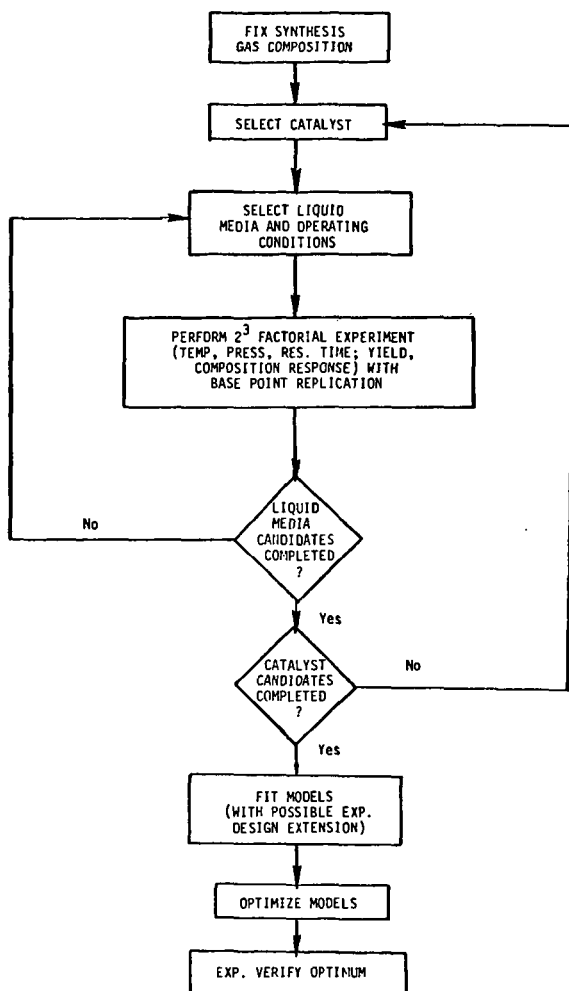
The work reported in this paper received support from the U.S. Department of Energy (Division of Industrial Programs) and the U.S. Department of Agriculture (Science and Education Administration)

## REFERENCES

1. Kuester, J. L., "Diesel Fuel via Indirect Liquefaction", Chapter 24 in Energy Applications of Biomass (M. Lowenstein ed.), Elsevier Applied Science Publishers Ltd (1985).
2. Kuester, J. L. "Diesel Fuel from Biomass, in Energy from Biomass and Wastes VIII, Institute of Gas Technology (1984).
3. Anderson, R. B. The Fischer-Tropsch Synthesis, Academic Press (1984).
4. Campbell, C. Synthesis of Liquid Hydrocarbon Fuels from Biomass in a Slurry Reactor, MSE Thesis, Arizona State University (December, 1983).
5. Zimmerman, W. Slurry Phase Synthesis of Liquid Hydrocarbon Fuels from Biomass Pyrolysis Gas Using Iron Catalysts, MS Thesis, Arizona State University (May, 1985).



Figure 1  
EXPERIMENTAL PLAN



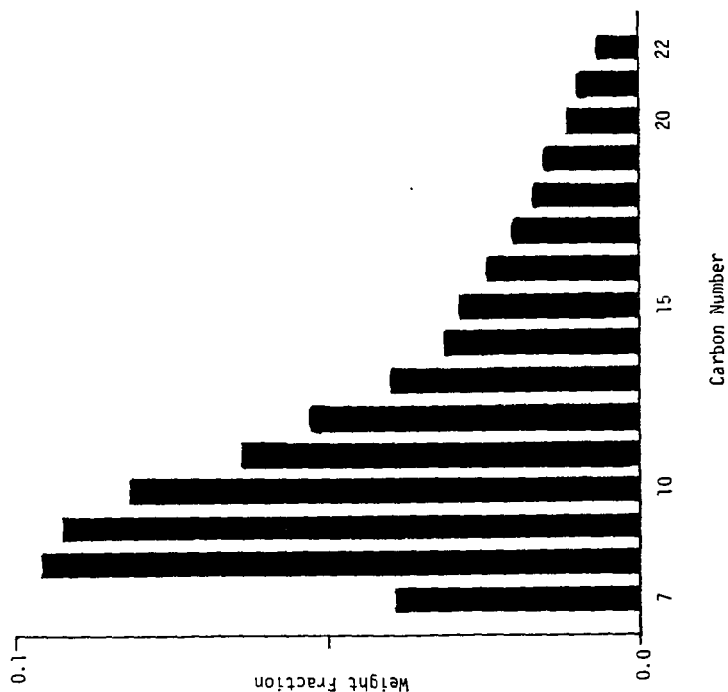


Figure 2  
Organic Product Distribution--Iron Catalyst  
Feed Composition: 26% H<sub>2</sub>, 32% CO, 16% CO<sub>2</sub>, 13% CH<sub>4</sub>, 13% C<sub>2</sub>H<sub>4</sub> (mole %)  
Temperature: 260 °C  
Pressure: 160 psig  
Superficial velocity: 1 cm/sec at T,P

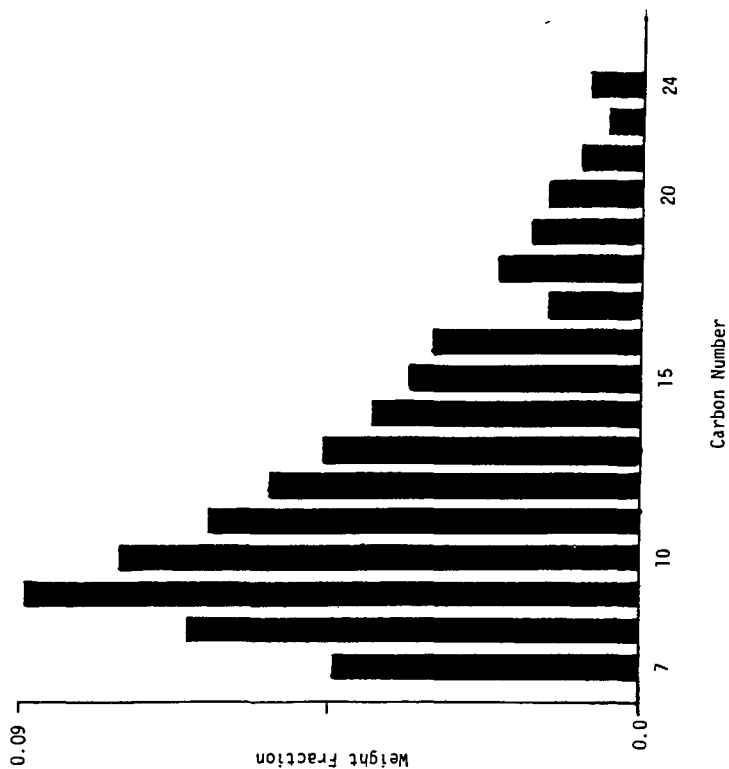


Figure 3  
Organic Product Distribution--Cobalt Catalyst  
Feed Composition: 26% H<sub>2</sub>, 32% CO, 16% CO<sub>2</sub>, 13% CH<sub>4</sub>, 13% C<sub>2</sub>H<sub>4</sub> (mole-%)  
Temperature: 260 °C  
Pressure: 160 psig  
Superficial velocity: 1 cm/sec at T,P

## THE CATALYTIC DECOMPOSITION OF METHANOL INTO SYNGAS FOR USE AS AN AUTOMOTIVE FUEL

David T. Wickham, Boyce W. Logsdon, and Scott W. Cowley

Department of Chemistry and Geochemistry  
Colorado School of Mines, Golden, CO 80401.

### ABSTRACT

Although methanol is thought to be an excellent automotive fuel, it has a smaller volumetric fuel value than gasoline. The catalytic decomposition of methanol into syngas, prior to its combustion in the engine, improves its fuel value by approximately 14%. Palladium and platinum on modified alumina supports demonstrate the necessary qualities for this process. The catalytic activity and thermal stability of palladium is strongly affected by the nature of the catalyst support used. A gamma-alumina support was modified with the oxides of Li, Mg, Cs, and La. The effect of the modified support on the activity, selectivity, and thermal stability of the palladium metal was studied during exposure to a thermal cycle of 300, 500, and 300°C. The profound difference in catalyst behavior may be due to strong metal-support interactions, to variations in metal dispersion, or to chemical alteration of the palladium. In order to determine the chemical state of the palladium metal and the modified support before and after testing, the catalysts were characterized by TPD, XRD, XPS, and volumetric chemisorption techniques.

### INTRODUCTION

Methanol is available from renewable sources, such as biomass, or from non-petroleum sources, such as coal. For this reason it is considered an attractive alternative to gasoline as an automotive fuel. However, it suffers the disadvantage of having a lower enthalpy content than gasoline, which translates into less mileage per gallon of fuel(1). The potential fuel value of methanol can be improved by catalytically decomposing it into syngas prior to its combustion in an internal combustion engine. Syngas, which is also referred to as dissociated methanol, has approximately a 14% higher enthalpy content than methanol. The combustion enthalpies for methanol, syngas ( $2\text{CO} + 4\text{H}_2$ ), and dimethyl ether (a side product of methanol decomposition) is given in Table I. A Chevrolet Citation and a Ford Escort have been retrofitted with catalytic converters in order to demonstrate the feasibility of this process. A schematic of the automotive system is shown in Figure 1. The design and testing of this system was carried out at the Solar Energy Research Institute (SERI). A more

detailed description of the automotive system employed in these studies is available in the literature(2).

At the time this study was initiated, no catalyst had been designed specifically for the decomposition of methanol into syngas in an automotive converter. In order to find an effective catalyst for this process, the following catalyst requirements were defined. First, the catalyst must demonstrate good selectivity for syngas over a large temperature range. Second, the catalyst should be able to withstand high temperatures without deactivating. Third, the catalyst should show significant activity at low temperatures. Fourth, the catalyst should be mechanically strong. Fifth, the catalyst cost should be reasonable. Several catalysts were prepared by placing active metals (Cu, Ni, Pd, and Pt) on a variety of supports (magnesia, silica, alumina) were tested and the results were compared with those obtained from several commercial formulations(3). All of the commercial formulations failed either the first, second or fourth requirements or a combination of those requirements. Palladium and platinum were found to be the best metals for the decomposition of methanol and alumina was found to be the best support, however, the alumina support is also active for the dehydration of methanol into dimethyl ether, which is an undesirable side reaction. Therefore, several catalysts were prepared in our laboratory in which active metals were impregnated onto a variety of modified gamma-alumina supports. The modified supports have a marked effect on the activity, selectivity, and thermal stability of some metals and little effect on others.

The objective of this study is to establish the function of these modified supports in controlling the behavior of the active metal. Many of the initial test and characterization results have been reported in the literature(3,4). However, some of the more interesting catalysts have been studied and characterized in more detail and are discussed below.

## EXPERIMENTAL

The catalysts were tested under the same temperature and flow conditions that would be experienced in the automotive system. The tests were conducted in a microcatalytic plug-flow reactor. Methanol was pumped into a heated inlet and vaporized. The catalyst was mounted on a fritted disk in a quartz tube. The methanol vapor was passed over the catalyst bed and the decomposition products were introduced by a gas sampling valve into a gas chromatograph. The gas chromatograph was equipped with a thermal conductivity detector and a 9 ft. x 1/8 inch stainless steel column packed with Poropak Q. Hydrogen analysis was accomplished by using a 5% hydrogen in helium carrier gas and a subambient program.

The modified supports were prepared by impregnating a gamma-alumina support with a solution containing the nitrate salt of the desired modifying agent. Subsequently, the modified supports were dried at 150°C, calcined at 550°C, and

impregnated with a solution containing either the nitrate or chloride salts of palladium or platinum. The drying and calcining steps were repeated for the finished catalyst. The catalysts were activated in the reactor under a flow of hydrogen at 300°C for 1 hour and at 400°C for 1 hour prior to testing.

Approximately 0.4 grams of 14-20 mesh catalyst particals were tested in each run, using a methanol flow rate of 0.19 g MeOH/g cat.-hr. The methanol was distilled over magnesium turnings and stored over 5A molecular sieve before use. Ultra high purity hydrogen was passed over a Matheson Model 450 purifier.

The total catalyst surface areas were obtained using conventional BET methods. The active metal surface areas were obtained with a volumetric apparatus using hydrogen chemisorption, carbon monoxide chemisorption, and hydrogen-oxygen titration techniques.

For the temperature programmed desorption studies, 0.4 grams of the catalyst were reduced in hydrogen at 400 or 500 °C for 2 hours. The hydrogen was stripped from the catalyst surface in a helium for 15 min. and then cooled in helium to 0°C. Subsequently, several pulses of carbon monoxide were introduced until the surface was saturated. The temperature desorption profile was obtained by increasing the temperature at a rate of 25°C/min. and analyzing the desorption products in a quadrupole mass spectrometer. The temperature programmed desorption apparatus is very similar to that used by other researchers(5). All the gases used during the characterization studies were of Ultra High Purity grade and they were further purified to remove traces of oxygen, water and other impurities.

The catalysts were also characterized before and after testing using a Rigaku x-ray diffractometer, a Perkin Elmer 5000 atomic absorption spectrometer, and a Surface Science SSX-100 x-ray photoelectron spectrometer.

## RESULTS AND DISCUSSION

### Catalyst Testing

All catalysts were tested at 300°C, the average operating temperature of the converter, and at 500 or 550°C to simulate a high temperature excursion. Subsequently, the temperature was lowered to 300°C to check for possible catalyst deactivation. The results of these tests are given in Table II. Each catalyst contains approximately 5 wt.% of the metal oxide modifying agent and a 0.5 wt% Pd or Pt. The modifying agents  $\text{Li}_2\text{O}$ ,  $\text{MgO}$ ,  $\text{Cs}_2\text{O}$ , and  $\text{La}_2\text{O}_3$  are represented in Table II as Li, Mg, and La. The gamma- $\text{Al}_2\text{O}_3$  support is represented as Al. The products observed in these tests were hydrogen, carbon monoxide, methane, carbon dioxide, water, dimethyl ether, and unconverted methanol. The mole % products in Table II are reported on a hydrogen free basis.

To begin with we will only consider the initial activity

of the catalysts at 300°C prior to a high temperature excursion at 550°C. The alumina support (Al) shows almost no activity for the formation of the desired CO decomposition product, but is very active for the formation of dimethyl ether. The formation of dimethyl ether is an exothermic reaction and should be avoided. In the case of the Pd-Al and Pt-Al catalysts, it is obvious that the metal plays the primary role in the production of CO, however, the dehydration activity of the support is still apparent. For those catalysts using the modified supports, Pd-Li-Al, Pd-Mg-Al, Pd-La-Al, Pt-Li-Al, Pt-Mg-Al, and Pt-La-Al the dehydration activity of the catalysts has been eliminated or reduced to an acceptable level. It is interesting to note that the modified supports have a pronounced effect on the initial activity of the Pd metal as indicated by the production of CO, with the Pd-Li-Al showing the lowest activity and the Pd-La-Al showing the highest activity. On the other hand, the initial activity of the Pt metal does not appear to be influenced by the nature of the modifier used.

At 550°C, the modified supports have a pronounced effect on the catalyst selectivity. All the Pt catalysts and the Pd-La-Al catalyst produce substantial amounts of methane, carbon dioxide, and water, while the Pd-Al, Pd-Li-Al, and Pd-Mg-Al catalysts are quite selective for the desired CO product. These results suggest that the latter catalysts have thermally deactivated and the resultant activity and selectivity is really due to the support and not the metal.

The final activity at 300°C, after testing at 550°C, shows all of the Pd catalysts (with exception of the 3% Pd catalyst) have thermally deactivated, while the Pt catalysts show no deactivation or an increase in activity.

The catalyst testing was extended to modified catalysts containing approximately 3 wt% Pd, and the results are shown in Table III. In these tests the hydrogen analysis was included. The effects of the modified supports on the initial and final activities of the catalysts is obvious, with the Pd-La-Al catalyst representing the best case and the Pd-Li-Al catalyst the worst case. The Pd-La-Al catalyst appears to experience a slight loss in activity after a thermal cycle. However, exposing the Pd-La-Al catalyst to repeated thermal cycling over a three day period resulted in no further deactivation. This catalyst was selected for use in the "dissociated methanol car" and has fulfilled all the catalyst requirements with exception of the cost of the material. In any case, it has allowed the feasibility of the process to be demonstrated in an automobile.

#### Catalyst Characterization

The modified supports have a marked influence on the catalyst activity, selectivity and thermal stability. Modified alumina supports may have an important impact on the behavior of metals other than Pd and Pt. The effects of these modified supports may extend to other important chemical reactions which involve hydrogenolysis, dissociation, or hydrogenation steps,

such as, Fischer Tropsch, and methanol synthesis. In order to understand the role of the modified support in controlling the behavior of the active metal component, selected catalysts were characterized using both bulk and surface techniques. Since the Pd-Li-Al and the Pd-La-Al catalysts represent the most extreme cases in activity, selectivity and thermal stability, they were selected for further detailed studies.

The complete thermal deactivation of the Pd-Li-Al catalyst could result from one of the following processes:

- 1) Loss of total surface area due to support sintering.
- 2) Loss of total surface area due to pore blockage.
- 3) Loss of the active Pd metal from the catalyst.
- 4) Sintering of the metal crystallites.
- 5) Migration of the metal into the support.
- 6) Covering the active metal with an inactive material.
- 7) Formation of a new inactive Pd compound.

The first two possibilities were eliminated by measuring the total surface area of the fresh and reduced Pd-Li-Al catalyst using the BET method. There was no significant change in the total surface area and the results are given in Table IV.

The metal content of the fresh, reduced and tested catalysts were determined using atomic adsorption and the results are also given in Table IV. It is apparent that the active metal does indeed remain with the catalyst.

Broadening of the Pd lines in x-ray diffraction would suggest sintering of the metal crystallites was involved. The XRD spectra for both the reduced and tested Pd-Li-Al catalyst is shown in Figure 2. There is no evidence of line broadening, however, all the palladium lines of the tested catalyst have shifted to lower  $2\theta$  values. This suggests that either a new compound has been formed or that the Pd lattice has expanded, possibly due to the palladium forming a solution with another element. These results would also argue against the migration of the Pd metal into the support as a cause for the thermal deactivation.

The catalyst deactivation was also found to be reversible, as shown in Figure 3. Although the catalyst was deactivated at high temperatures, its activity could be restored by recalcining the catalyst in air and reducing in hydrogen. The catalyst demonstrated an activity almost identical to its initial activity. However, the catalyst was again deactivated after a thermal cycle. This result strongly argues against migration of the Pd metal into the support, which should be an irreversible process. It also suggests that the element which is causing the deactivation is easily removed by treatment with oxygen, an example of such an element would be carbon.

XPS analysis of the fresh, reduced, and tested Pd-Li-Al and Pd-La-Al catalysts is shown in Figure 4. These survey scans provided information about the elemental composition of the catalyst surfaces before and after testing. The peaks of most interest are the Pd 3d peaks. For the Pd-La-Al catalyst the Pd is present at the surface of the fresh, reduced, and tested catalyst. In fact, the Pd signal is enhanced after



testing. On the other hand, the Pd-Li-Al catalyst shows that the Pd signal has almost disappeared on the tested catalyst. This would suggest that the catalyst is being covered by some other element. The carbon signal, just to the right of the Pd peak, appears to increase on the Pd-Li-Al catalyst but not for the Pd-La-Al catalyst. A depth profile of the surface was obtained by sputtering the surface with argon ions. The results are shown in Figures 6 and 7. The Pd signal for the Pd-Li-Al catalyst increased as the surface was sputtered away, while the carbon signal disappeared at the same time. The Pd-La-Al catalyst showed little effect with sputtering of the surface.

Finally, temperature programmed desorption/reaction of carbon monoxide from the surface was conducted to study the ability of the two catalysts to disproportionate carbon monoxide into carbon dioxide and carbon. The disproportionation reaction may be the primary source of the carbon for the deactivation of the Pd-Li-Al catalyst, see Figure 5. It is apparent that much more carbon dioxide is produced over the Pd-Li-Al catalyst and the reaction takes place at a much lower temperature. This suggests that the modified supports have a pronounced effect on the surface activity of the Pd metal.

#### SUMMARY

The activity, selectivity, and thermal stability of Pd metal is strongly influenced by the use of the modified supports. This suggests that either the modified support is influencing the behavior of the metal by either controlling the dispersion of the metal crystallites or by exhibiting a strong metal-support interaction.

#### REFERENCES

- 1) J. Finegold, J.T. McKinnon, and M. Karpuk, "Reformed Methanol", Non-petroleum Fuels Symposium III, October 1980.
- 2) J. Finegold, G.P. Glinsky, and G.E. Voecks, "Dissociated Methanol Citation: Final Report", SERI/TR-235-2083, August 1984.
- 3) S.W. Cowley and S.C. Gebhard, "The Catalytic Decomposition of Methanol into Synthesis Gas for Use as an Automotive Fuel", CSM Quarterly, 7(3), 41 (1983).
- 4) S.C. Gebhard, B.W. Logsdon, and S.W. Cowley, "The Decomposition of Methanol Over Supported Palladium and Platinum Catalysts", manuscript in preparation.
- 5) J.M. Zowtiak and C.H. Bartholomew, J. Catal., 83, 107 (1983).

TABLE I. Combustion Enthalpies for Methanol, Dimethyl Ether, Methane, and Synthesis Gas.

Combustion Reactions	$H_f$ (kcal/mole)	
	400°K	800°K
1. $2\text{CH}_3\text{OH} + 3\text{O}_2 \rightarrow 2\text{CO}_2 + 4\text{H}_2\text{O}$	-322.4	-321.5
2. $\text{CH}_3\text{OCH}_3 + 3\text{O}_2 \rightarrow 2\text{CO}_2 + 3\text{H}_2\text{O}$	-317.1	-316.8
3. $2\text{CH}_4 + 4\text{O}_2 \rightarrow 2\text{CO}_2 + 4\text{H}_2\text{O}$	-365.0	-341.4
4. $2\text{CO} + 4\text{H}_2 + 3\text{O}_2 \rightarrow 2\text{CO}_2 + 4\text{H}_2\text{O}$	-367.7	-371.0

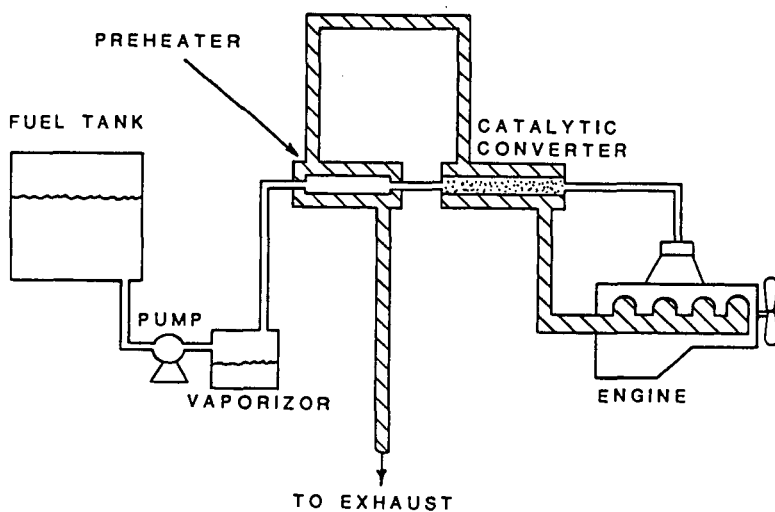


Figure 1. Automotive system for methanol decomposition. The unhatched pathway delineates the transport of fuel toward and into the engine; the hatched pathway illustrates the discharge of exhaust gases from the engine.

TABLE II. Methanol Decomposition Over Pd and Pt Catalysts.

CATALYST*	TEMP. (°C)	%Pd or %Pt	MOLE % PRODUCTS					
			CO	CH <sub>4</sub>	CO <sub>2</sub>	H <sub>2</sub> O	CH <sub>3</sub> OH	DME
Al	300	0	0.9	0	0	25.1	47.5	26.6
	550		78.9	7.5	6.7	5.8	0	0
	300		0.9	0	0	25.5	46.7	27.0
Pd-Al	300	0.5	60.8	0.9	0.8	13.5	12.2	21.3
	550		72.5	10.3	6.7	8.1	0.8	0
	300**		0.4	0	0	2.5	95.0	0
Pd-Li-Al	300	0.5	36.5	0	0	1.5	62.0	0
	550		94.3	0	1.3	2.7	1.0	0.8
	300**		1.0	0	0	0.8	98.0	0
Pd-Mg-Al	300	0.5	36.6	0	0	1.5	61.9	0
	550		92.9	1.2	1.3	3.5	0.7	0.5
	300**		0.7	0	0	2.5	95.0	1.8
Pd-La-Al	300	0.5	85.6	0.8	0.7	3.2	9.2	1.5
	500		61.7	2.0	2.6	13.6	7.1	12.9
	300**		-	-	-	-	-	-
Pd-La-Al	300	3.0	85.4	2.4	1.0	5.8	2.7	2.4
	550		18.0	41.8	17.7	22.1	0	0
	300**		83.5	2.0	0.7	7.6	2.5	2.6
Pt-Al	300	0.5	25.2	2.7	1.8	25.4	23.3	21.1
	550		40.9	28.4	13.0	16.4	0.6	0
	300**		35.8	1.5	0.7	22.0	19.3	20.0
Pt-Li-Al	300	0.5	46.8	0.8	0.8	1.0	49.5	0
	550		65.2	16.0	8.1	9.7	0	0
	300**		45.0	0.9	0.6	1.2	51.2	0
Pt-Mg-Al	300	0.5	45.8	0.6	0.5	1.6	51.8	0
	550		52.7	22.0	11.4	12.3	0	0
	300**		50.1	1.0	0.4	2.5	44.5	0
Pt-La-Al	300	0.5	48.3	0	2.0	4.6	42.1	0
	550		26.6	35.5	16.8	19.8	0.6	0
	300**		69.6	0	1.2	2.9	23.0	0

\* Catalyst Wt. = 0.400 g, approx. 5% metal oxide modifier present  
Space Velocity = 1.9 g MeOH/g cat.-hr.

Pressure = 608.0 mm Hg

\*\* After testing at 500°C

TABLE III. Methanol Decomposition Over Modified 3% Pd Catalysts.  
Hydrogen Analysis Included in Product Analysis

CATALYST*	TEMP. (°C)	MOLE % PRODUCTS						
		H <sub>2</sub>	CO	CH <sub>4</sub>	CO <sub>2</sub>	H <sub>2</sub> O	CH <sub>3</sub> OH	DME
Pd-Al	300	57.8	31.0	0.7	0.3	6.5	1.1	2.5
	550	25.6	5.4	31.0	15.8	22.3	0	0
	300**	59.2	32.2	0.8	0.3	5.0	0	0
Pd-Li-Al	300	53.4	29.2	0	0	1.1	16.3	0
	550	60.8	30.2	0.8	2.3	3.0	0.2	2.7
	300**	1.4	0.5	0	0	2.3	96.8	0
Pd-Cs-Al	300	34.8	19.9	0.5	0	4.1	40.6	0
	550	56.7	27.9	6.4	4.2	4.9	0	0
	300**	34.2	18.2	0.3	0	2.5	44.8	0
Pd-La-Al	300	56.7	30.4	0	0	0	13.0	0
	500	33.9	10.5	25.0	14.2	16.1	0	0
	300**	51.6	28.0	0	0	1.7	18.6	0

\* Catalyst Wt. = 0.400 g, approx. 5% metal oxide modifier present  
Space Velocity = 1.9 g MeOH/g cat.-hr.  
Pressure = 612-622 mm Hg

\*\* After testing at 500°C

TABLE IV. Elemental Composition and Surface Analysis of Pd Catalysts.

Catalyst	Catalyst History	Pd Metal*	Metal Oxide**	BET	Chemisorp. ( mole Pd/g)		
		(wt.%)	(wt.%)	(m <sup>2</sup> /g)	H <sub>2</sub>	CO	H <sub>2</sub> -O <sub>2</sub>
Pd-Al	fresh	2.6	0	-	-	-	-
	reduced	2.6	-	-	115.1	102.8	107.4
	tested	2.6	-	-	-	-	-
Pd-Li-Al	fresh	2.9	5.0	75.6	-	-	-
	reduced	2.9	-	-	45.7	37.0	-
	tested	2.9	-	75.6	-	-	-
Pd-Cs-Al	fresh	2.8	5.0	-	-	-	-
	reduced	2.8	-	-	67.7	64.5	57.0
	tested	2.9	-	-	-	-	-
Pd-La-Al	fresh	3.4	5.0	-	-	-	-
	reduced	3.3	-	-	66.0	53.8	48.7
	tested	3.4	-	-	-	-	-

\* Wt. % metal was determined by atomic absorption

\*\* Estimated from preparation

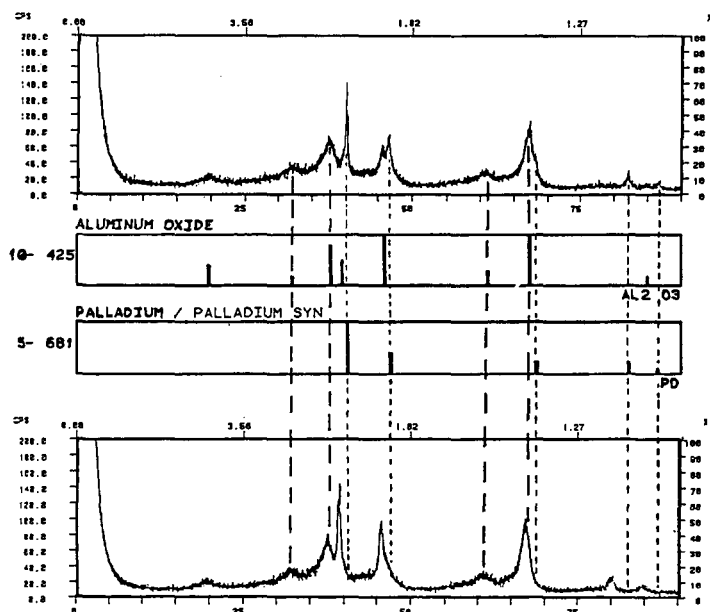


Figure 2. The XRD spectra of a reduced (top) and a tested (bottom) Pd/alumina catalyst modified with lithia.

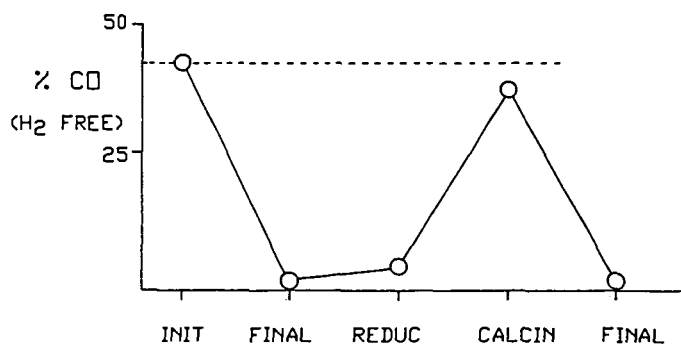


Figure 3. The lithia modified Pd/alumina catalyst always shows severe deactivation (final) after exposure to high temperature, but its activity can be restored after calcining in air and reducing the catalyst (calcin).

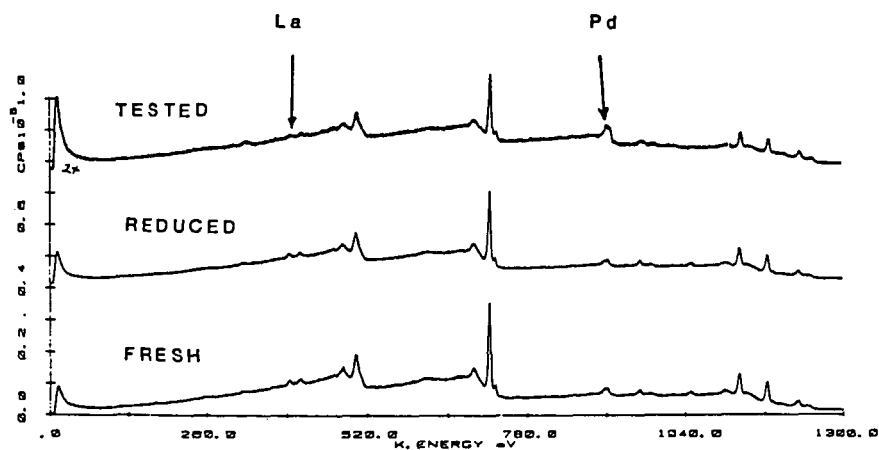
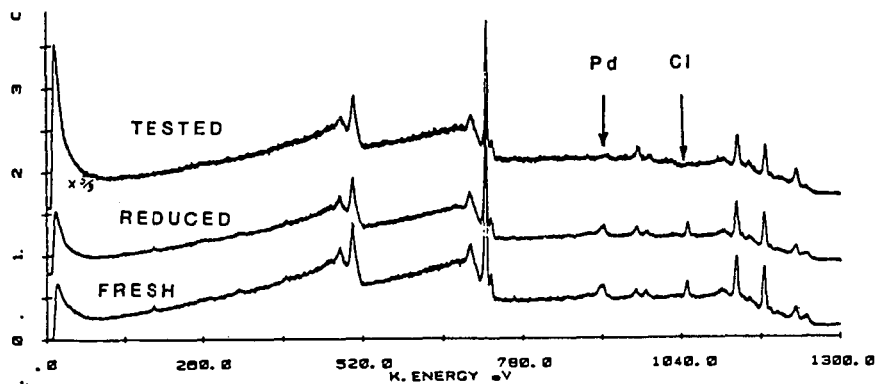


Figure 4. XPS survey scan of a lithia (top) and a lanthana (bottom) modified Pd/alumina catalyst which has been either freshly calcined, reduced, or tested.

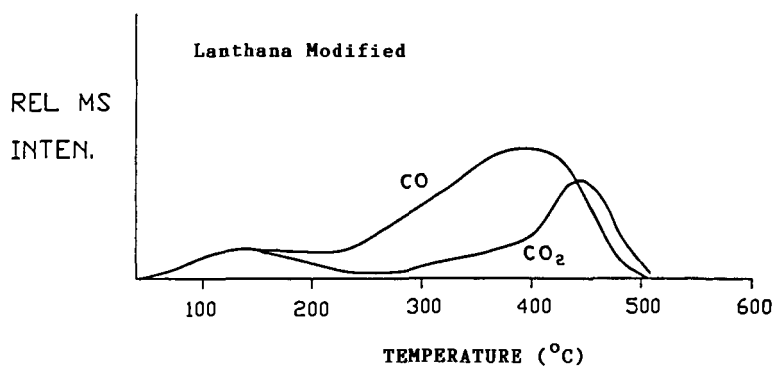
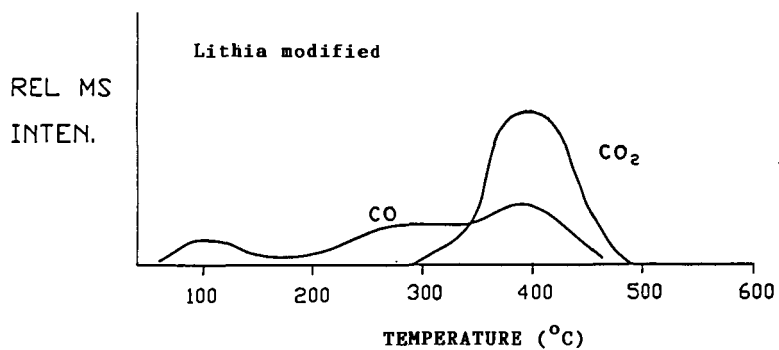


Figure 5. TPD profile of CO from a lithia (top) and a lanthana (bottom) modified Pd/alumina catalyst.

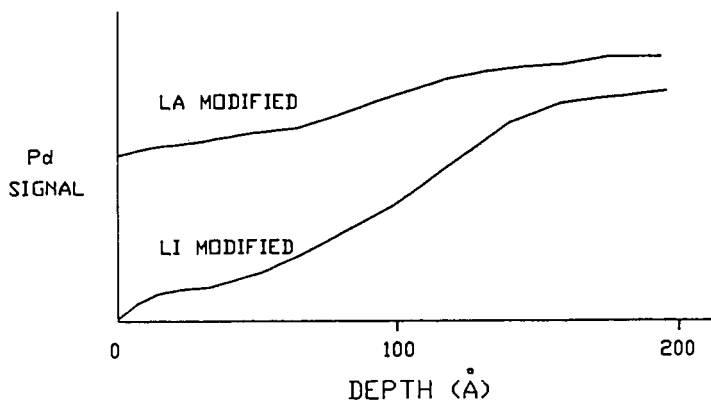


Figure 6. The depth profiles of the XPS  $Pd_{3d}$  signal for Pd/alumina catalysts modified with lanthana or lithia.

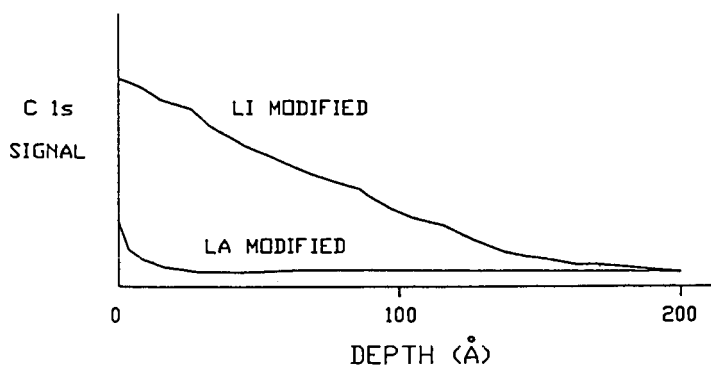


Figure 7. The depth profiles of the XPS  $C_{1s}$  signal for Pd/alumina catalysts modified with lanthana or lithia.



## TESTING OF A SULFUR TOLERANT DIRECT METHANATION PROCESS

Allan Skov  
Haldor Topsoe, Inc.  
P. O. Box 58767  
Houston, Texas 77258

Karsten Pedersen  
Haldor Topsoe A/S  
P. O. Box 213, Nymollevvej 55  
DK-2800 Lyngby, Denmark

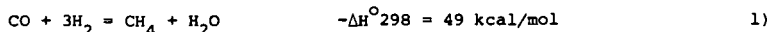
Chiang-liu Chen and Ralph L. Coates  
Questar Development Corporation  
141 East First South  
Salt Lake City, Utah 84147

### ABSTRACT

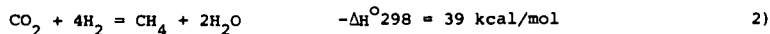
A new sulfur tolerant catalyst for methane formation from carbon monoxide and hydrogen has been tested at Haldor Topsoe's laboratory and at Mountain Fuel Resources' entrained coal gasification Process Development Unit. The catalyst also effectively catalyzes the shift reaction, which permits direct methanation of raw coal gas. In contrast to nickel-based methanation catalyst, it is not necessary to add steam for prevention of carbon formation. Physical and chemical properties of the catalyst have been characterized and reliable reaction rate expressions have been derived for optimization of the reactor design. Results of 1080 hours of testing time with raw gases produced from five different type coals showed no poisoning of the catalyst by impurities contained in the raw gas and no carbon formation on the catalyst surface. Near 100 percent conversion was achieved with respect to CO or  $H_2$ . Besides methane, the product gas also contained ethane and a small amount of propane.

### INTRODUCTION

Conventional methanation is normally carried out by reacting one molecule carbon monoxide with three molecules hydrogen to produce methane and steam:

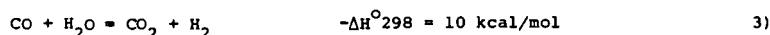


or one molecule carbon dioxide with four molecules of hydrogen to produce one molecule of methane and two molecules of steam:



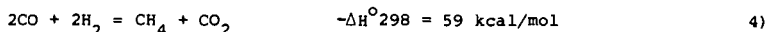
The reactions are catalyzed by various metals of which supported nickel is commonly employed (1).

The raw product gas from coal gasification typically contains higher concentrations of carbon monoxide than hydrogen, and the  $CO/H_2$  ratio ranges from 1 to 2 depending on the process. Therefore, in order to produce methane via reaction (1) above, the gas compositions have to be adjusted by the shift reaction:



and the excess  $CO_2$  has to be removed. Steam addition before methanation is required to prevent carbon formation on nickel catalysts and catalyst deactivation (2). Furthermore, since conventional catalysts are susceptible to sulfur poisoning, the hydrogen sulfide contained in the raw gas must be removed prior to methanation.

An alternate reaction for methane synthesis, which is known as direct methanation, is represented by the following reaction:



Haldor Topsoe, Inc., has recently developed a sulfur resistant catalyst for direct methanation as well as for the general reaction:



The main product of this reaction is methane. The hydrocarbons formed in addition to methane are saturated. Since the catalyst is activated by sulfur, the hydrogen sulfide contained in the raw feed gas has a positive effect on the reaction rate. The catalyst was first tested at Haldor Topsoe's laboratory in Denmark with synthetic gas simulating raw coal gas composition.

Besides being tolerant to sulfur, it is an effective catalyst for the shift reaction. Thus it offers the potential of greatly simplifying the coal to SNG process by eliminating the need for a shift reactor and sulfur removal upstream of the methanation reactor. Figure 1 presents a simplified block flow diagram to produce SNG from coal using sulfur tolerant direct methanation catalyst.

#### DESCRIPTION OF THE TEST UNIT

The methanation test unit was fabricated and partially assembled at the Haldor Topsoe Research Laboratory in Denmark and shipped to Mountain Fuel Resources (MFR) entrained coal gasification process development unit (PDU) in Utah. The unit was assembled and connected to the plant facility.

Figure 2 presents a simplified piping and instrument diagram of the unit. The unit consists of rotameters for hydrogen, hydrogen sulfide, nitrogen, and air, the methanation reactor, a fluidized sand bed for temperature control, heating elements, product gas condenser, product gas meter, temperature controller, temperature recorder, and other ancillary instruments.

The raw product gas slip stream from the gasifier was piped from the recycle gas surge tank to the reactor. The pressure was controlled by a pressure regulator upstream of the reactor and the flow rate was controlled by a needle valve downstream of the reactor. The temperature in the catalyst bed was measured with thermocouples placed inside thermowells centrally located along the length of the bed. The sand bath temperature was monitored with thermocouples embedded in the bath at several locations.

The catalyst has been tested previously in the Haldor Topsoe laboratory with synthetic raw gas in several experiments including a long-duration test of 1100 hours. This particular batch of catalyst installed at the PDU site, designated SMC 324, had been tested 440 hours at Haldor Topsoe's laboratory before it was shipped to the PDU.

#### EXPERIMENTAL

During the test, raw feed gas samples and product gas samples were taken periodically, approximately three to six times daily, and sent to Mountain Fuel Supply Company's gas laboratory for analysis. The samples were analyzed with a gas chromatograph for  $\text{H}_2$ ,  $\text{CO}$ ,  $\text{CO}_2$ ,  $\text{H}_2\text{S}$ ,  $\text{CH}_4$ ,  $\text{C}_2\text{H}_6$ ,  $\text{C}_3\text{H}_8$ , and  $\text{N}_2$ . The water vapor content of the product gas was measured by periodically weighing the condensate collected in the condenser.

The needle valve at the reactor exit was adjusted to obtain a desired gas flow rate. The space velocity was calculated based on the inlet gas flow. The conversion of carbon monoxide and hydrogen was calculated by:

$$X_{\text{CO}+\text{H}_2} = 1 - \frac{\text{Flow}_{\text{exit}} \cdot (\text{CO} + \text{H}_2)_{\text{exit}}}{\text{Flow}_{\text{in}} \cdot (\text{CO} + \text{H}_2)_{\text{in}}}$$

6)

Direct sulfur resistant methanation testing was conducted at the MFR PDU for a cumulative total of 1080 hours between October 4 and November 21, 1984. Raw feed gases were produced from five different coals, Pittsburgh No. 8 eastern bituminous, North Dakota lignite, petroleum coke, Price River Utah bituminous and SUFPCO Utah bituminous.

During the tests conversion was kept at 90 percent in order to evaluate the catalyst activity. Occasionally, the  $\text{CO}/\text{H}_2$  ratio was adjusted with the addition of pure hydrogen into the feed. Hydrogen sulfide, in addition to that present in the feed gas from the coal, was added from time to time to study the effect of sulfur on the activity of the catalyst. Most of the tests were conducted at 300 psia pressure. When the pressure was varied to study the effect of pressure on the activity the feed flow to the reactor was reduced to attain the desired conversion.

## RESULTS

Table 2 presents the range of test conditions and test results and Figure 3 presents a plot of catalyst activity versus time. The activity was calculated as the space velocity for 90 percent conversion based on the rate limiting component; i.e., the minor component which is  $\text{H}_2$  for  $\text{CO}/\text{H}_2$  ratio of greater than 1.1 and CO for  $\text{CO}/\text{H}_2$  ratio of less than 1.1. Since the tests were conducted at different pressures and feed gas compositions, the space velocity to attain 90 percent conversion in pure  $\text{H}_2$  + CO at 300 psia total pressure was calculated to obtain a standard value of the catalyst activity.

Figure 3 also includes the activity of the catalyst during the tests at Haldor Topsoe with synthetic raw gas. The figure shows that the activity remained constant for the first 500 hours tested at the PDU. At this time a plant air compressor failure occurred which resulted in a temperature runaway of the methanator for more than 10 hours. Temperatures exceeded  $600^\circ\text{C}$ . After that the activity stabilized at a level of 0.87 times the initial value. The activity remained at this value throughout the rest of the test period despite two more temperature runaways at about 720 hours of operation.

The type of coal appeared to have no effect on the activity of the catalyst. The effect of variations in hydrogen sulfide concentration were also small. There appeared to be no effect of hydrogen sulfide on activity below 0.07 volume percent concentration. The catalyst activity remained constant during a 100 hour test with hydrogen sulfide partial pressure as low as 1 ppm.

## CONCLUSIONS

The direct, sulfur resistant methanation catalyst developed was successfully tested for 1080 hours at the MFR PDU with gases produced from five different type coals.

The catalyst was tested in several experiments with synthetic raw gas at the Haldor Topsoe laboratory in Denmark, including an 1100-hour continuous test. The particular batch sent to the PDU site had been tested for 440 hours in the laboratory.

Tests were conducted at 90 percent conversion level to evaluate catalyst activity at various test conditions. Near 100 percent conversion was achieved with respect to CO or  $\text{H}_2$ . The main hydrocarbon product was methane, which was produced in concentrations near 25 percent in the product gas. The product gas also contained ethane (about 2.5 percent) and propane (about 0.5 percent).

The activity was stable after more than 1500 hours of total operation. A slight drop in catalyst activity was observed after a temperature runaway above 600°C. This caused the activity to drop to 87 percent of the initial value. Two more temperature runaways thereafter had no effect on the activity.

The activity was not affected by the type of feedstocks to the gasifier. No poisoning of the catalyst by impurities contained in the raw feed gas was observed. The catalyst was examined after the tests and no carbon formation on the catalyst surface was observed.

The catalyst appears to be preferable to conventional methanation catalysts, especially in processing gas from coal gasification which contains high carbon monoxide.

The ethane and propane produced in addition to the methane provide a significant boost to the heating value of the product gas.

#### REFERENCES

- (1) "Catalytic Aspects of High Temperature Methanation," Pedersen, K., Skov, A., and Rostrup-Nielsen, J.R., Amer. Chem. Soc. Preprints Fuel Chemistry Division 25(2), March 1980, Houston, Texas
- (2) "Deactivation Phenomena of a Ni-based Catalyst for High Temperature Methanation," Gierlich, H. H., Fremery, M., Skov, A., Rostrup-Nielsen, J. R., pp. 459-469, Catalyst Deactivation, Elsevier, Amsterdam, 1980.

TABLE 1  
PHYSICAL CHARACTERISTICS OF THE CATALYST

Name	SMC 324
Size, L x D	4.5 mm x 4.5 mm (0.18" x 0.18")
Density	1.75 gm/cm <sup>3</sup> (109 lb/cf)
Bulk Density	1.275 Kg/l (80 lb/cf)
Surface Area	100 m <sup>2</sup> /gr
Crushing Strength	600 Kg/cm <sup>2</sup> (8700 lb/in <sup>2</sup> )

TABLE 2  
SUMMARY OF DIRECT METHANATION TEST CONDITIONS AND RESULTS

	Range of Test Conditions	Typical Test Data
Pressure, psia	90 - 300	300
Volumetric Flowrate, SCFH	1 - 8	3
Inlet Conditions (Adjusted with H <sub>2</sub> ), %		
CO/H <sub>2</sub> Ratio	0.7 - 1.5	1.0
H <sub>2</sub>	30 - 45	35
CO	30 - 45	40
CO <sub>2</sub>	10 - 40	15
H <sub>2</sub> S	1 ppm - 3.5	0.1
CH <sub>4</sub>	0 - 13	1
N <sub>2</sub>	2 - 11	5
Outlet Conditions, %		
H <sub>2</sub>	0 - 15	8
CO	2 - 15	8
CO <sub>2</sub>	40 - 55	50
H <sub>2</sub> S	2 ppm - 4.5	0.1
CH <sub>4</sub>	16 - 39	25
C <sub>2</sub> H <sub>6</sub>	1 - 4	2.5
C <sub>3</sub> H <sub>8</sub>	0.2 - 0.7	0.5
N <sub>2</sub>	Balance	Balance
Fractional Conversions		
CO	70 - 100	90
H <sub>2</sub>	70 - 100	90

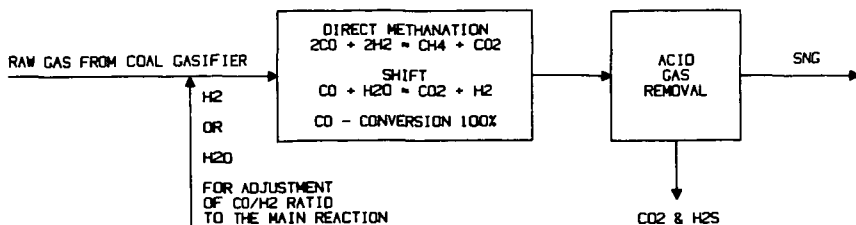


FIGURE 1. Block Flow Diagram, SNG from Coal by Direct Methanation Process

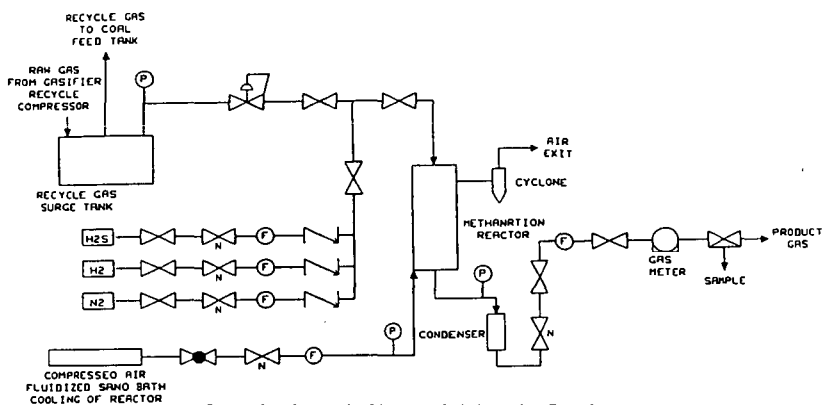


FIGURE 2. Schematic Diagram of Methanation Test System

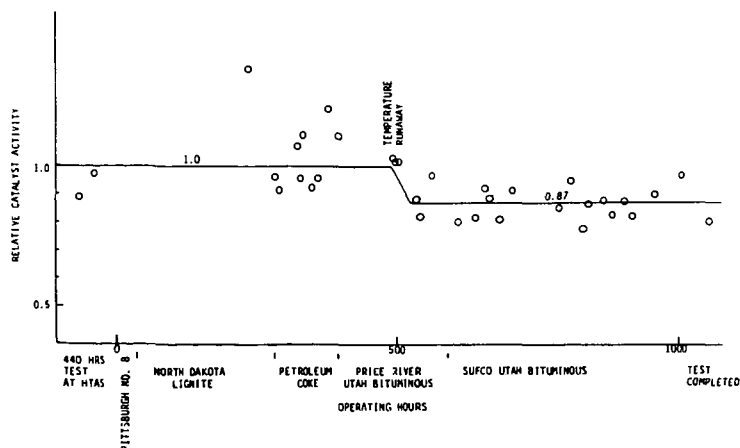


FIGURE 3. Relative Catalyst Activity Versus Time